EXPERIMENTAL STATUS OF GAUGE THEORIES

D.H. Perkins
Oxford University, United Kingdom

1. INTRODUCTION

Our present thinking is that all theories of the interactions between the fundamental constituents of the universe are renormalizable gauge theories. In these lectures, my task is to try to critically assess the experimental evidence for this conclusion; to compare the data in detail with the predictions of the gauge theories of the electroweak and strong interactions; and to discuss the prospects for obtaining experimental evidence relating to the schemes (GUTs) unifying strong and electroweak interactions.

The experimental support for the different gauge models is on a different level in each case. The electroweak (SU(2) × U(1)) interactions involve weak couplings ($\alpha \sim 10^{-2}$), the theoretical predictions are in most cases unambiguous and a meaningful and quantitative comparison is possible with a wide variety of experiments. For the strong (colour SU(3)) interactions, on the contrary, the couplings are much stronger ($\alpha_s > 0.1$), the predictions of perturbation theory have only been evaluated to leading or next to leading order, and are in any case complicated by the effects of non-perturbative (and uncalculated) terms in the q^2 range presently available experimentally. So far, clear, quantitative tests of the theory have not been possible. Finally, experimental evidence in support of grand unified theories (e.g. SU(5), SO(10)) is indirect and tentative and crucial tests of the grand unified models - for example the definitive observation of nucleon decay - are probably some years away (although clearly, rumours of signals are to be expected long before that).

2. ELECTROWEAK INTERACTIONS

Experimental verification of the standard SU(2) × U(1) electroweak theory of Weinberg, Salam and Glashow (WSG) comes from two distinct sectors: the study of lepton-lepton interactions:-

- neutrino-electron scattering ($\bar{\nu}_e e$, $\nu_\mu e$, $\bar{\nu}_\mu e$)
- $e^+e^- \to e^+e^-$, $\mu^+\mu^-$, $\tau^+\tau^-$;

and the study of lepton-quark interactions:-

- νN, $\bar{\nu} N$ inclusive and exclusive reactions
- polarized electron-deuteron scattering
- $e^+e^- \to Q\bar{Q} \to$ hadrons
- parity violation in atoms.

The purely leptonic interactions in principle provide very clear and direct tests of the standard model, which is, primarily, a model of the interaction of free leptons via the mediating gauge bosons $W^{\pm}$, Z^0 and γ. The extension of the electroweak model to lepton-hadron interactions - made by Weinberg in 1972 - involves the quark-parton description of hadrons (including the couplings of the bosons to the various quark flavours) and corrections to the quark parton model arising from strong interaction (QCD) effects as well as electromagnetic radiative corrections.

2.1 LEPTONIC ELECTROWEAK INTERACTIONS

In leading order, these are described by the diagrams of Fig.1(a) and 1(b); that is, single γ exchange and single Z^0 exchange. In addition, in the process $\bar{\nu}_e e \to \bar{\nu}_e e$, the $W^{\pm}$ exchange in Fig.1(c) is involved.

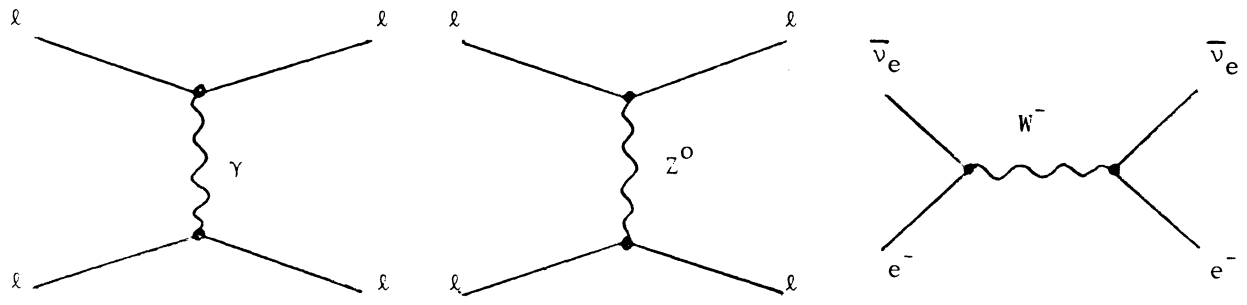

(a) (b) (c)

Fig. 1

The couplings of the leptons to the Z^0 boson have V and A coefficients defined by

$$g_V = g_L + g_R \qquad g_A = g_L - g_R \tag{1}$$

where g_L, g_R are the couplings to left-handed and right-handed states. In the WSG model,

$$g_L = I_3 - Qx \quad , \quad x = \sin^2\Theta_W \tag{2}$$
$$g_R = - Qx$$

where I_3 is the third component of weak isospin of the lepton, Q is its charge in units of |e|, and the assignments are

	I_3	Q
$\begin{pmatrix} \nu_\ell \\ \ell^- \end{pmatrix}_{LH}$	$+\frac{1}{2}$	0
	$-\frac{1}{2}$	-1
$(\ell^-)_{RH}$	0	-1

(3)

2.2 NEUTRINO-ELECTRON SCATTERING

The differential cross-section has the pointlike form (for $s=2ME \ll M_Z^2$)

$$\frac{d\sigma}{dy} = \frac{G^2 mE}{2\pi}\left[(g_V + g_A)^2 + (1-y)^2 (g_V - g_A)^2 + \frac{my}{E}(g_V^2 - g_A^2)\right] \tag{4}$$

where $G^2 mE/2\pi = 4.25E(GeV).10^{-42}$ cm^2 and E = neutrino energy, m = electron mass, and y is the fractional energy carried off by the electron, $E_e = yE$. For E > 1 GeV (accelerator experiments) the last term can be neglected. The first term in brackets corresponds to the coupling g_L of (1) and the second, to g_R. The factor $(1-y)^2$ arises as follows. In the CMS, the scattering of LH particle on LH particle (or of RH on RH) is isotropic, since the

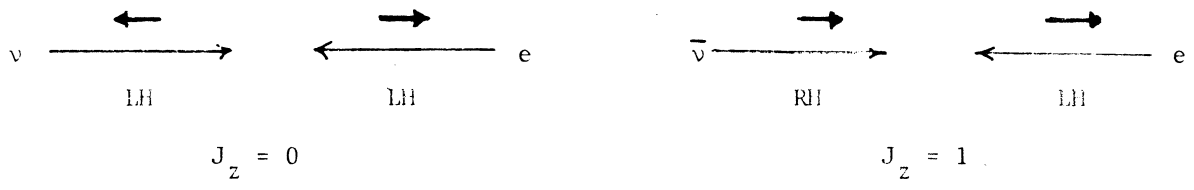

Fig. 2

overall angular momentum is J=0. (See Fig.2). So

$$\frac{d\sigma^{LL}}{d\Omega} = 4\pi E \frac{d\sigma}{dE_e} = 4\pi \frac{d\sigma}{dy} = \text{const},$$

while for scattering of a RH (anti) particle on LH particle (or LH on RH), $J=J_z=+1$, and 180° scattering is impossible since it would require $\Delta J=2$. In this case,

$$\frac{d\sigma^{RL}}{d\Omega} \propto (1 + \cos\theta_{CMS}), \qquad \text{or} \qquad \frac{d\sigma^{RL}}{dy} \propto (1 - y)^2$$

since $2y=1-\cos\theta_{CMS}$. The actual values of g_V and g_A to be inserted in (4) are as follows:

$$\begin{array}{lllll} \nu_\mu e & g_V = 2x-\tfrac{1}{2} & g_A = -\tfrac{1}{2} & \text{(i)} & \\ \bar{\nu}_\mu e & g_V = 2x-\tfrac{1}{2} & g_A = +\tfrac{1}{2} & \text{(ii)} & \\ \nu_e e & g_V = 2x+\tfrac{1}{2} & g_A = +\tfrac{1}{2} & \text{(iii)} & (5) \\ \bar{\nu}_e e & g_V = 2x+\tfrac{1}{2} & g_A = -\tfrac{1}{2} & \text{(iv)} & \end{array}$$

These values follow from (1), (2) and (3) for $\nu_\mu e$ scattering; for $\nu_e e$ scattering, the g_V, g_A coefficients are simply obtained by adding 1 to those for $\nu_\mu e$, corresponding to the $W^\pm$ exchange diagram of Fig.1(c). The values of g_V, g_A are obtained from those for antineutrinos by the substitution $g_V \to g_V$, $g_A \to -g_A$.

Integrating (4), the reactions (5) will provide four total cross-sections which are quadratic in g_V, g_A. Reaction (iii) has not been observed, (iv) has been observed at a reactor and (i) and (ii) have been observed in about 6 experiments with bubble chambers or counters at CERN and Fermilab. These three reactions give ellipses in the g_V, g_A plane, the ones for $\nu_\mu e$ and $\bar{\nu}_\mu e$ being centred at (0,0) while the one for $\bar{\nu}_e e$ is centred at (-1,-1). The three ellipses (see Fig.3) intersect in two regions, given by $g_V \sim -\tfrac{1}{2}, g_A \sim 0$ and $g_V \sim 0$, $g_A \sim -\tfrac{1}{2}$. The former solution is excluded by observations on $e^+e^- \to \ell^+\ell^-$, as discussed below, so that the allowed solution is consistent with the standard model, with $g_A=-\tfrac{1}{2}$ and $x=0.25$, giving $g_V=2x-\tfrac{1}{2}=0$. The world average cross-sections in fact give the results (Langacker et al 1979, Liede and Roos 1979):

$$\sigma(\nu_\mu e) = (1.5 \pm 0.3).10^{-42}\ \text{cm}^2 \to \sin^2\theta_W = 0.24^{+.06}_{-.04}$$

$$\sigma(\bar{\nu}_\mu e) = (1.3 \pm 0.6).10^{-42}\ \text{cm}^2 \to \sin^2\theta_W = 0.23^{+.09}_{-.23} \qquad (6)$$

Including the reactor data (on $\bar{\nu}_e e$) as well leads to the value

$$\sin^2\theta_W = 0.24 \pm .04 \qquad \nu_\mu e,\ \bar{\nu}_\mu e,\ \bar{\nu}_e e. \qquad (7)$$

This figure does not include recent results on $\bar{\nu}_\mu e$ from the CHARM (CERN EP 81/66 (1981)) collaboration at CERN, which is to be published soon, and gives $\sin^2\theta_W = 0.29 \pm .05$.

The result (7) is based on a world total of only about 100 events. Fig.4 shows the first, historic example of $\bar{\nu}_\mu e$ scattering in the Gargamelle chamber. One observes a single electron of E=500 MeV energy projected almost exactly in the beam direction (within 1.8°, consistent with the kinematic limit $\Theta \leq \sqrt{2m/E}$). This first event, found at Aachen in December 1972, was for me the first clear evidence for neutral currents. Although just one event, the background (from $\nu_e n \to pe^-$, where the proton is absorbed in the nucleus) was known to be <<0.1 event. In the total of 1.4 million pictures taken, only 3 $\bar{\nu}_\mu e$ events were eventually observed in 3 years of analysis.

It is of interest to remark that study of neutral currents was not the first goal of Gargamelle PS neutrino experiments; when they started in 1970 the scanning and measuring was directed to study of νN charged current interactions. Only after the paper of t'Hooft in 1971, showing that the Weinberg-Salam-Glashow model was renormalizable, was it decided to embark on the difficult task of scanning the film for low energy electrons. Eventually, (in 1973) the main evidence for neutral currents was to come from the observation of the inclusive reactions on nucleons $\nu N \to \nu$ + anything, with 10^3 times larger cross-section than the νe reaction but with larger relative background.

2.3 $e^+e^- \to \ell^+\ell^-$

In this process, both Z° and γ exchange are involved. In the case $e^+e^- \to e^+e^-$ (Bhabha scattering) the exchanges can take place in s as well as t-channels. Let us consider first the reaction $e^+e^- \to \mu^+\mu^-$. Again for $s<<M_Z^2$, the differential cross-section is given in terms of CMS scattering angle by:

$$\frac{d\sigma(e^+e^-\to\mu^+\mu^-)}{d(\cos\Theta)} = \frac{\pi\alpha^2}{2s}\{(1+\cos^2\Theta) + 8\chi[g_V^2(1+\cos^2\Theta) - 2g_A^2\cos\Theta]$$

$$+ 16\chi^2[(g_V^2 + g_A^2)^2(1+\cos^2\Theta) + 8g_V^2g_A^2\cos\Theta]\} \qquad (8)$$

where the first and last terms are due to pure γ and pure Z° exchanges, and the second is the interference term. The quantity

$$\chi = -\frac{GS}{8\sqrt{2}\pi\alpha} = -\frac{4.4}{10^5}\, s(GeV^2) \qquad (9)$$

while the couplings of the charged leptons are g_V and g_A as before. The derivation of (8) can be found in the lectures of Kajantie at this school, or in the lectures by J. Ellis, SLAC 215 (1978 Summer School). Integration of (8) gives for the forward-backward asymmetry ($\chi \ll 1$):

$$A = \frac{F-B}{F+B} = -6\chi g_A^2 = -\frac{6.6}{10^5}\, s(\mathrm{GeV}^2) \tag{10}$$

where the final expression is from the standard model with $g_A(\text{lepton}) = +\frac{1}{2}$, and is independent of $x=\sin^2\theta_W$. Experiments at PETRA (with $s \sim 10^3 \mathrm{GeV}^2$) with the JADE, MARKJ, PLUTO and TASSO detectors (see Figs.5 and 6) gave, on average (Wiik 1980)

$$(\bar{A}_{\mu\mu})_{obs} = -2.8 \pm 3.4\% \qquad (\bar{A}_{\mu\mu})_{theory} = -6.7\%$$

$$(\bar{A}_{\tau\tau})_{obs} = -\ 3 \pm\ 8\% \qquad (\bar{A}_{\tau\tau})_{theory} = -7.2\% \tag{11}$$

The absolute cross-sections for $e^+e^- \to \mu^+\mu^-$ or $\tau^+\tau^-$ from (8) are given in terms of the pointlike cross-section $\sigma(\text{point})=4\pi\alpha^2/3s$ by:

$$R_{\mu\mu} = \frac{\sigma_{\mu\mu}}{\sigma(\text{point})} = 1 - 8\chi g_V^2 + 16\chi^2(g_V^2+g_A^2)^2 \tag{12}$$

$$= 1 - 2\chi(4x-1)^2 + \chi^2[(4x-1)^2+1]^2 \quad \text{(SWG)}$$

$$= 1 - \frac{6s}{10^7} + \frac{2s^2}{10^9} \qquad (x = 0.23)$$

where in the second line we have substituted the values for g_V and g_A in the standard model (Equ.(3)) and in the third line, the coefficients for x=0.23, the present day best value.

Measurement of $R_{\mu\mu}$, $R_{\tau\tau}$ and R_{ee} (using the Bhabha scattering at small angle for normalization) gave the following values for g_V^2 and g_A^2, averaged over the JADE, MARKJ, PLUTO and TASSO experiments at PETRA:

	g_V^2	g_A^2	
Observed	-0.037 ± 0.05	$0.16 \pm .08$	(13)
SWG(x=0.23)	0.0016	0.25	

These numbers clearly agree with the standard model, with $\sin^2\theta_W \sim 0.25$. They do not provide very strong constraints (the error on $\sin^2\theta_W$ is of order ± 0.13), because in the presently attainable energy region ($S < 1500\ GeV^2$) the expected deviations of R from unity are at the per cent level - for example for $g_V=1$ and $S=10^3$, $\Delta R=10\%$, which is comparable with the systematic uncertainty (from apparatus acceptance) in calibrating the R values from the small angle Bhabha scatters.

The insensitivity of the data on $\sigma(e^+e^-\to\ell^+\ell^-)$ to $\sin^2\theta_W$ arises because, for $\sin^2\theta_W=0.25$, the vector coupling g_V of the charged leptons vanishes. This is not the case for quarks, and, as discussed below, the value of $R(\text{hadron}) = \sigma(e^+e^-\to Q\bar{Q})/\sigma(\text{pt})$ is in principal a more sensitive measure of $\sin^2\theta_W$.

2.4 Lepton-Quark Electroweak Interactions

In this section, we shall discuss neutrino-nucleon scattering, polarization asymmetry in the scattering of LH or RH electrons by deuterons, the ratio $R=\sigma(e^+e^-\to Q\bar{Q})/\sigma(e^+e^-\to\mu^+\mu^-)$, and optical rotation in atoms. All the interpretation depends on

(i) the extension of the SWG model to quarks

(ii) the quark-parton description of hadrons

(iii) QCD (or other) modifications to the QP model.

Regarding (i), the LH states of quarks of charge Q=+2/3 are assigned weak isospin $I_3=+\frac{1}{2}$, those of charge Q=-1/3, $I_3=-\frac{1}{2}$; and, as for leptons, RH quarks are assigned $I_3=0$. Inserting these in (1) and (2) we get Table I for the V and A couplings of the known fermions:

Table 2.1

V and A Couplings of fermions to Z° in standard model

$$x = \sin^2\theta_W \qquad v=2g_V \ , \quad a=2g_A$$

$$g_L = I_3 - Qx$$

$$g_R = -Qx$$

$$v = 2g_V = 2(g_L+g_R) = 2I_3-4Qx$$

$$a = 2g_A = 2(g_L-g_R) = 2I_3$$

$I_3 = +\frac{1}{2}$ $\quad \nu$; u, c, t

$= -\frac{1}{2}$ $\quad \ell^-$; d, s, b

Leptons

$$v_e = v_\mu = v_\tau = 4x-1 \ : \ a_e = a_\mu = a_\tau = -1$$

$$v_\nu = 1 \ : \ a_\nu = 1$$

Quarks

$$v_u = v_c = v_t = 1-\frac{8x}{3} \ : \ a_u = a_c = a_t = 1$$

$$v_d = v_s = v_b = \frac{4x}{3}-1 \ : \ a_d = a_s = a_b = -1$$

2.5 Neutrino-Nucleon Inclusive Neutral Current Reactions

This is the simplest case, as only Z^0 exchange is involved (the neutrino being uncharged). In order to keep the analysis as model-independent as possible, we shall use the Sakurai notation for the chiral couplings. For simplicity, we shall first consider the nucleon to be composed of u, d, $\bar{u}$, $\bar{d}$ quarks only.

The effective Lagrangian for the neutrino-nucleon neutral current coupling has the form (for $q^2 << M_Z^2$):

$$\mathcal{L}_{NC} = \frac{G}{2\sqrt{2}} [\bar{\nu} \gamma_\mu (1+\gamma_5)\nu][\{\bar{u}\gamma_\mu (\alpha+\beta\gamma_5)u - \bar{d}\gamma_\mu (\alpha+\beta\gamma_5)d\}$$

$$+ \{\bar{u}\gamma_\mu (\gamma+\delta\gamma_5)u + \bar{d}\gamma_\mu (\gamma+\delta\gamma_5)d\}$$

$$+ - - - -] \qquad (14)$$

The first term in brackets is the neutrino current, with coupling to Z^0 of v=a=1 and thus involving the usual operator $\gamma_\mu (1+\gamma_5)$ familiar in the charged current case. The quark combinations $(u\bar{u}-d\bar{d})$ and $(u\bar{u}+d\bar{d})$ represent the I=1 and I=0 parts respectively, with vector and axial vector coupling coefficients to Z^0 denoted α and β, and γ and δ, respectively. The dashes in the final term represent the neglected s,c..... contributions. In terms of the LH and RH coefficients, which we call U_L, U_R and D_L, D_R, we have (from (1)):

$$\begin{array}{llll} I=1 & V & \alpha = U_L + U_R - D_L - D_R & 1-2x \\ I=1 & A & \beta = U_L - U_R - D_L + D_R & 1 \\ I=0 & V & \gamma = U_L + U_R + D_L + D_R & -2x/3 \\ I=0 & A & \delta = U_L - U_R + D_L - D_R & 0 \end{array} \qquad (15)$$

In the parton model, we have to make an incoherent sum over u and d quarks, and on isoscalar targets, u and d always occur in equal amount. It is useful to define

$$g^- = U_L^2 + D_L^2$$
$$g^+ = U_R^2 + D_R^2 \qquad (16)$$

Recalling that the RH states involve the factor $(1-y)^2$, yielding a factor 1/3 upon y-integration, the inclusive cross-sections have the form

$$\sigma_{NC}^{\nu N} = \frac{G^2 ME}{\pi} \int x dx \left[(u+d)\left(g^- + \frac{g^+}{3}\right) + (\bar{u}+\bar{d})\left(g^+ + \frac{g^-}{3}\right) + - -\right] \qquad (17)$$

$$\sigma^{\bar{\nu}N}_{NC} = \frac{G^2ME}{\pi} \int xdx \left[(\bar{u}+\bar{d}) \left(g^- + \frac{g^+}{3}\right) + (u+d) \left(g^+ + \frac{g^-}{3}\right) + - - \right] \tag{18}$$

while for the charged current cross-sections, which are pure V-A and involve the LH(RH) states of quarks (antiquarks) only (thus $g^-=1$, $g^+=0$):

$$\sigma^{\nu N}_{CC} = \frac{G^2ME}{\pi} \int xdx \left[(u+d) + \frac{(\bar{u}+\bar{d})}{3} + - - -\right] \tag{19}$$

$$\sigma^{\bar{\nu}N}_{CC} = \frac{G^2ME}{\pi} \int xdx \left[(\bar{u}+\bar{d}) + \frac{(u+d)}{3} + - - -\right] \tag{20}$$

In (17) to (20), $u=u(x)$, $d=d(x)$ etc. represent the density of u, d.... quarks with fraction x of the nucleon momentum. Let us first neglect the $\bar{u}$, $\bar{d}$ sea, so that, using the notation σ and $\bar{\sigma}$ for neutrinos and antineutrinos:

$$\bar{R} = \frac{\bar{\sigma}_{NC}}{\bar{\sigma}_{CC}} = 3g^+ + g^- \tag{21}$$

$$R = \frac{\sigma_{NC}}{\sigma_{CC}} = g^- + \frac{g^+}{3} \tag{22}$$

The experimental results, from CERN counter experiments (CDHS and CHARM) are as follows:

$$g^+ = U_R^2 + D_R^2 = \frac{3}{8}(\bar{R}-R) = 0.029 \pm .006 \quad \left(= \frac{5x^2}{9}\right) \tag{23}$$

$$g^- = U_L^2 + D_L^2 = \frac{3}{8}\left(3R-\frac{\bar{R}}{3}\right) = 0.298 \pm .008 \quad \left(= \frac{1}{2} + \frac{5}{9}x^2 - x\right) \tag{24}$$

From these results, and making a reasonable estimate of "sea" contributions, one finds

$$\sin^2\theta_W = 0.23 \pm .02 \qquad (25)$$

The plot of R versus $\bar{R}$ is shown in Fig.7.

This value depends on cross-section ratios $(R,\bar{R})$ and is thus independent of absolute neutrino flux estimates. It does depend on knowing the shape of the neutrino spectrum. In the experiments, NC events are differentiated from CC events on the basis of penetration: the muon in the CC event, $\nu + N \to \mu^- +$ anything, must penetrate through the calorimeter and beyond the hadron cascade (so that a cut in $y(<1)$ has to imposed). Furthermore, NC events can only be discriminated against hadronic background if a minimum total hadron energy (E_H=6 GeV say) is required ($y > y_{min}=E_H/E_\nu$). In either case, the spectrum shape has to be known. Uncertainty about the "sea" contributions will tend to cancel in taking the ratios.

The quantities g^+ and g^- can also be separated by measuring the y distributions, using (17) and (18) in un-integrated form. Fig.8 shows results from the CHARM collaboration experiment at CERN, using a narrowband beam to provide information on the neutrino energy in individual events (Jonker et al 1981).

If the absolute cross-sections (17)-(20) are measured, and the difference taken between neutrino and antineutrino cross-sections, one obtains

$$(\sigma-\bar{\sigma})_{NC} = \frac{2}{3}x(g^- - g^+)[(u+d) - (\bar{u}+\bar{d})]$$

$$(\sigma-\bar{\sigma})_{CC} = \frac{2}{3}x[(u+d) - (\bar{u}+\bar{d})] \qquad (26)$$

$$\frac{(\sigma-\bar{\sigma})_{NC}}{(\sigma-\bar{\sigma})_{CC}} = (g^- - g^+) = \frac{1}{2} - \sin^2\theta_W$$

where NC and CC differences depend only on the "valence" quark distributions and are independent of the "sea" contributions of $u\bar{u}$, $d\bar{d}$, $s\bar{s}$, $c\bar{c}$, ... pairs. Using this method, the ABCLOS collaboration obtained (Deden et al 1979)

$$\sin^2\theta_W = 0.19 \pm 0.04 \qquad (27a)$$

Experiments on isoscalar targets, as described above, leave the relative magnitudes of $U_{L,R}$ and $D_{L,R}$ undetermined. They may be separated by comparing the cross-sections in hydrogen, where $u(x)=2d(x)$, with those in neon (with $u(x)=d(x)$). This has been done in experiments in the BEBC chamber with the result shown in Fig.9 (Blietschau et al 1979), giving again in the standard model

$$\sin^2\theta_W = 0.19 \pm 0.04 \qquad (27b)$$

2.6 EVALUATION OF INCLUSIVE AND EXCLUSIVE νN DATA

So far we have described results of analysis of the inclusive reactions of neutrinos and antineutrinos on nucleons, determining (if we include the hydrogen data) U_L^2, D_L^2, U_R^2, D_R^2. Since the signs of U_L, D_L, U_R, D_R are unknown, this is not sufficient information to determine the parameters α, β, γ, δ of (15) uniquely: there is a 4-fold ambiguity, two of the solutions being isoscalar dominant, the others isovector dominant. The former solutions were eliminated for example by the observation in bubble chambers of strong Δ-resonance production in neutral current reactions involving single pion production. Thus purely on the basis of neutrino-nucleon scattering, a unique solution for α, β, γ, δ could be found, and this unique solution coincided with the SWG model. The following Table shows the comparison of the fit of the world data by Langacker et al (1979) to U_L, D_L, U_R, D_R (or equivalently α, β, γ, δ), with the model predictions:

Table 2.2 Langacker et al (1979) fit to chiral coupling constants of quarks to Z^0.

	Fit	SWG(x=0.23)
U_L	$0.351 \pm .037$	$\frac{1}{2}-\frac{2x}{3} = 0.345$
D_L	$-0.415 \pm .055$	$-\frac{1}{2}+\frac{x}{3} = -0.423$
U_R	$-0.179 \pm .032$	$-\frac{2x}{3} = -0.155$
D_R	$-0.010 \pm .046$	$+\frac{x}{3} = 0.077$

2.7 POLARIZED ELECTRON-DEUTERON SCATTERING

Apart from that from neutrino experiments, strong experimental support for the standard superweak model comes from experiments at SLAC on the scattering of (longitudinally) polarized electrons by deuterons, again in the lepton-quark sector.

Asymmetries between LH and RH scattering rates arise from the interference between the γ exchange and Z^0 exchange diagrams (Fig.10). The former amplitude is of order e^2/q^2 and the latter of order G (the Fermi constant). Hence the ratio of the two, determining the asymmetry, must be of order

$$A = \frac{\sigma_R - \sigma_L}{\sigma_R + \sigma_L} \sim \frac{G}{(e^2/q^2)} \sim 10^{-4}\, q^2 \quad (q^2 \text{ in GeV}^2) \tag{28}$$

Let us denote by Q^Z_{Le}, Q^Z_{Re} the "charge" coupling LH and RH electron states to the Z^0, Q^Z_{Li} and Q^Z_{Ri} the corresponding quantities for quarks of the type 'i'. The couplings to the photon are denoted by $Q^\gamma_{Le} = Q^\gamma_{Re} = -e$ and $Q^\gamma_{Li} = Q^\gamma_{Ri} = Q^\gamma_i$. Adding the two amplitudes in Fig.10 we have for the cross-section for RH electrons on RH quarks:

$$\sigma_{RR} \propto \left[\frac{Q^\gamma_{Re}\, Q^\gamma_{Ri}}{q^2} + \frac{Q^Z_{Re}\, Q^Z_{Ri}}{q^2+M_Z^2}\right]^2$$

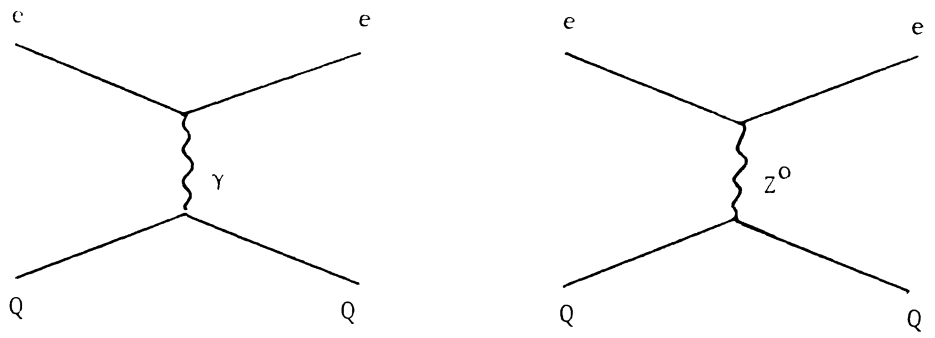

Fig. 10

while that for RH electrons on LH quarks is:

$$\sigma_{RL} \propto \left[\frac{Q^{\gamma}_{Re}\, Q^{\gamma}_{Li}}{q^2} + \frac{Q^{Z}_{Re}\, Q^{Z}_{Li}}{q^2+M_Z^2}\right]^2 (1-y)^2$$

In the experiment $q^2 \sim 1\ GeV^2 << M_Z^2$, so in calculating σ we need keep only the square of the first term and the cross-term. Making an incoherent sum over all (LH and RH) quarks, it is easy to show that

$$A = \frac{\sigma_R - \sigma_L}{\sigma_R + \sigma_L} = -\frac{q^2}{M_Z^2 e^2} \frac{\sum^{u,d} f_i(x)\,(Q_i^{\gamma}/e)\left[Q^{Z}_{Re}Q^{Z}_{Ri} - Q^{Z}_{Le}Q^{Z}_{Li}) + (1-y)^2 (Q^{Z}_{Re}Q^{Z}_{Li} - Q^{Z}_{Le}Q^{Z}_{Ri})\right]}{\Sigma f_i(x)\,(Q_i^{\gamma}/e)^2 [1 + (1-y)^2]} \qquad (29)$$

In the standard model

$$Q^{Z}_{L} = \frac{e}{\sin\Theta\cos\Theta}\left[I_{3L} - Q^{\gamma}\sin^2\Theta\right]$$

$$Q^{Z}_{R} = \frac{e}{\sin\Theta\cos\Theta}\left[I_{3R} - Q^{\gamma}\sin^2\Theta\right]$$

where

$$I_{3R} = 0$$

$$I_{3L} = +\tfrac{1}{2} \text{ for u quarks}$$

$$= -\tfrac{1}{2} \text{ for } e^- \text{ and d quarks}$$

With the definitions

$$M_Z^2 = \frac{\pi\alpha\sqrt{2}}{2G\sin^2\theta\cos^2\theta}$$

$$e^2 = 4\pi\alpha$$

we then obtain

$$A = Bq^2 \{a_1 + a_2 \frac{[1 - (1-y)^2]}{[1 + (1-y)^2]}\} \qquad (30)$$

where

$$B = \frac{9}{10}\frac{G}{2\sqrt{2}\pi\alpha} = \frac{16.08}{10^5} \text{ (for } q^2 \text{ in GeV}^2\text{)}$$

deuterium:

$$a_1 = 1 - \frac{20}{9}\sin^2\theta_W$$

$$a_2 = 1 - 4\sin^2\theta_W$$

hydrogen:

$$a_1 = \frac{5}{6} - 2\sin^2\theta_W$$

$$a_2 = \frac{5}{6} - \frac{10}{3}\sin^2\theta_W$$

These formulae should be checked by the student; in case of difficulty, consult the standard paper by Cahn and Gilman, Phys.Rev. 17,1313(1977).

From the observed asymmetry - which was found to have a y-distribution in agreement with (30) - the value

$$\sin^2\theta_W = 0.22 \pm 0.02 \qquad (31)$$

was obtained.

Fig.11 shows the stages in the experiment (Prescott et al 1978,79). Linearly polarized light from a dye laser traverses a calcite prism, allowing the plane of polarization to be rotated, and then falls on a Pockels cell. This is a birefringent crystal, which transforms the linear to circular polarization. The sense (left-handed or right-handed) can be selected by changing the sign of voltage applied to the cell. The circularly polarized light is then used to optically pump a GaAs crystal, which emits

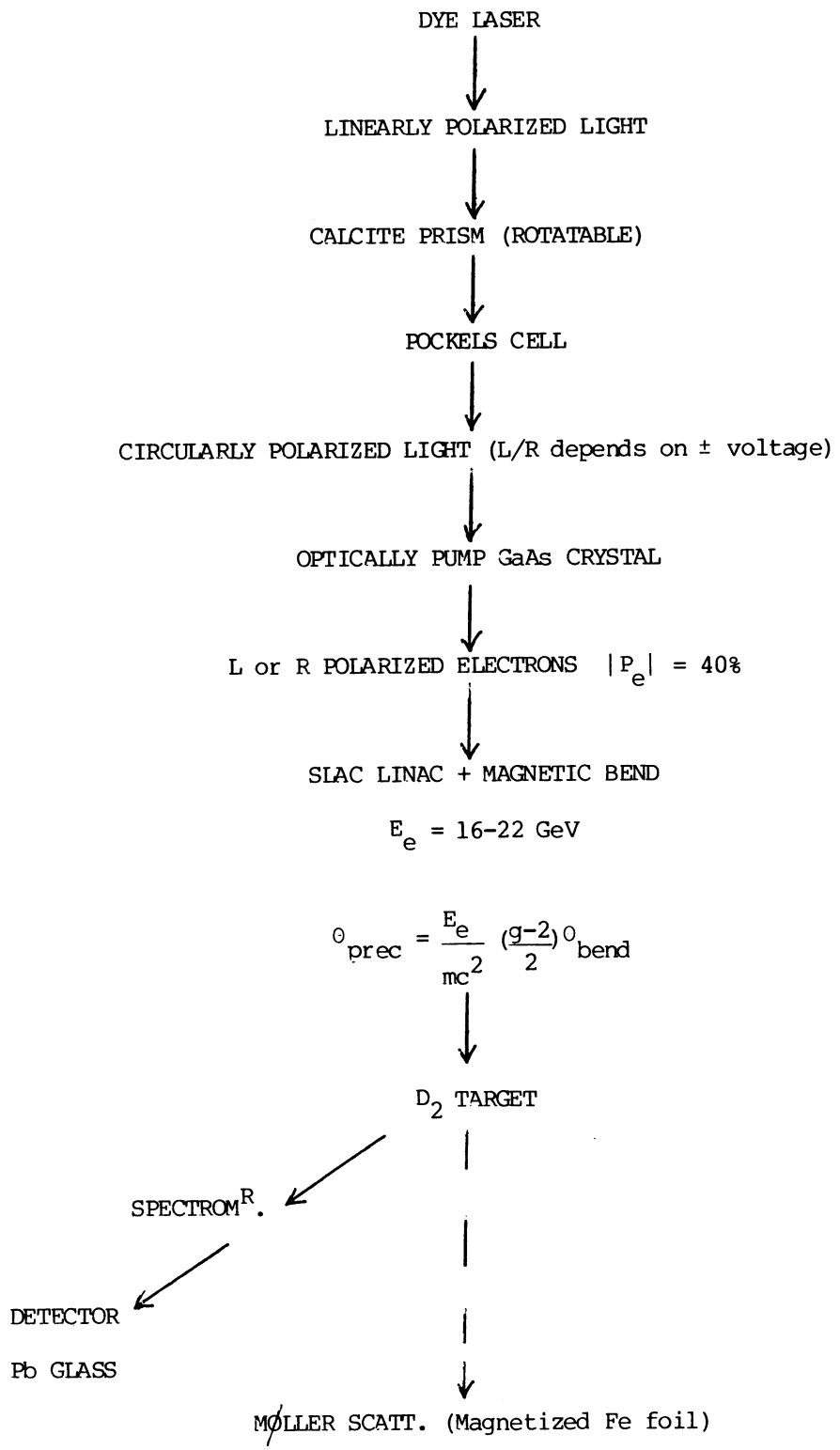
DYE LASER
LINEARLY POLARIZED LIGHT
CALCITE PRISM (ROTATABLE)
POCKELS CELL
CIRCULARLY POLARIZED LIGHT (L/R depends on ± voltage)
OPTICALLY PUMP GaAs CRYSTAL
L or R POLARIZED ELECTRONS |P_e| = 40%
SLAC LINAC + MAGNETIC BEND
E_e = 16-22 GeV
θ_prec = (E_e / mc^2) ((g-2)/2) θ_bend
D_2 TARGET
SPECTROM^R.
DETECTOR
Pb GLASS
MØLLER SCATT. (Magnetized Fe foil)
+ MONITOR
L/R ASYMM. → P_e

Fig.11

electrons with the same (LH or RH) polarization (i.e. helicity) as the incident light. The degree of electron spin-polarization is $|P_e| \sim 40\%$. These electrons were then injected into the SLAC electron linac and accelerated to energy E = 16-22 GeV (using more or less RF cavities). A magnetic bend is included, which serves to rotate the electron spin vector relative to the momentum vector by the "g-2" precession angle

$$\Theta_{prec} = \frac{E}{mc^2} \frac{(g-2)}{2} \Theta_{bend}$$

where Θ_{bend} is held constant so that the electron beam, independent of E, falls on the deuterium target. The beam passing through the target impinges on a beam monitor and also a magnetized iron foil. The left/right asymmetry of the Møller (electron-electron) scattering from the foil measures the electron polarization P_e. Electrons scattering inelastically from the target (with $q^2 \sim 2GeV^2$) are momentum-selected by means of a spectrometer magnet and recorded with a shower counter. The average asymmetry was measured by frequent changes of Pockels cell voltage. Several checks were made that the results were measuring a real physical effect, even at the 10^{-5} level. First, the experiment was carried out with unpolarized electrons (from an electron-gun) to check that there was no effect. Second, the calcite prism was rotated through various angles ϕ, to check that the asymmetry $A(\propto \cos 2\phi)$ reversed for $\phi = 90°$ and that it went to zero for $\phi = 45°$. Finally, the electron beam energy was varied to check that 'A' changed in sign and magnitude as the spin vector rotated through the angle Θ_{prec}.

2.8 THE PROCESS $e^+e^- \to$ HADRONS

Neutral weak current effects are expected in the process $e^+e^- \to Q\bar{Q} \to$ hadrons, just as in $e^+e^- \to$ lepton pair. We simply have to make a sum over quark flavours f, so that the expression for the cross-section, generalizing (12) will be

$$R = \frac{\sigma(e^+e^- \to Q\bar{Q})}{\sigma(\text{point})} = 3\left[\sum_f Q_f^2 - 2\chi \Sigma Q_f v_e v_f + \chi^2 (v_e^2 + a_e^2)(v_f^2 + a_f^2)\right] \qquad (32)$$

where the factor 3 stands for the number of colours, Q_f is the charge of quark flavour f, and I have set $2g_V^e = v_e$, $2g_A^e = a_e$, $2g_V^f = v_f$ and $2g_A^f = a_f$ for clarity. The first, second

and third terms stand for the γ exchange (QED), γ-Z^0 interference and Z^0 exchange terms respectively. The quantity $\chi = -4.4s(GeV^2).10^{-5}$ as before. Because the vector charge v_f of the quarks depends differently on x than that of the leptons (see Table 2.1), the departures from pure QED for the hadron reaction are different (and larger) than for $e^+e^- \to \ell^+\ell^-$. For x=0.23, however, the effect is small:

$$R(x=0.23) = \frac{11}{3}\left[1 - .0071\,\frac{s}{10^3} + .0038\,\frac{s^2}{10^6}\right] \qquad (33)$$

if we sum over u, d, s, c and b quarks. (32) describes a parabolic relation of R on $x=\sin^2\Theta_W$, and Fig.12 shows that for the JADE experiment at PETRA. For any given value of R, there are two possible solutions, in this case x=0.23 and x=0.58. From the limits set from asymmetries in $e^+e^- \to \ell^+\ell^-$ described before, the second solution can be excluded (see Fig.3). The JADE and MARKJ experiments together give

$$\sin^2\Theta_W = 0.23 \pm 0.08 \qquad (34)$$

In this analysis, we have so far neglected QCD corrections, which at finite q^2 give a first-order correction

$$R(q^2) = R(\infty)\left(1 + \frac{\alpha_s}{\pi}\right) \qquad (35)$$

Inserting α_s=0.17 (from the analyses of 3-jet events to be described later), this correction was first applied in arriving at the result (34). What is the significance of these results? First we can say that they give some check on the neutral current couplings - previously unmeasured - of the c, b and s quarks: they are not 10 times the GSW values, or anything crazy like that. Second, they depend on electroweak couplings at very high energy (q^2 up to 1400 GeV^2, compared with ~20 GeV^2 in neutrino experiments). Thirdly, however, it has to be said that they (the JADE/MARKJ physicists) seem to have more confidence in QCD than in electroweak theory. I would have <u>assumed</u> the standard electroweak coupling and the value of $\sin^2\Theta_W$ from the neutrino results (i.e. equation (33)), and used the observed value of R to estimate α_s from (35). The point is that (35) is a fairly safe (leading order) formula, and I could believe that it really does measure α_s (as compared with the ratio of "3 jet"/"2 jet" events to be considered later, which may or may not measure α_s). If one takes the JADE data for example, then one obtains from

(35) $\alpha_s = 0.25 \pm 0.25$, not earthshaking but to me more interesting than (34).

2.9 PARITY VIOLATION IN ATOMIC TRANSITIONS

Parity violation in atomic transitions is expected on the basis of γ/Z^0 interference in the coupling of the atomic electrons to the nucleus (quarks). Suppose we consider a very weak (M1) electromagnetic transition, say between two s-states of the same parity. The Z^0 exchange can lead to a mixing of s and p states, leading to an E1(s→p) transition. Thus, one has a predominantly M1 transition with an E1 admixture. If the transition is excited by plane polarized light, the effect is to rotate the plane of polarization of the transmitted light in one direction by a very small angle. Such optical rotation has been measured in atomic transitions in Bi vapour excited by laser beams, and we discuss these experiments briefly.

In its most general form the parity non-conserving part of the Lagrangian for the electron-nucleus interaction will be

$$\mathcal{L}_{PV} = \frac{G}{\sqrt{2}} \sum_{u,d} \left[(\bar{e}\gamma_\mu\gamma_5 e)\, 2g_A^e \{\alpha\,(\bar{u}\gamma_\mu u - \bar{d}\gamma_\mu d) + \gamma\,(\bar{u}\gamma_\mu u + \bar{d}\gamma_\mu \bar{d})\}\right.$$

$$\left. + (\bar{e}\gamma_\mu e)\, 2g_V^e \{\beta\,(\bar{u}\gamma_\mu\gamma_5 u - \bar{d}\gamma_\mu\gamma_5 d) + \delta\,(\bar{u}\gamma_\mu\gamma_5 u + \bar{d}\gamma_\mu\gamma_5 \bar{d})\}\right] \qquad (36)$$

representing an axial electron current interacting with a vector quark current, or vice-versa.

In a nucleus, at low q^2, one obtains the coherent effect of all nucleons (quarks). However,

(i) Σ (nuclear axial) ~ nuclear spin ~ 1 N.M. - most quark spins are paired off.

(ii) Σ (nuclear vector) ~ A (=mass no.) (the weak quark charges add).

Thus, in comparison with the first term in (36), the second term involving nuclear axial currents can be discarded. Further $2g_A^e = -1$, and since the nucleons are non-relativistic, $\gamma_\mu = \gamma_4$ only, the time component.

Hence

$$\mathcal{L}_{PV} = -\frac{G}{2\sqrt{2}} (\bar{e}\gamma_4\gamma_5 e)\Big[\sum_{u,d} (\alpha+\gamma)\bar{u}\gamma_4 u + (\gamma-\alpha)\bar{d}\gamma_4 d\Big]$$

$$= +\frac{G}{2\sqrt{2}} \frac{\underline{q}\cdot\underline{p}}{m_e}\big[\alpha(Z-N) + 3\gamma(Z+N)\big]$$

The rotation thus depends on the quantity

$$Q_W = \alpha(Z-N) + 3\gamma(Z+N) \qquad (37)$$
$$= -N + Z(1-4x)$$

where the second expression, from the standard model, results from the substitution $\alpha=1-2x$, $\gamma=-2x/3$. For bismuth (Z=83, N=126) we have for example

x = 0	Q_W = - 43
x = 0.10	Q_W = - 76
x = 0.25	Q_W = -126
x = 0.50	Q_W = -209

The results of various experiments on optical rotation in bismuth are shown in Table 3, from a review by Fortson and Wilets (1981). There are seen to be substantial discrepancies between experiments. Furthermore the theoretically expected rotations depend on details of atomic shielding calculations and different estimates vary by a factor 2. All that can be said is that 3 of the 4 groups now find rotations which agree in sign and in approximate magnitude with what is expected in the standard model.

Table 2.3 OPTICAL ROTATION EFFECTS IN BISMUTH

(after Fortson and Wilets, Advances in Atomic and Molecular Physics, 16,319 (1981)

Group	Wavelength & transition	R_{exp}(radian $\times 10^8$)	$R_{th}(\times 10^8)$	$r=\frac{R_{exp}}{R_{th}}$
Seattle I	876nm $(\frac{3}{2} \rightarrow \frac{3}{2})$	-8 ± 3	-11	0.73
Seattle II	" "	-0.7 ± 3.2		0.06
Seattle III	" "	-9.3 ± 2.9		0.85
Oxford I, II	648nm $(\frac{3}{2} \rightarrow \frac{5}{2})$	$+2.7 \pm 4.7$	-13	-0.17
Oxford III	" "	-10.7 ± 1.5		0.80
Novosibirsk I	" "	-18 ± 5	-20	~1
Novosibirsk II	" "	-20.6 ± 3.2		~1
Moscow	" "	0 ± 1		0

Other atomic experiments are currently under way in hydrogen and other elements; one, by the Berkeley group in thallium, obtains a preliminary result within a factor 2 of that expected.

2.10 Summary on Electroweak Experiments

The data described above have been analysed in terms of the simplest electroweak model of Salam, Weinberg and Glashow, which incorporates a single isospin doublet of Higgs scalars to provide the spontaneous symmetry-breaking mechanism. One can also do fits for models involving more than one Higgs doublet, and these involve a parameter ρ, which is the ratio of the squares of the intrinsic couplings of NC and CC respectively ($\rho = M_W^2/(M_Z^2 \cos^2\theta_W)=1$ in the WSG model). For the two parameter fit, one obtains for the

SLAC experiment

$$\sin^2\theta_W = 0.29\ ^{+.03}_{-.10}$$
$$\rho = 1.74 \pm 0.36 \qquad (38)$$

while for the neutrino-nucleon data (cf (25)), one obtains

$$\sin^2\theta_W = 0.234 \pm .013$$
$$\rho = 1.002 \pm .015 \qquad (39)$$

Experimentally therefore, $\rho=1$. Note that in the eD scattering, ρ and $\sin^2\theta_W$ are strongly correlated, and the neutrino data provides a much stronger constraint on the model.

Fig.13 shows the results for $\sin^2\theta_W$ from the various experiments plotted against q^2. If we exclude the atomic results, which are uncertain, no dependence of $\sin^2\theta_W$ on q^2 is discernible over the range $q^2 \sim 10^{-4}$ GeV^2 (from $\bar{\nu}_e e$ scattering) to $|q^2| \sim 1400$ GeV^2 (the top end of the PETRA range). All the data incorporate residual uncertainties, principally on background subtraction in νe scattering and on the use of the parton model (plus QCD corrections) for the other experiments.

The νN results will also be uncertain due to electromagnetic radiative corrections to the cross-sections, which could reduce $\sin^2\theta_W$ by ~ 0.005. It has also been recently pointed out by Glück and Reya (1981) that high twist (coherent quark) effects, which are different for NC and CC events, may change $\sin^2\theta_W$ by as much as 0.02. The very close correspondence of the $\sin^2\theta_W$ values from different experiments probably implies that the errors are somewhat overestimated, since the probability that the numbers in Fig.13 should agree so closely is <1% if one accepts the stated errors. Finally, it should be stressed that the data are, within the considerable uncertainties, in very good agreement with the prediction of the SU(5) version of grand unification, with $(\sin^2\theta_W)_{SU5} \simeq 0.21$.

3. QUANTUM CHROMODYNAMICS (QCD)

3.1 QCD IN BOUND STATES

While these lectures are mostly concerned with high q^2 processes such as deep-inelastic lepton-nucleon scattering and e^+e^- annihilation to hadrons at high energy, it should be emphasized that much of the qualitative support for QCD comes from the study of bound states of quarks (and antiquarks).

For example, the existence of the colour degree of freedom is necessitated by the value of $R = \sigma(e^+e^- \to \text{hadrons})/\sigma(e^+e^- \to \mu^+\mu^-)$ for $10 < E < 35$ GeV, shown in Fig. 14, which is compatible (within $\sim$10% errors) with the value 11/3 expected for u,d,s,c,b quarks in $N_c = 3$ colours. But the measured rate for $\pi^\circ \to 2\gamma$, via a u,d quark loop, is proportional to N_c^2 and gives the more precise estimate $N_c = 2.98 \pm 0.11$. The colour force between quarks is assumed to be carried by an octet of colour-anticolour massless vector gluons. The one-gluon exchange potential is then attractive for a colour singlet $Q\bar{Q}$ pair, and for a colour singlet combination of 3 quarks, but repulsive for all other multiquark (or antiquark) colour combinations. Further, the hyperfine mass splitting of the vector and pseudoscalar mesons, $m_\rho - m_\pi \sim 0.6$ GeV is expected to be, as is observed, approximately twice that for baryons, $m_\Delta - m_N \sim 0.3$ GeV. The narrowness of the onium bound states ψ, γ can perhaps be understood in the colour model. For example, the decay of $\psi(=c\bar{c})$ to pions involves gluon exchange between quarks in colour singlets. Thus at least 2 gluons must be involved, and, since ψ has odd C-parity (it couples to the photon), 3 gluon exchange is the simplest possibility. Denoting the quark-gluon coupling constant by α_s it is found that

$$\Gamma(\psi \to 3G) = \frac{160}{81} \frac{(\pi^2-9)\alpha_s^3}{M_\psi^2} |\chi(0)|^2 = 70 \text{ keV} \qquad (40)$$

where $\chi(0)$ is the $Q\bar{Q}$ wavefunction at the origin. The leptonic decay width is

$$\Gamma(\psi \to e^+e^-) = \frac{16\pi\alpha^2}{M_\psi^2} \cdot |\chi(0)|^2 \cdot Q_c^2 = 5 \text{ keV} \qquad (41)$$

where $Q_c = {}^2/3$ is the charge of the charmed quark. (40) and (41) together give $\alpha_s \simeq 0.2$.

The level sequence in charmonium and the upsilon system also give some information on α_s. The expected $2^3S_1 - 1^3S_1$ level separation $\Delta E \propto \mu$, the quark mass, for a ${}^1/r$ potential while $\Delta E \propto \mu^{-1/3}$ for a potential proportional to r. The values $\Delta E_\psi = (M_{\psi'}-M_\psi)c^2 = 589$ MeV and $\Delta E_\gamma = (M_{\gamma'}-M_\gamma)c^2 = 560$ MeV are indeed nearly equal. This can be achieved for a combination of Coulomb and confining terms:-

$$V = -\frac{4}{3}\frac{\alpha_s}{r} + kr \qquad (42)$$

by choice of k and α_s. In fact, $k = 0.2$ GeV^2 is set from the string model of Regge trajectories, where the Regge slope $(2\pi khc)^{-1} = 0.9$ GeV^2. One then finds $\alpha_s \simeq 0.40$, that is substantially larger than the value from the leptonic branching ratio.

The approximate chiral symmetry in nature ($m_\pi \curvearrowright 0$) also indicates a vector gluon theory. These examples show that many of the detailed properties of the bound states of mesons and baryons are qualitatively what we expect from QCD. They cannot be quantitative because quantitative calculations require the perturbative approach, with $\alpha_s << 1$. Moreover, the useful range of q^2 available from bound states is somewhat restricted. Really significant tests of QCD require a much larger dynamic range in q^2, in order to answer the crucial questions:-

(i) Does the running coupling constant α_s really run?

(ii) Is the theory non-Abelian, i.e. is there a strong gluon-gluon coupling?

It is, of course, precisely the non-Abelian nature of QCD (ii) which makes α_s decrease with q^2, as in (i). But it would be useful to see the existence of the 3-gluon vertex demonstrated directly. Qualitatively, the success of the parton model implies that α_s is small at large q^2, and the existence of bound states, that the coupling is probably large at small q^2, but one wants to see a quantitative and reliable measurement of α_s over a big range in q^2.

3.2 DEEP INELASTIC LEPTON-HADRON SCATTERING - THE PARTON MODEL

The first point to remember is that the "naive" parton model is a very good approximation. Neutrino total cross-sections are very nearly proportional to energy, over the range 2-200 GeV (see Fig. 15). This fact can easily be understood in terms of the elastic scattering of the neutrino by pointlike, quasi-free constituents. Since there are no form-factors, the cross-section (for $q^2 << M_W^2$, so that W-propagator effects can be neglected) can then depend only on the phase-space in a 2-body → 2 body collision. This goes as p^{*2} or E_ν, the square of the CMS momentum or the laboratory neutrino energy, for a stationary target.

The pointlike parton constituents scattering the neutrino can be identified with quarks. First they have spin $^1/_2$ because, from lepton scattering and e^+e^- experiments we find:-

(i) The ratio $2xF_1/F_2$ in SLAC e-d experiments (Fig. 16) measures the ratio of backward (magnetic or spin-flip) scattering, to the forward (electric or non spin-flip) scattering. Indeed

$2xF_1/F_2 = {}^{g}/_{2}$ where g is the gyromagnetic ratio of the parton. Thus $2xF_1/F_2 = 1$ for spin $^{1}/_{2}$ partons (this is the so-called Callan-Gross relation (1969) for the limit of large q^2).

(ii) The angular distribution of 2-jet events in e^+e^- annihilation at W = 25-35 GeV has a $(1+\cos^2\theta)$ distribution relative to the beam, just as in $e^+e^- \to \mu^+\mu^-$ - see Fig. 17.

(iii) In the Drell-Yan process of dilepton production in hadron-hadron collisions, interpreted as fusion of quark and antiquark from projectile and target, $Q\bar{Q} \to \gamma \to \mu^+\mu^-$, the angular distribution of the muons in the dimuon rest-frame, relative to the beam axis, is also $(1+\cos^2\theta)$ - see Fig. 18.

Early (1972) inelastic electron and neutrino scattering from nucleons also gave evidence for fractional quark charges and for gluons. Fig. 19 shows Gargamelle (PS) neutrino bubble chamber data measuring the structure function $F_2^{\nu N}(x)$, which is equal to the total fractional momentum carried by parton constituents, each carrying a fraction x of the nucleon momentum. In terms of u,d,$\bar{u}$, $\bar{d}$ quark constituents,

$$F_2^{\nu N}(x) = x\,\{u(x) + d(x) + \bar{u}(x) + \bar{d}(x)\} \qquad (43)$$

where u(x) etc. is the population of u quarks at x in the proton. For electron scattering, the corresponding structure function is $F_2^{eN}(x)$, where the contributions from the different quarks are weighted by the squares of their charges:-

$$F_2^{ep}(x) = x \{\frac{4}{9} \{u(x)+\bar{u}(x)\} + \frac{1}{9} \{d(x)+\bar{d}(x)\} \}$$

$$F_2^{en}(x) = x \{\frac{4}{9} \{d(x)+\bar{d}(x)\} + \frac{1}{9} \{u(x)+\bar{u}(x)\} \}$$

$$F_2^{eN}(x) = \frac{1}{2}(F_2^{ep}+F_2^{en}) = \frac{5}{18}x \{u(x)+d(x)+\bar{u}(x)+\bar{d}(x)\} \qquad (44)$$

where the s,c... quark content of the nucleon has been neglected. Thus we expect

$$F_2^{\nu N}(x) = \frac{18}{5}F_2^{eN}(x) \qquad (45)$$

In Fig. 19, the experimental points show the neutrino data while the curve is drawn smoothly through the SLAC electron data, for a similar range in q^2. The ratio of the two distributions clearly is compatible with the value of $^5/_{18}$, the mean square quark charge in the nucleon. If a nucleon consisted only of quarks then clearly we would expect the integral $\int F_2^{\nu N}(x)dx \simeq 1$, since it represents the total fractional momentum carried by quarks. Instead we see that it is 0.50 ± 0.05, so that half the momentum is carried by partons which are inert to the electric or weak charges of the leptons. This fraction is ascribed to the neutral gluons, the carriers of the field between the quarks, which can interact only with strong charges.

3.3 QCD AND THE RUNNING COUPLING CONSTANT α_s

We now discuss the radiative corrections, or deviations from the naive parton model, resulting from the interquark interactions, as described by QCD.

First, let us briefly recall some results from QED, on lepton magnetic moments (the (g-2) anomaly). In QED it is possible to estimate the theoretical value for the anomaly as a perturbation series in α, the fine structure constant. Thus

$$a_e=\left(\frac{g-2}{2}\right)_{\text{electron}} = 0.5\frac{\alpha}{\pi} - 0.32848\left(\frac{\alpha}{\pi}\right)^2 + 1.19\left(\frac{\alpha}{\pi}\right)^3 + \ldots = 1159652.10^{-9} \quad (46)$$

$$a_\mu=\left(\frac{g-2}{2}\right)_{\text{muon}} = 0.5\frac{\alpha}{\pi} + 0.76578\left(\frac{\alpha}{\pi}\right)^2 + 24.45\left(\frac{\alpha}{\pi}\right)^3 + \ldots = 1165852.10^{-9} \quad (47)$$

in precise agreement with experiment (after small strong-interaction effects are included in the muon case). One observes that $a_\mu > a_e$ and $m_\mu > m_e$. It is <u>as if</u> the anomaly could be accounted for by keeping the first term of the series (46) and (47) but postulating $\alpha_{eff}(\mu) > \alpha_{eff}(e)$ where α_{eff} is an effective or <u>running</u> coupling constant which depends on the masses or q^2 values involved.

In QCD the q^2 dependence of the running coupling constant is described by the β function which can be expanded in perturbation theory as:-

$$\frac{d\alpha_s}{d\ell nq} = \beta(\alpha_s) = -b_0\frac{\alpha_s^2}{2\pi} - b_1\frac{\alpha_s^3}{8\pi^2} + \ldots \quad (48)$$

Where the constants

$$b_0 = (33-2f)/3$$
$$b_1 = (306-38f)/3 \quad (49)$$

where f = number of quark flavours. Thus, provided $f \leq 16$, $b_0, b_1 > 0$ and $d\alpha_s/d\ell nq < 0$. Retaining the first term of the renormalization group equation (48), integration gives

$$\frac{1}{\alpha_s(q^2)} - \frac{1}{\alpha_s(\mu^2)} = \frac{b_0}{4\pi}\ell n\left(\frac{q^2}{\mu^2}\right)$$

or

$$\alpha_s(q^2) = \frac{\alpha_s(\mu^2)}{1+\frac{b_0}{4\pi}\alpha_s(\mu^2)\ell nq^2/\mu^2} \quad (50)$$

or

$$\alpha_s(q^2) = \frac{1}{B\ell nq^2/\Lambda^2} = \frac{12\pi}{(33-2f)\ell nq^2/\Lambda^2} \tag{51}$$

where

$$B = b_0/4\pi$$

$$\Lambda^2 = \mu^2 \exp\{-4\pi/b_0\alpha_s(\mu^2)\} \tag{52}$$

Equations (50), (51) are satisfactory provided $\alpha_s(q^2) << 1$ over the range $\mu^2 \to q^2$. This is the so-called leading log or leading order (LO) approximation. In this case, one can see from (48) that the error in α_s through neglect of the second term will be (setting f = 4):-

$$\frac{\Delta\alpha_s}{\alpha_s} \simeq \frac{b_1\alpha_s}{8\pi b_0} \sim \frac{\alpha_s}{3} \tag{53}$$

However,

$$\frac{\Delta\Lambda^2}{\Lambda^2} \simeq B \gtrsim 0.75 \tag{54}$$

Thus, if a measurement is made and interpreted according to LO theory, and the value of α_s obtained is ~ 0.1, the higher order corrections to this estimate are likely to be a few per cent only. On the contrary, if the scaling deviations are quoted in terms of Λ^2, higher order corrections are likely to change it by $\sim 100\%$, no matter at which value of q^2 it is measured. This arbitrariness in Λ just arises from the fact that it depends exponentially on α_s, and relatively small errors in α_s are very big in Λ.

The q^2 dependence of α_s is determined by the sign of b_0 in (49). In QED (as distinct from QCD), β is negative and in (50), $b_0\alpha_s/4\pi$ is replaced by $-\alpha/3\pi$. This corresponds to the fact that in QED, the virtual fermion pairs produce a polarization of the vacuum leading to a decrease in the effective charge, or shielding at small q or large distance as in Fig. 20(a). In QCD, there are, in addition to the fermion loop shielding effects, gluon pair diagrams as in Fig. 20(b), in which one of the gluons is longitudinal and leads to an antishielding effect (the gluon-gluon

interaction effectively "spreads out" the distribution of the strong charge), leading to a decrease in α_s at large q and small distance (Fig. 20(c)).

This is the vital difference between QED and QCD. QED is Abelian, that is the carrier (the photon) does not carry electric charge and thus there is no photon-photon coupling (in leading order). QCD is non-Abelian, the gluon carriers do carry a colour charge and therefore there is a strong gluon-gluon interaction, which results in the phenomenon of asymptotic freedom ($\alpha_s \to 0$ as $q^2 \to \infty$) and explains the success of the parton model.

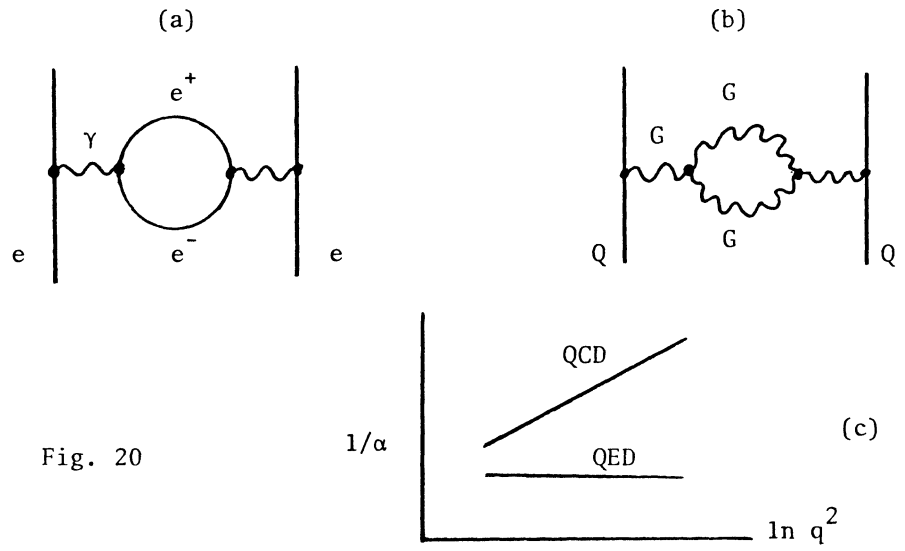

Fig. 20

There are several very crucial questions which we would expect experiments to answer about QCD. For example:-

- Does α_s actually run with q^2?
- Is the quark-gluon theory believable, for example can one obtain direct evidence for gluon radiation by quarks (as distinct from indirect evidence, for example the fact that charged parton constituents only carry half the nucleon momentum), and for the gluon-gluon self coupling?
- Can one establish the "existence" of gluons as constituents, for example producing jets of hadrons which are distinct from those

apparently produced by quarks? Can one perhaps determine the gluon quantum numbers?

3.4 SCALING DEVIATIONS IN DEEP INELASTIC SCATTERING

Clear evidence for a QCD-type behaviour of the deep inelastic structure functions has been found in numerous experiments on electron, muon and neutrino scattering showing that such functions are indeed q^2-dependent. In general, the deviations from the "naive parton model", which has no q^2 dependence, are small and quite hard to measure. Figs. 21-23 show recent results for the nucleon structure functions measured in neutrino and muon scattering experiments. There are clear deviations, especially at large x and very small x. The difficult task is to quantify these deviations in a systematic way and compare the measurements with QCD predictions.

The q^2 dependent effects expected in structure functions (or, equivalently, quark distribution functions) can be best illustrated from the Altarelli-Parisi developmental equation. The q^2 dependence of the quark distribution is obtained in a self-evident way from the diagram of Fig. 24.

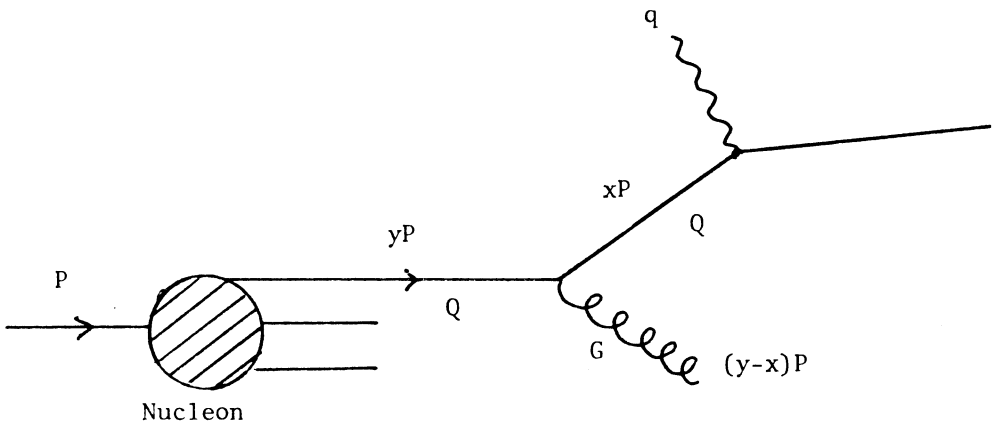

Figure 24

First, we consider the valence (or non-singlet flavour) quark distribution. Thus $(Q_u - Q_d)$, $(Q_u - Q_{\bar{u}})$ are non-singlets, because the sea-quarks - which

originate from gluon → $Q\bar{Q}$ - are then excluded. $(Q_u - Q_d)$ can be obtained from the difference of cross-sections for electrons or muons on neutrons and protons, while $(Q_u - Q_{\bar{u}})$ is obtained from the difference of neutrino and antineutrino cross-sections on nucleons. In this simplest situation, we obtain

$$\frac{q^2 dQ_{NS}(x,q^2)dx}{dq^2} = \frac{\alpha_s(q^2)dx}{2\pi} \int_{y=x}^{y=1} P_{QQ}(\frac{x}{y}) Q_{NS}(y,q^2) \frac{dy}{y} \qquad (55)$$

On the LHS, there is no scale given, hence only the fractional change in q^2 can be involved. The change dQ_{NS} in the quark distribution, as one increases q^2, results from gluon bremsstrahlung, with probability α_s. The contribution to the quark density at x will come from quarks $Q_{NS}(y,q^2)dy$ with nucleon momentum fraction $y \to y + dy$, where $1 > y > x$, weighted by the splitting function $P_{QQ}(z)$ for finding a quark in a quark with energy fraction $z = x/y$, and the whole integrated over y. Upon writing

$$P_{QQ}(z)dz = P_{QQ}(x/y)dx/y$$

the result (55) follows. The actual formula for P_{QQ} is that for the radiation process fermion → fermion + boson and is given by the Weizsacker-Williams formula, with the colour factor already seen in (42):-

$$P_{QQ}(z) = \frac{4}{3} \frac{(1+z^2)}{(1-z)}$$

This has a singularity at z = 1. But the total probability of finding a quark in a quark is unity, which implies, in the way in which it is defined, that the integral over $P_{QQ}(z)$ is zero. We can achieve this by writing

$$P_{QQ}(z) = \frac{4}{3} \{\frac{1+z^2}{1-z} - \delta(1-z) \int_0^1 \frac{1+y^2}{1-y} dy\} \qquad (56)$$

so that

$$\int_0^1 P_{QQ}(z)dz = 0 \qquad (57)$$

3.5 DIRECT DETERMINATION OF α_s

From (55) and (56) it is easy to find α_s from the non-singlet functions by numerical integration of the expression (at fixed q^2), for $F_{NS}(x,q^2) = xQ_{NS}(x,q^2)$:-

$$\frac{dF_{NS}(x,q^2)}{d\ell nq^2} = \frac{\alpha_s}{2\pi}\cdot\frac{4}{3}\left\{\int_{z=x}^{z=1}\left[\frac{(1+z^2)F_{NS}(x/z)-2F_{NS}(x)}{(1-z)}\right]dz + \{\frac{3}{2} + 2\ell n(1-x)\}\,F_{NS}(x)\right\} \quad (58)$$

where all the F's are defined at a single value of q^2. There are some difficulties. Firstly, the most precise lepton scattering experiments at high q^2 have data extending only to $y = x/z = 0.7$, so that the contributions from larger y have to be estimated (e.g. by parameterising in the form $(1-y)^3$). This turns out not to be a serious source of error, as most of the contribution to the integral depends on y not much larger than x. Secondly, most of the experiments measure $F_2(x)$, not $F_{NS}(x)$, that is, they do not separate the non-singlet. In some cases (the CDHS experiment) the non-singlet function xF_3 is actually determined but for some inexplicable reason they still use the function F_2. This means that one has to stay in the region of largish x (>0.3), otherwise the sea-quark contribution will affect the q^2-dependence. So, all the useful, accurate data, from the CDHS neutrino, and the NA2 and NA4 muon experiments, is confined between $x = 0.3$-0.7. The range of q^2 is more extensive, from $q^2 \curvearrowleft 10$ GeV^2 to $q^2 \curvearrowleft 150$ GeV^2.

From the data published already, or given in preliminary graphical form at conferences, I have estimated values for α_s, with the results shown in Fig. 25. The main error on α_s comes from the smallness of the q^2 dependence and the consequently large error in evaluating the LHS of (58). Using starting values of $x = 0.35$ or 0.45, values of $\alpha_s \curvearrowleft 0.2$ are obtained for

some average q^2. Actually, it is only in leading order that α_s is a function of q^2. When higher order effects are considered, it turns out that α_s becomes effectively a function of $w^2 \simeq q^2(1-z)/z$. w^2 varies over the integration region of (58), and a weighted average is therefore taken (typically $w^2 \simeq (0.4\text{-}0.6)q^2$ depending on the value of x). So in Fig. 25, α_s is plotted as a function of w^2. We repeat that it is already corrected for most of the second order effects, and values of Λ should be compared with second-order values obtained in other analyses, to be described below.

The results given for α_s are likely to be slight overestimates, because of (a) kinematic target (nucleon) mass effects which introduce an extra dependence. Since $w^2 >> M^2$ for most of the data, this effect should be small; (b) higher twist terms also contribute; these are discussed below.

The main result is that $\alpha_s \simeq 0.2$ in the region of $w^2 \curvearrowright 5\text{-}40$ GeV^2, corresponding to $\Lambda \simeq 0.15 \pm .05$ GeV. It is important to emphasize that the method is independent of arbitrary parameterizations or mathematical tricks, as employed in other methods to be discussed later.

3.6 MOMENT METHOD

If both sides of (55) are multiplied by x^{N-1} (where N is any integer ≥ 2), they can be integrated from $x = 0 \rightarrow 1$. Upon changing the order of x and y integrations, the RHS factorizes into two integrals from $0 \rightarrow 1$ in y and z. One obtains

$$\frac{d}{d\ell nq^2} M_{NS}(N,q^2) = \frac{\alpha_s(q^2)}{2\pi} A_N M_{NS}(N,q^2) \tag{59}$$

where

$$M_{NS}(N,q^2) = \int_0^1 x^{N-1} Q_{NS}(x,q^2)dx \tag{60}$$

$$A_N = \int_0^1 z^{N-1} P_{QQ}(z)dz \tag{61}$$

so

$$\ell n M_{NS} = \frac{A_N}{2\pi B} \ell n(\ell n q^2/\Lambda^2) + C$$

$$M_{NS} = \frac{C_N}{\ell n q^2/\Lambda^2 \; {}^{d_{NS}}} \tag{62}$$

where B is defined under (51), C_N is a constant for fixed N and

$$d_{NS} = -\frac{A_N}{2\pi B} = -\frac{6A_N}{(33-2f)} = \frac{4}{(33-2f)} \quad 1 - \frac{2}{N(N+1)} + 4\sum_{2}^{N} \frac{1}{j} \tag{63}$$

The prediction (62) is <u>beautifully simple</u>. It is that the (N-1)th moment (60) of the quark distribution varies as an inverse, known, power d_{NS} of $\ell n q^2/\Lambda^2$. d_{NS} is called the anomalous dimension. There are, again, snags of an experimental nature in employing this method. First, since an integral from $x = 0 \to 1$ is involved, one <u>has</u> to separate the non-singlet piece of the quark distribution, that is $(Q_i - Q_j)$, where $i \neq j$. For example in neutrino and antineutrino experiments on nucleon targets, $F_3 = (u+d-\bar{u}-\bar{d})$ is a non-singlet $(Q-\bar{Q})$ obtained from the difference between $d\sigma/dx$ for neutrinos and antineutrinos. This was done in the BEBC and Gargamelle bubble chamber experiments at CERN. In electron/muon scattering experiments, the difference $F_1^{\mu p} - F_1^{\mu n}$, obtained from proton and neutron targets, is a non-singlet (proportinal to u-d), and such moments were measured in the E98 (FNAL muon) and SLAC/MIT (electron) experiments. The CDHS group also combined their F_3 data at high x with the SLAC/MIT data, using the approximate 18/5 ratio (44) for relative normalization.

Secondly, it is difficult to measure complete moments at small N or large N. The maximum beam energy E_o implies $x_{min} = q^2/2ME_o > 0$ and especially so at large q^2. Furthermore, since F(x) falls rapidly at large x (as $\simeq(1-x)^3$), experimental energy resolution becomes a dominant factor, since events at smaller x are smeared to larger (and smaller) x, and corrections are required. In principal, this is no problem if one knows accurately the resolution in hadron energy ν (where $x = q^2/2M\nu$). However,

high N momenta may in principle involve large systematic errors.

Setting these problems to one side, we now discuss the results. First, there is a technical detail: the moments actually calculated are so-called Nachtmann moments, which involve a modification to the x variable in (60), to take account of the target (nucleon) mass correction, of purely kinematic origin, the effect of which can be and has been calculated exactly. To compare experiment with prediction, one first observes that (62) predicts power-law relations between the moments of different N:-

$$\ell n\, M_{NS}(N_1,q^2) = -d_1 \ell n(\ell n q^2/\Lambda^2) + \ell n\, A_1$$
$$\ell n\, M_{NS}(N_2,q^2) = -d_2 \ell n(\ell n q^2/\Lambda^2) + \ell n\, A_2$$

so

$$\frac{d\ell n M_1}{d\ell n M_2} = \frac{d_1}{d_2} \qquad (64)$$

Thus, a plot of moment N_1 against moment N_2 on a log-log scale, for the various values of q^2, should give a straight line of slope d_1/d_2. Fig. 26 shows some results. The plots are indeed linear, and the slopes are consistent with the QCD predicted ratios d_1/d_2 - equal to the ratios of the square-bracket in (63). More details are given in Table 4. The first columns give the QCD predictions (QCDI refers to the leading order ratio from (63), QCDII to small modifications from second-order corrections). The column headed "scalar gluon" is computed from (63) with the last term in the square bracket - characteristic of vector gluons - omitted. The results appear to be in favour of vector gluons, and indeed, these moment slopes are one of the important tests of QCD, since the theoretical value is predicted unambiguously. One can only regret that the most recent lepton scattering experiments (NA2 and NA4 at CERN) have been designed in such a way that it seems impossible to obtain complete (or nearly complete) moments.

TABLE 4

NON-SINGLET NACHTMANN MOMENTS: LOG MOMENT RATIO SLOPES

N_1, N_2	ABCLOS (Bosetti et al 1978)	CH1O (Anderson et al 1978)	CDHSI (de Groot et al 1979)	CDHSII (Wahl 1981)	QCD I	QCD II	Scalar Gluon
	q^2 = 1-60	q^2 = 2-25	q^2 = 5-10	q^2 = 5-10			
3 , 4	-	-	-	1.38 ± .06	1.26	1.32	1.08
4 , 5	-	-	-	1.20 ± .03	1.16	1.20	1.04
3 , 5	1.50 ± .08	1.80 ± 0.25	1.34 ± .12	1.68 ± .11	1.46	1.57	1.12
4 , 6	1.29 ± .06	1.45 ± 0.10	1.18 ± .09	-	1.29	1.36	1.06
3 , 7	1.84 ± .20	-	-	-	1.76	1.94	1.16

Notes: The different ratios from a given experiment are not independent.

QCDII includes higher-order (α_s^2) corrections.

The experiments quoted in Table 4 naturally gave fits to Λ via (62), the values obtained being Λ = 0.70 GeV for BEBC/Gargamelle (Bosetti et al, 1978) and for CHIO (Anderson et al, 1978) and $\Lambda \simeq 0.35$ for CDHSI (de Groot et al, 1979); a re-analysis with more data, CDHSII, gave $\Lambda = 0.3 \pm 0.1$ (Wahl, 1981). The first two experiments consisted of data heavily weighted to low q^2, with an effective mean value of order 4-5 GeV^2. However, these values of Λ are clearly in disagreement with those obtained from Fig. 25 - but they are at lower q^2.

Higher-order corrections can be considered to the leading-order (LO) expressions for the non-singlet moments. Considering the next to leading order (NLO), that is the second term in (48), one obtains instead of (51) and (52):-

$$\alpha_s(q^2)_{NLO} = \frac{4\pi}{b_0 \ell n q^2/\Lambda^2_{MS}} - \frac{4\pi b_1}{b_0^3} \frac{\ell n(\ell n q^2/\Lambda^2_{MS})}{\ell n^2(q^2/\Lambda^2_{MS})} + \ldots \qquad (65)$$

where

$$\Lambda^2_{MS} = \mu^2 \exp\{-\frac{4\pi}{b_0 \alpha_s(\mu^2)} - \frac{b_1}{b_0^2} \ell n \left[4\pi b_0 \alpha_s(\mu^2)\right]\} \qquad (66)$$

This procedure is for a particular renormalization scheme, the so-called minimal subtraction scheme, in which there are no further terms in (65) in $(\ell n q^2/\Lambda^2)^{-2}$. The value of Λ in (66) in this scheme is denoted Λ_{MS}. The effect on the NS moment (62) is to introduce a further factor:-

$$M_{NS}(N,q^2) \to \frac{C_N}{(\ell n q^2/\Lambda^2_{MS})^{d_{NS}}} \left[1 + \frac{f_N + g_N \ell n(\ell n q^2/\Lambda^2_{MS})}{\ell n q^2/\Lambda^2_{MS}}\right] \qquad (67)$$

where f_N and g_N are numerical constants.

It is found experimentally that (67) and (62) give <u>equally good fits</u> to the moment data; the only effect of the NLO corrections is to change Λ: typically $\Lambda_{MS} \simeq 0.6\Lambda_{LO}$. All this is in line with what we said before, that

Λ is a lousy parameter to specify the strong-interaction scale.

We should perhaps emphasize here what the moment analysis does NOT test. Non-singlet functions specifically exclude the gluon-gluon interaction and thus the non-Abelian character of the theory. To get at that, one has to include the singlet structure functions as well. In principle, given the singlet function (i.e. F_2) and the non-singlet (F_3), the difference measures the quark sea contribution and hence, the gluon distribution. There is a snag, of course. Increasing the Λ value would make the valence quark contribution to F_2 fall off more steeply with increasing q^2, but this fall-off can be compensated by pumping in more gluons and hence $Q\bar{Q}$ pairs which will boost F_2. Thus one can trade off changes in Λ by changes in the gluon contribution for a given q^2 dependence of F_2. F_{NS} in principal fixes Λ and the q^2-dependence of the $Q\bar{Q}$ sea in principal fixes the gluons. But in practice, it is very difficult to get unambiguous numbers on the gluons (apart from their N = 2 moment, known since 1972 from momentum conservation).

3.7 DIRECT FITS TO STRUCTURE FUNCTIONS

The Λ values usually quoted today are obtained from the most recent and hopefully most accurate experiments - namely the CDHS neutrino experiment (Eisele 1980, Wahl 1981), the NA2 muon experiment (EMC, Aubert et al, 1980) and the NA4 muon experiment (Bollini et al, 1981). These experiments do not generally separate non-singlet functions. The approach is to parameterize the quark distributions empirically, as suggested by Buras and Gaemers (1978). For the valence quarks (which dominate for $x > 0.25$) the fits are of the form

$$xF_3(x,q^2) = \text{const.}x^{\alpha}(1-x)^{\beta} \qquad (68)$$

where $\alpha \sim 0.5$, $\beta \sim 3$.* Choosing a particular value of $q^2 = q_o^2$, α and β are first determined. Next, as q^2 varies, the variation of α and β, of the form $A + B\ell n\ (\ell nq^2/\Lambda^2/\ell nq_o^2/\Lambda^2)$ where A and B are constants, is found, and in this way, Λ can be obtained from the best fit of the constants. A similar method can be used for F_2, over a wider x range, by suitable parameterization of the gluon distribution. From the neutrino data, the distribution of the sea quarks is first found from the neutrino and antineutrino cross-sections, since, neglecting s and c quarks,

$$\frac{d\sigma^{\nu N}}{dxdy} = \frac{G^2ME}{\pi}\, x\, \{(u+d) + (1-y)^2(\bar{u}+\bar{d})\}$$

$$\frac{d\sigma^{\bar{\nu}N}}{dxdy} = \frac{G^2ME}{\pi}\, x\, \{(\bar{u}+\bar{d}) + (1-y)^2(u+d)\} \qquad (69)$$

with the results shown in Fig. 27. Typically, the valence quarks can be described at $q_o^2 \sim 5\ GeV^2$ by

$$2x(u+d-\bar{u}-\bar{d}) = xF_3(x) = const.x^{0.5}(1-x)^3 \qquad (70a)$$

and the sea quarks by

$$x(\bar{u}+\bar{d}) = const.(1-x)^{10} \qquad (70b)$$

Assuming the gluon distribution to be of similar form, the fits give

$$xG(x) = const.(1-x)^5 \qquad (70c)$$

For the parameterization (68), Buras and Gaemers checked that the calculated non-singlet moments did behave (almost) logarithmically with q^2,

---

* The constant in (68) is fixed by the requirement $\int_0^1 F_3 dx = 3$ (Gross/Llewellyn-Smith sumrule).

as required by QCD, over a fair range in q^2 ($q^2 = q_o^2$ to $q^2 = 10^4 q_o^2$). Most of the recent fits are concerned with F_2 in the region $x > 0.25$, so that a knowledge of the sea and gluon distributions is unnecessary, provided the sea makes no contribution to F_2 in this region. Values obtained are shown in Table 5, which includes the results from moment fits.

A great deal of discussion has appeared in the literature about the pros and cons of fitting structure functions, or moments of structure functions or using some other method. All methods must use the Altarelli-Parisi equation (55) as a starting point and thus necessarily have to use data from $x = x$ to $x = 1$ in order to extract α_s or Λ. If good data is not available near $x = 1$, it has to be guessed and the results must be correspondingly doubtful. Obviously, moments of high N will emphasize large x and be very unreliable if the data there is suspect. The main problem with moments is practical in nature - namely that the experimentalists do not measure accurately enough the energy resolution function in order to "unsmear" the data at large x, or are unable to isolate the non-singlet part of the structure function. One cannot remedy this experimental failure by fancy mathematics, use of inverse Mellin transforms etc., which make it appear as if only data over a limited x range is needed. Somewhere, hidden assumptions have been made about the behaviour of the structure functions in x regions where they have not been measured.

Using the Buras-Gaemers method, one parameterizes the valence-quark, sea-quark and gluon x distributions, and their q^2 dependence, in an ad-hoc way. These parameters are chosen to satisfy the QCD developmental equations (over a restricted q^2 range) but there are clearly many choices possible. We have already noted that changes in the gluon shape can be compensated by changes in Λ. The advantage of this approach is that it can be used when data are available only over a limited range of x, and the weakness is that Λ is only one of the fitted parameters, and necessarily depends to some degree on the assumed shape parameters of the quark and gluon distributions.

TABLE 5

VALUES OF Λ FROM VARIOUS ANALYSES

Experiment		q^2	Λ_{LO}	Method
νN BEBC/GGM	1978	1-60	$0.74 \pm .05$	xF_3 moments
μN / eN CH1O/SLAC	1979	3-40	$0.64 \pm .15$	$(F_2^p - F_2^n)$ moments
νN / eN CDHS/SLAC	1979	5-100	$0.35 \pm .20$	$(xF_3 + F_2)$ moments
νN CDHS	1979	5-100	$0.50 \pm .20$	xF_3, F_2 BG
νN CDHS	1981	2-200	$0.20^{+.15}_{-.10}$	xF_3, F_2 BG
νN GGM	1981	2-50	$0.26 \pm .16$	xF_3+F_2 BG
νN CHARM	1981	3-180	$0.29 \pm .16$	xF_3+F_2 BG
μFe EMC	1980	5-200	$0.13^{+.11}_{-.08}$	$F_2(x>0.2)$ BG
μH EMC	1981	5-200	$0.10^{+.14}_{-.08}$	$F_2(x>0.2)$ BG
μC BCDMS	1981	25-200	$0.01^{+.04}_{-.01}$	$F_2(x>0.3)$ BG
eN SLAC	1980	1-20	0.25-0.70	F_2, $F_2^p - F_2^n$ BG + HT
νN, μN		10-100	$\alpha_s \simeq 0.2$	
			$\Lambda_{MS} \sim 0.15 \pm .05$	AP $x>0.3$

3.8 HIGHER-ORDER CORRECTIONS

Higher order corrections have been discussed ad nauseam in the literature. As stated in the discussion of the moment analysis (see Equns. (65)-(67)), the main effect is to change the fitted value of Λ. There have been claims from time to time that second-order corrections lead to better fits, but in view of the large variations in Λ_{LO} found in different experiments, these can hardly be taken seriously. The magnitude of the α_s^2 corrections depends on the renormalization scheme employed - that is, whether one chooses to try to minimize even higher order (α_s^3...) terms, include all possible terms of order α_s^2, etc. It is arbitrary because no-one has computed corrections to the higher orders (that is the $(\ell n)^{-3}$, $(\ell n)^{-4}$-terms). We do not discuss these matters since the experimental situation does not need it or warrant it, at the present time.

3.9 HIGH TWIST EFFECTS

The "enfants terrible" of the testing of QCD via nucleon structure functions are the high twist terms. Implicit in our analysis thus far, has been the assumption that we are dealing with the strong radiative corrections to one quark, that which absorbs the current. But, of course, the nucleon contains other quarks, which interact with the struck quark via gluon exchange, and this "cross-talk" leads to additional terms proportional to $1/q^2$, $1/q^4$ etc. Thus, a possible form for the structure function would be

$$F(x,q^2) = F(x,q^2)_{QCD}\left(1 + \frac{m_1^2}{q^2(1-x)} + \frac{m_2^4}{q^4(1-x)^2\ldots} + \ldots\right) \qquad (71)$$

and for the moments would be

$$M_{NS}(N,q^2) = M_{NS}(n,q^2)_{QCD}\left(1 + \frac{Na_1^2}{q^2} + \frac{N^2a_2^4}{q^4} + \ldots\right) \qquad (72)$$

In these empirical expressions, the $1/(1-x)$ dependence in (71) and N dependence in (72) are justified because high twist effects must dominate as $x \to 1$. (For example, in the elastic scattering process, $x = 1$, and the three quarks must recoil coherently and thus the q^2 dependence is dominantly $1/q^4$.) Other forms, for example replacing N/q^2 or $N\ell n^2 N/q^2$ are also possible. The coefficients m_1, $m_2 \ldots a_1$, $a_2 \ldots$ in (71) and (72) are arbitrary, but may be expected to be of the order of the typical intrinsic transverse momentum of a quark in a hadron.

The existence of high twist effects can be illustrated from the values of the quantity $R = \sigma_S/\sigma_T$, meaning the ratio of absorption cross-sections of scalar (helicity 0) to transverse (helicity = 1) mediating bosons (photons in the electromagnetic case, $W^{\pm}$'s in the weak scattering case). In the naive parton model, the transverse momentum of a quark is neglected and in the reference frame where the parton momentum is reversed upon absorption of the current $W^{\pm}$ - the so-called Breit frame - only the $H = \pm 1$ helicity components contribute, that is $\sigma_S = 0$ - see Fig. 28(a). If however

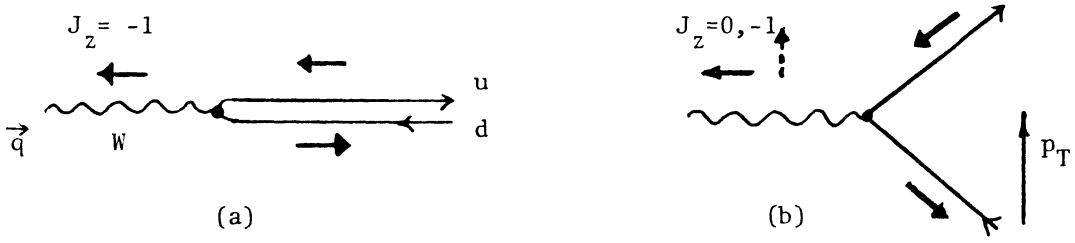

Heavy arrows denote spin projections

Fig. 28

the parton has a transverse momentum p_T relative to $\vec{q}$, both H = 0 and -1 components are involved and the ratio

$$R = \frac{\sigma_S}{\sigma_T} \simeq \frac{4\langle p_T^2 \rangle}{q^2} \qquad (73)$$

The quantity p_T of the quark-parton can arise from the (non-perturbative) "primordial" transverse momentum K_T of the quark in the nucleon; or, perturbatively, by radiation by the quark of a hard gluon at large angle, as discussed later. In the latter case, $(p_T^2)_{QCD} \sim q^2(\frac{1}{x} - 1)$ and the expression for R takes the form

$$R = \frac{\sigma_S}{\sigma_T} = \frac{4<p_T^2>}{q^2} = \frac{4}{q^2}\{<K_T^2> + \alpha_s.q^2(\frac{1}{x} - 1)\} \qquad (74)$$

where $<k_T^2>$ is expected to have only a weak x dependence.

Fig. 29 shows recent CDHS data (Wahl, 1981) on R as a function of x at fixed q^2. R shows no x dependence and one can conclude that high twist (k_T) contributions are present and dominant at large x. At the present time, it is fair to say that all the experimental data on R has very large errors, but it is clear that perturbative effects alone cannot account for the results.

Assuming the validity of perturbative QCD at large q^2, it is clear also that the rather large values of Λ obtained in the analyses of moments at low q^2 - the first three entries in Table 5 - when compared with the lower values from the data at higher q^2, can be accounted for in terms of high twist effects.

How can we quantify this statement? First it has to be pointed out that any one set of data can be equally well fitted by either a $1/q^2$ (non-perturbative) in $1/\ell nq^2$ (perturbative) dependence. This is illustrated in Fig. 30, showing the q^2-dependence of one of the non-singlet moments of the CHIO/SLAC eN and μN data. Obviously a combination of HT and P contributions also gives good fits, and Fig. 31 shows the relation between b and Λ for the fits of the data to the form

$$M_{NS}(N,q^2) = \frac{\text{const}}{(\ell nq^2/\Lambda^2)^{d_{NS}}}\left(1 + \frac{b(N-1.5)}{q^2}\right) \qquad (75)$$

All the fits on the b, Λ curve are equally good. Clearly, if one adopts a Λ value $\sim$0.1 GeV from the high q^2 data, that in Fig. 31 implies b $\sim$ 1.0 GeV^2.

In most of the experimental analyses, limits n high twist contributions have been set, by assuming them to be of the form

$$F(x,q^2) = F(x,q^2)_{QCD}\left(1 + \frac{\mu^2}{q^2(1-x)}\right) \qquad (76)$$

The upper limits on the values of μ^2 are $\sim$0.1 GeV^2 from the high q^2 data (the lower entries in Table 5) and $\sim$1.0 GeV^2 from the low q^2 data (BEBC/GGM, CHO/SLAC). If Λ is very small, and the scaling deviations are attributed mostly to high twist effects, it therefore appears necessary to postulate $1/q^4$ as well as $1/q^2$ terms in the low q^2 data.

Statements have sometimes been made to the effect that, in some analyses, high twist effects and the non-perturbative, QCD, dependence can be separated. In general this cannot be true. What is meant is that HT effects can be distinguished <u>if</u> they have a certain assumed form, e.g. involve a factor $1 + \mu^2/q^2(1-x)$ in the structure function, or a factor $1 + m^2N/q^2$ in the moment. But very many other forms, involving slightly different x or N dependences are possible and cannot be excluded. It is also clear that a combination of $1/q^2$ and $1/q^4$ terms can always mimic a logarithmic dependence over a substantial range in q^2. Fig. 32 shows, by way of illustration, the q^2 dependence of the two terms in (75) for the N = 3 and 7 moments. The differences over the range q^2 = 2-100 GeV^2 are only a few per cent. Only at very large q^2 (>10^3 GeV) are the two types of q^2 dependence easily differentiated.

The existence of high twist terms appears to be an inevitable consequence of the use of nucleon (i.e. multi-quark) targets, but it is

possible that their effects might be minimized by analyzing data at small x or with small N. An example of a situation where this might be true is the N = 1 moment of xF_3 where the main contribution comes from the small x region. The moment is given by the Gross-Llewellyn-Smith sumrule

$$\int_0^1 F_3 dx = 3(1 - \frac{\alpha_s}{\pi} + \ldots) \qquad (77)$$

Fig. 33 shows unpublished data on this integral from the BEBC/GGM experiments (ABCLOS collaboration). Very little q^2 dependence is observed, even at very low q^2, and this is consistent with a small Λ value. This demonstrates the fact that it is possible to find small Λ values from suitable moments at low q^2. Indeed I heard recently fron Jaffel (MIT) that twist 4 ($^1/q^2$) contributions to the GLS sumrule vanish identically.

3.10 NON-ABELIAN NATURE OF QCD

A crucial feature of QCD, distinguishing it from QED, is the non-Abelian nature of the coupling, that is the existence of gluon self interaction, G → G + G. As pointed out by Glück and Reya (1979) the q^2 dependence of the N = 2 moment of $F_2(x,q^2)$ provides such a test. An asymptotically free non-Abelian gauge theory predicts that the moment should decrease monotonically with q^2. For a non-asymptotically free theory with a fixed point (coupling α_s tending to a constant value as $q^2 \to \infty$), the integral is expected to <u>increase</u>. So, superficially, the data (Fig. 34) support QCD, since there is a small decrease, and certainly no large increase, of the integral with q^2. Of course, such a conclusion must again be qualified by reservations about high twist terms which may mimic the q^2 dependence of the perturbative QCD. For N = 2 moments, we <u>expect</u> high twist effects to be small. An explicit calculation by Jaffe at MIT (private communication) using the bag model gives for the N = 2 high twist

modification

$$M_{NS}(N = 2,q^2) = M_{NS}(N = 2,q^2)_{QCD} + \Delta^2_{NS}/q^2$$

where $\Delta_{NS} \sim 70$ MeV. The corrections to Fig. 34 to account for twist 4 effects are, in this case, quite negligible. If so, this demonstrates for the first time the asymptotically-free nature of QCD.

3.11 SUMMARY

Let me try to summarize the situation on scaling deviations in deep inelastic lepton-nucleon scattering. Scaling deviations are observed in all experiments, with a pattern qualitatively consistent with QCD (decrease of $F_2(q^2,x)$ with increasing q^2 for $x > 0.3$, increase of $F_2(q^2,x)$ with q^2 for $x < 0.2$). For analyses in the q^2 region 10-150 GeV^2, the deviations from the parton model are small, corresponding to derived values of the QCD parameters $\alpha_s \sim 0.2$ and $\Lambda_{LO} \sim 0.1$-.2 GeV. The x dependence of $R = \sigma_s/\sigma_T$ and the stronger q^2 dependence of the structure functions and moments at lower q^2 and large x indicate the importance of additional non-perturbative, high twist terms ($\sim 1/q^2$, $1/q^4$...). Their importance seems to be much less at small x, or for moments of low N (for example, in the Gross-Llewellyn-Smith sumrule for F_3).

Quantitative verification of QCD by such experiments seems to be difficult and is probably some years away. In particular, the crucial features of the model - the dependence of the coupling constant α_s on q^2 and the existence of the gluon-gluon coupling - have not yet been convincingly demonstrated experimentally.

4. TESTING QCD FROM FINAL STATE HADRONS IN LEPTOPRODUCTION

QCD makes predictions about the q^2 dependence of the momentum distributions of hadrons produced in leptoproduction.

4.1 THE LONGITUDINAL MOMENTUM DISTRIBUTIONS (FRAGMENTATION FUNCTIONS)

From Fig.24 it is apparent that QCD will make predictions about the momentum distributions of quarks and gluons produced in lepto-quark collisions, and thus of the secondary hadrons into which the quarks/gluons fragment. The development with q^2 of the longitudinal momentum distributions of the hadrons are governed, like that of the structure functions, by the Altarelli-Parisi equations. This is intuitively obvious: the hadronic fragments depend on the respective quantum numbers of the quarks or gluons from which they originate, and the change of the momentum distributions of the various hadrons reflects the change with q^2 of the quark and gluon populations in the target. As in the case of structure functions, the absolute values of the fragmentation functions depend on non-perturbative processes and have to be determined empirically, and perturbative QCD only makes predictions about the fractional change in the fragmentation functions with q^2.

The fragmentation functions are denoted $D^h_{Q_i}(z,q^2)$ for the fragmentation of a quark of type Q_i to a hadron of type h, carrying a fraction z of the quark energy. Several definitions of z are possible. The usual one is

$$z = \frac{P.h}{P.q} = \frac{ME_h}{M\nu} = \frac{E_h}{\Sigma E_h} \tag{78}$$

where h, P, q are the 4-momenta of the hadron, the nucleon target and the current, E_h is the energy of the hadron and ΣE_h the total energy of all hadrons, measured in the laboratory system. One can also evaluate $z = E_h/\Sigma E_h$ in other systems; for example in the CMS

$$z(CMS) = \frac{2E_h(CMS)}{W} \tag{79}$$

There are sum rules from energy momentum conservation. Thus $\sum_h \int_0^1 z\,D(z)\,dz = 1$. Empirically,

it is observed that the CMS definition (79) tends to give more consistent results. The situation is also complicated by experimental deficiencies. First, not all hadrons are detected (e.g. K_L^o are lost) so in an individual event, a correction to the total hadron energy is required. This is the case in neutrino experiments in bubble chambers where the incident neutrino energy is not known, and the same overall correction factor is applied to all events (the factor being determined from experiments with 100 GeV hadron (π^-, K^-) beams). Thus z is (over) underestimated, depending on whether, in an individual event, the energy correction was too (small) big. Second, the momentum of a secondary is measured, and the energy estimate depends on the particle mass. In general, positives of $p > 2$ GeV/c are not identified and could be protons or pions (or kaons). The pion hypothesis is adopted in these cases. All these deficiencies can be taken into account via Monte Carlo programs in comparing with theory, but it is important to be aware of them.

Any particular hadron can come from a quark, antiquark or gluon, i.e. $D^h = D_Q^h + D_{\bar{Q}}^h + D_G^h$. Suppose the current q has been absorbed by a quark of type 'i'. If we take the difference between D^h values for quarks 'i' and 'j', the sea and gluon distributions will drop out and we have a non-singlet fragmentation function

$$D_{NS}(z) = D_i^h(z) - D_j^h(z) \tag{80}$$

For example, for positive hadrons

$$\begin{aligned} D_{NS}(z) &= D_u^+(z) - D_{\bar{u}}^+(z) \\ &= D_u^+(z) - D_u^-(z) \end{aligned} \tag{81}$$

where the last step follows from C-conjugation invariance. In neutrino reactions, one deals with the transitions

$$\begin{aligned} \nu + d &\to u + \mu^- \\ \nu + \bar{u} &\to \bar{d} + \mu^- \end{aligned} \tag{82}$$

so that, if we neglect the small (5%) sea contribution of antiquarks present in the nucleon, we are dealing with u-quark fragmentation and (81) is the non-singlet combination effectively measured. Then from the non-singlet moment relations written down before, the perturbative QCD prediction is

$$M_{NS}(N,q^2) = \int_0^1 z^{N-1} D_{NS}(z,q^2)\,dz = \frac{\text{const}}{(\ln q^2/\Lambda^2)^{d_{NS}}} \tag{83}$$

We note yet another problem here: the moments involve integrals from $z = 0 \to 1$ but they are supposed to refer to hadrons from the struck quark only. Some of the low energy hadrons come from the spectators (diquark). Provided we take $N \geq 3$ these make very little contribution. An alternative procedure is to evaluate the moment for $z = z(\text{CMS})$ in (79) and take only hadrons travelling forward ($x_F > 0$). The two methods give very similar results.

Fig.35 shows results for the q^2 dependence of the non-singlet moments (83) from the BEBC experiments at CERN (Blietschau et al 1979). The errors are very large but the q^2 dependence is clearly consistent with the prediction (for $\Lambda \sim 0.5$ GeV). Fig.36 shows the moment-moment plots, again in good agreement with QCD, just as in Fig.26. Everything looks fine, but there are two problems: first there is the phenomenon of non-factorization, because experimentally, the single-particle cross-section is not a simple product $F(x,q^2)D(z,q^2)$, but $D = D(z,x,q^2)$. Not surprisingly, large z values and large x values tend to be correlated (think of the elastic process $z = x = 1$). This non-factorization is actually a QCD prediction, and it should disappear as q^2 becomes large and $\alpha_s \to 0$ - as it does. However, the magnitude of the non-factorization - technically specified by the values of double moments of structure and fragmentation functions - is not in agreement with QCD and must be dominated by non-perturbative terms. Hence the agreement of z moments (integrated over x) with perturbative QCD may be fortuitous.

Secondly, it is found that the q^2 dependence in Fig.35 is associated with the low W region ($W < 4$ keV), where final state resonances are likely to be important. For $W > 4$ there is much less q^2 dependence of the fragmentation function moments - or, in QCD terms, $\Lambda << 0.5$ GeV. We see here parallel phenomena to those found in the structure function moments, where at low q^2 the situation is dominated by non-perturbative effects.

In summary, the data obtained so far on longitudinal hadron distributions - of which I have only discussed a small fraction here - does not seem to provide clear-cut tests of perturbative QCD, and I shall not discuss it further. This does not mean that the experimental results are not important. Why the low q^2 data, both in structure functions and in fragmentation functions, mimics QCD so closely provides a theoretical problem for the distant future, when, hopefully, the mystery of confinement has been solved and one

knows how to handle the non-perturbative aspects of the interquark interactions.

4.2 TRANSVERSE MOMENTUM DISTRIBUTIONS OF HADRONS IN DEEP INELASTIC SCATTERING

As compared with longitudinal distributions, the transverse momentum distributions of hadrons in leptoproduction have provided a more relevant testing ground for QCD. The reasons for this are easily understood in the context of the naive parton model. The deviations from this model of the longitudinal distributions, arising from interquark reactions, vary only logarithmically with q^2 and are correspondingly hard to detect. On the contrary, the NPM predicts that the transverse momentum of quarks (relative to the $\vec{q}$ vector) is zero, while QCD predicts that transverse momenta should be large and increase with q. This follows from a simple dimensional argument. When q is large compared with any particle masses involved, then p_T must be proportional to q. Only for the NPM is the constant of proportionality zero. In fact, of course, one does not observe the quarks directly, only the hadron fragmentation products. In the fragmentation process, the hadrons will carry a fraction z of the quark p_T, but they will also acquire an additional, non-perturbative component associated with the process of fragmentation, which however is known to be small and constant.

In the discussion of hadronic transverse momenta, the magnitude of p_T from the fragmentation process is a vital factor, and it is important to understand what this is. Thirty years ago, Fermi had a thermodynamic model of meson production in hadron-hadron reactions in which the CMS angular distribution of the mesons was isotropic and thus their transverse momenta increased indefinitely with incident energy. An important early discovery in studies of cosmic ray jets was that the p_T of hadrons was in fact limited ($\langle p_T \rangle \sim 0.3$ GeV/c) and independent of incident energy over the range E(lab) = 10-10^6 GeV. This can be understood from the Uncertainty Principle. A typical p_T must be of order of the inverse hadron size. There is a distribution in p_T, but it must fall off sharply at large values, with $\langle p_T^2 \rangle \sim 0.1$ GeV^2. If $\langle p_T^2 \rangle$ in a particular process is measured to be much larger than this, or increases with energy/momentum transfer, it is a clear indication of processes on a scale more pointlike than a hadron.

Fig.37 shows the three contributions to the hadronic p_T in deep inelastic scattering. The QCD contribution is assumed to arise from hard gluon bremsstrahlung at wide angle. Assuming quarks and gluons are massless on the scale of q, it is straightforward kinematics to show that for the Compton process, $\gamma + Q \rightarrow Q + G$, that is for single gluon bremsstrahlung,

$$\langle p_T^2 \rangle_{QCD} \propto \alpha_s q^2 (\frac{1}{x} - 1) \propto \alpha_s W^2 \tag{84}$$

Putting all the above factors together, we get

$$\langle p_T^2 \rangle_{hadron} = \langle p_T^2 \rangle_{frag} + \langle z^2 \rangle [\langle p_T^2 \rangle + c\alpha_s W^2] \tag{85}$$

where the constant c depends on integrals of structure functions with the approximate value 0.05. Of course, we have no idea if the terms in (85) can be treated separately, as assumed. If they can, then clearly we can deduce the QCD term from the (z,W) dependence.

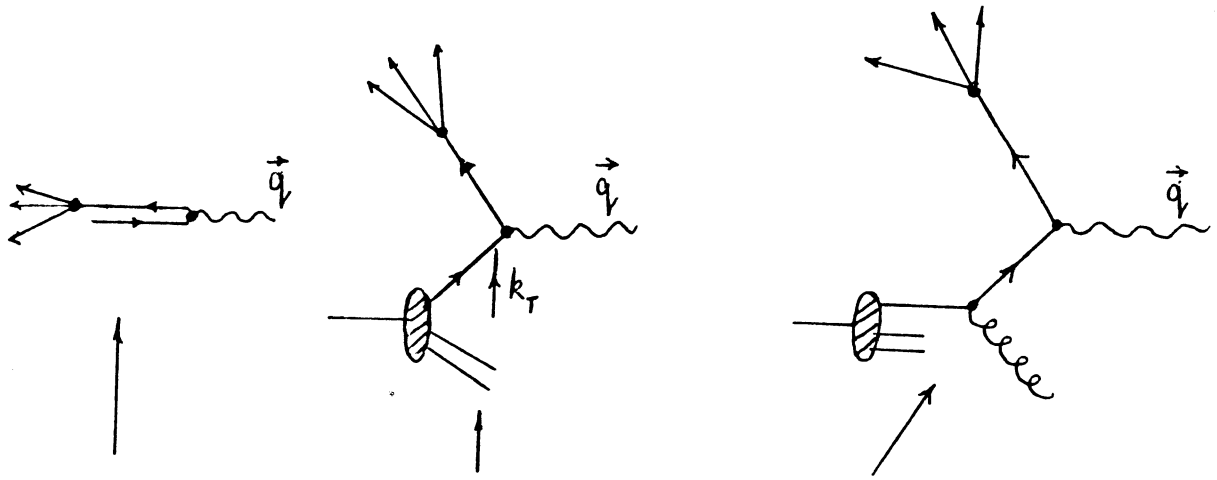

NPM

$(p_T)_Q = 0$

$(p_T)_H = (p_T)_{frag}$

Primordial k_T

$(p_T)_H = (p_T)_{frag} + zk_T$

QCD

$(p_T)_H = (p_T)_{frag} + zk_T + z(p_T)_{QCD}$

$(p_T)_{QCD} = \text{const.}\ W$

Fig.37

There is however one point to be made about $\langle p_T^2 \rangle_{frag}$. At small W, the p_T distribution will be limited by energy-momentum conservation, since $p_T < W/2$. This so-called "seagull" effect depends of course on the shape of the fragmentation p_T distribution, which from hadron-hadron collisions is known to have the approximate form

$$\frac{dN}{dp_T^2} = \text{const.}\ \exp[-\alpha m_T^2], \quad m_T^2 = p_T^2 + m^2 \tag{86}$$

where m_T is the transverse mass and m is the rest-mass of the produced hadron, and where $\alpha = 6\ \text{GeV}^{-2}$. Thus, $(p_T^2)_{frag}$ will increase with W at low W before reaching its asymptotic value α^{-1} (for $W^2 > 50$, approximately).

4.3 THE DEPENDENCE OF p_T^2 ON W^2 IN LEPTOPRODUCTION

Figs.38(a) and (b) show data from the BEBC neutrino experiments on p_T^2 as a function of W^2 and z, where $z = z(\text{CMS}) = 2E_H^*/W$ is the fractional energy of a hadron in the CMS and z is counted as positive (negative) for hadrons going forward (backward). For small W (< 4 GeV) the distributions are forward/backward symmetric. The dependence of p_T^2 on z at small |z| is just the seagull effect. At larger W, the p_T^2 of forward hadrons increases with z and is larger than at small W, while the backward hadrons show no W dependence. This effect is seen also in Fig.38(b), for hadrons of large z, $|z| \geq 0.4$. So, the hadrons originating from the accelerated (struck) quark behave differently from those from the recoiling diquark. If the backward hadrons represent the typical non-perturbative effects (fragmentation, primordial k_T), the origin of the larger p_T for forward hadrons has to be ascribed to some other process associated with acceleration of quarks. Hard gluon bremsstrahlung is one possible process leading to a broadening of the p_T distribution of hadrons from the struck quark. It is important to establish that this F-B asymmetry is not instrumental. The forward hadrons have high energy and errors in their momentum measurement, or in the direction of the $\vec{q}$ axis with respect to which p_T is measured, will clearly be larger than for the backward hadrons. Recall that the $\vec{q}$ vector is found from momentum balance, using the measured muon momentum and the neutrino energy deduced from the muon energy and the total hadron energy, after correction for undetected (neutral) hadrons. Any error in $\vec{q}$ will clearly increase p_T^2 in average. The effect has been investigated by Monte Carlo calculations and by varying the energy correction factor used in event analysis, and it is sure that only a small part of the increase of p_T^2 with W^2 can be ascribed to such causes.

It is very important to emphasize at this point that these effects are not necessarily evidence for QCD and particularly for single hard gluon bremsstrahlung, as in Fig.39(a). Multiple gluon bremsstrahlung must equally, in our dimensional arguments, lead to $\langle p_T^2 \rangle$ increasing with W^2 (Fig.39(b)). We note only that in (a), the hadrons will tend to be confined to a plane (the QG scattering plane) while in (b) they will not (since the directions of successive gluons are uncorrelated). One of the tasks of the data analysis will clearly be to see if one can extract events corresponding to the process (a). This is just like finding the single (Rutherford) scattering acts among the multiple scattering distribution of charged particles traversing a thick scattering foil.

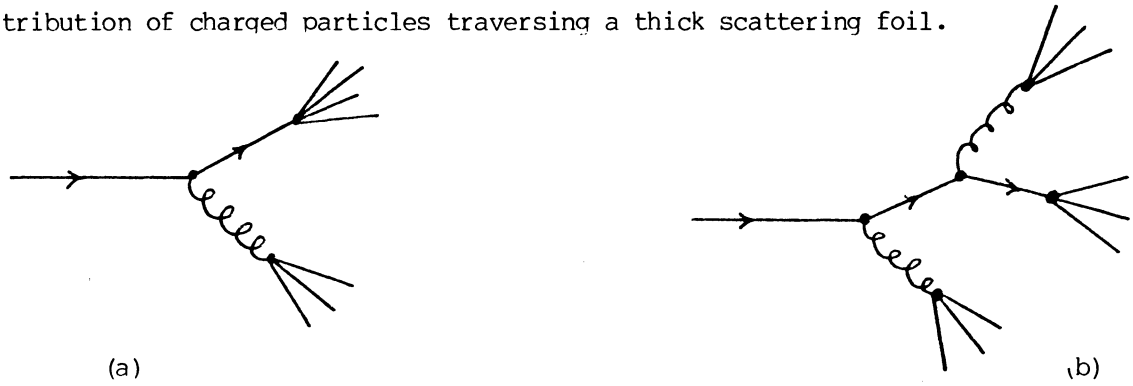

Fig.39

Fig.40 shows results in the growth of p_T^2 with W^2 from both neutrino and muon scattering experiments. If we apply (85) to this data, that is assume the p_T broadening is due to single gluon bremsstrahlung, using the observed value of $\langle z^2 \rangle$ and $\langle k_T^2 \rangle = 0.4$ GeV^2, as obtained from a separate analysis of 3C events, one finds $\alpha_s \sim 0.5$-1. This is so large that higher-order processes, proportional to α_s^2, α_s^3..... cannot be neglected. This simply tells us that multiple hard scattering processes are dominant. This fact is confirmed in the analysis of planar events, discussed below.

4.4 PLANAR EVENTS

In single hard gluon bremsstrahlung as in Fig.39(a), the p_T broadening should be principally in the quark-gluon scattering plane, and the events shoud be "planar", with the forward hadrons forming a fan-shaped configuration, with p_T^2 large in one plane and small perpendicular to this plane.

* In the leptoproduction experiments, one can determine the preferred plane of the hadrons, as that which maximises the component of p_T^2 in the plane, and minimizes that normal to it. In these experiments, the $\vec{q}$ vector is known, and by a minimization procedure one can find that vectors $\vec{Q}_2$ and $\vec{Q}_1$ normal to $\vec{q}$ such that Σp_T^2 is maximum in the plane defined by $\vec{Q}_2$ and $\vec{q}$. The corresponding mean value per hadron is called $\langle p_T^2 \rangle_{in}$, and that in the orthogonal direction (in the plane defined by $\vec{Q}_1$ and $\vec{q}$), $\langle p_T^2 \rangle_{out}$. These quantities are evaluated from the forward hadrons only.

We shall also compare the leptoproduction data with that from $e^+e^- \to$ hadrons at high energy (at PETRA). In the latter case, there is no $\vec{q}$ vector, and the direction of the forward and backward jets from the process $e^+e^- \to Q\bar{Q}$ is determined by a minimization procedure. Thus the TASSO and JADE groups evaluated the 3 × 3 matrix

$$M_{\alpha\beta} = \sum_{j=1}^{j=N} p_{j\alpha}\, p_{j\beta} \qquad (87)$$

here $\alpha,\beta = x,y,$ or z and the sum extends over all N secondaries of the event. Diagonalizing (87) one finds the eigenvalues Λ_1, Λ_2, Λ_3 of the momentum ellipsoid and hence the normalized eigenvalues

$$Q_{1,2,3} = \Lambda_{1,2,3} / \Sigma p_j^2 \qquad (88)$$

such that $Q_1 + Q_2 + Q_3 = 1$, and $Q_3 > Q_2 > Q_1$. Q_3 defines the sphericity axis (roughly equivalent to the $\vec{q}$ axis in lepton scattering) normal to which p_T^2 is minimal, and Q_2 and Q_1 the transverse axes, with $\langle p_T^2 \rangle_{in}$ the mean square component in the Q_2-Q_3 plane, $\langle p_T^2 \rangle_{out}$ that in the Q_1-Q_3 plane.

Fig.41 shows the values of $\langle p_T^2 \rangle_{in}$ and $\langle p_T^2 \rangle_{out}$ from the BEBC neutrino and e^+e^- (PETRA) experiments. Both $\langle p_T^2 \rangle_{in}$ and $\langle p_T^2 \rangle_{out}$ are seen to grow at about the same relative rate with W^2. The values of p_T^2 in νN and e^+e^- experiments are somewhat different; in particular, the values from e^+e^- are smaller, simply because they are measured relative to the sphericity axis and have been minimized with respect to it. However, the trend of $\langle p_T^2 \rangle_{in,out}$ with W^2 is clearly similar in the two cases. The neutrino data can be fitted by a simple power law:

$$\langle p_T^2 \rangle_{in}^{\nu N} = A_1\, W^{0.54 \pm 0.06}$$
$$\langle p_T^2 \rangle_{out}^{\nu N} = A_2\, W^{0.58 \pm 0.04} \qquad (89)$$

with $\langle p_T^2 \rangle_{in} \sim 3 \langle p_T^2 \rangle_{out}$. The e^+e^- data show a similar ratio.

Obviously, $\langle p_T^2 \rangle_{in}$ is greater than $\langle p_T^2 \rangle_{out}$, by definition. For events with finite multiplicity, one can always find a preferred event plane, and the ratio of the two components will clearly depend on the angular distribution of secondaries and the multiplicity (e.g. it is infinity for N=2!). In fact, the observed ratio (~3) is consistent with average isotropy of the azimuthal distribution around the $\vec{q}$ (or $\vec{Q}_3$) vector.

These results are consistent with what one expects from "2 jet" events, with a random azimuthal angular distribution about the jet axis. Of course, in the absence of hard scattering (gluon bremsstrahlung) processes, we cannot easily account for the rise of p_T^2 with W^2 at large W. So, if these processes occur, they lead to a broadening of the p_T distribution in all directions. In fact this is also a prediction of QCD. If a quark radiates a hard gluon at large angle, this will define an event plane. But further (and unavoidable) gluon emission will be in arbitrary directions and will lead to a growth of p_T^2 both in and out of the initial plane. It turns out that, in the high W limit, $\langle p_T^2 \rangle_{out} / \langle p_T^2 \rangle_{in} = K\alpha_s$, where K is a numerical coefficient, not so far calculated as far as I know, but of order unity.

So much for the average behaviour of events at high W. One can now see whether it is possible to isolate events ascribable to single hard gluon bremsstrahlung (i.e. those in which several energetic gluons may be involved, but one of them is dominant and essentially fixes the event plane). If this is possible then one should be able to distinguish gluon jets and quark jets and hence get information about gluon quantum numbers. As in our single/multiple scattering analogy, one might expect to enhance the number of interesting events by selecting those with hadrons of exceptionally high p_T. Different selection methods have been used, but they all essentially amount to this.

In the e^+e^- experiments, the TASSO and JADE groups have determined the sphericity S and aplanarity A,

$$S = \frac{3}{2}(Q_1 + Q_2) = \frac{3}{2}(1 - Q_3) = \frac{3}{2} \text{ Min } \frac{\Sigma p_{T_j}^2}{\Sigma p_j^2}$$

$$A = \frac{3}{2} Q_1 \tag{90}$$

Events of large S involve large p_T values, those of small A have p_T preferentially in the Q_3/Q_2 plane, i.e. they are pancake-like. Fig.42 shows a Dality plot, where 2-jet events (small S) occur in the L.H. bottom corner, "spherical" or isotropic events in the R.H. bottom corner and events of large S and small A near the R.H. upper boundary. The observed numbers of events were compared with those predicted according to the generation of "2 jets" by $e^+e^- \to Q\bar{Q}$ with the quark fragmentation described by the Feynman-Field prescription (essentially, an exponential distribution in Feynman x_F, combined with a limited (Gaussian) p_T distribution); and with the numbers predicted including also the "3 jet" process $e^+e^- \to Q\bar{Q}G$ (hard gluon bremsstrahlung by one quark).

The TASSO group, for example, found:

Solution	Observed	$Q\bar{Q}$ MC	$Q\bar{Q}G$ MC
$S > 0.25$; $A < 0.04$	[illegible]	4.5	17
$S > 0.25$; $A > 0.04$	38	38	35

indicating an excess of small A events ascribable to the QCD process.

It is important to emphasize that the parameters of the fragmentation process are empirical, and that in principle the number of planar events can always be increased by changing the shape of the p_T distribution in the fragmentation process. The $Q\bar{Q}$ model can also be made to reproduce the number of planar events by changing the p_T distribution from $dN/dp_T^2 = \text{const.}\exp(-6\, p_T^2)$ to $dN/dp_T^2 = \text{const.}\exp(-2p_T)$. But the second distribution is <u>not</u> a reasonable description of hadronisation, for which we already know the p_T distribution from (86).

The MARKJ group at PETRA adopted slightly different criteria, defining the thrust T and oblateness O, in terms of principal axes defined by orthogonal unit vectors $\vec{e}_1$, $\vec{e}_2$, $\vec{e}_3$:

$$\begin{aligned} T &= \max \Sigma\, \vec{p}_j.\vec{e}_1/\Sigma|p_j| \\ \text{ajor} &= \max \Sigma\, \vec{p}_j.\vec{e}_2/\Sigma|p_j| \\ \text{Minor} &= \vec{e}_3 = \vec{e}_2 \wedge \vec{e}_1 \end{aligned} \tag{91}$$

$$O = (\text{Major} - \text{Minor})$$

The oblateness distribution (Fig.43) is again in better agreement with the $Q\bar{Q}G$ Monte Carlo than that for the process $Q\bar{Q}$. The $Q\bar{Q}G$ process gives rise to "3 jet" events, and the ratio of 3-jet to 2-jet events is clearly proportional to α_s. All four PETRA groups give similar values for α_s, and the average is

$$\alpha_s \ (3 \text{ jet}/2 \text{ jet}, \ S \sim 10^3 \text{ GeV}^2) \simeq 0.18 \pm .05 \qquad (92)$$

The value of the argument $|q^2| = W^2$ of α_s is a matter of debate; it is not clear if it is equal to s, or the invariant mass of (gluon + quark) system, or what. Probably one should assume $\alpha_s(q^2)$ where $q^2 \sim 0.4s$. In any event, the value of α_s is compatible with the one deduced from lepton-nucleon scattering at $q^2 \sim 10\text{-}100$ GeV^2.

Tests of this identification of jets as due to quarks or gluons are to look in the 3-jet events at the fragmentation functions of each - but they seem to be quite similar - or the angular distributions. Fig.44 shows TASSO data. The angle $\tilde{\theta}$ is that of the (oppositely-directed) quark to gluon momentum vectors in the rest-frame of the broad jet (assigned to $Q+G$), measured relative to the slim jet (assigned to $\bar{Q}$). The expected distribution, as calculated by Ellis and Karliner (1979) is fairly complicated, but with the cuts $T \sim 0.8\text{-}0.9$, $\cos\tilde{\theta} < 0.5$ needed to define the separated 3-jet structure, they acquire the approximate form

$$\begin{aligned} dN/d\cos\tilde{\theta} &\propto 1 + 2\cos^2\tilde{\theta} \quad \text{vector gluon} \\ &\propto 1 + 0.2\cos^2\tilde{\theta} \quad \text{scalar gluon} \end{aligned} \qquad (93)$$

The observed distribution favours vector gluons. The difficulty with this analysis is that the cuts required to make the separate jets recognizable are such that the sensitive region, $\cos\tilde{\theta} \sim 1$, is excluded.

4.5 ENERGY FLOW

Even if separated 3-jet events are not recognizable, the wide-angle bremsstrahlung process $Q \to Q+G$ may have a detectable effect on the pattern of energy flow in the events. In particular, if a quark radiates a hard gluon at wide angle, the broad jet of hadrons produced should have an energy flow pattern with a minimum in the forward direction. However, the selection of the likely events, that is of planar events with large transverse momenta principally in one plane, will tend in any case to deplete the forward region. Everything depends on comparison with events generated by Monte Carlo, using the experimental cuts.

Fig.45 shows the CERN EMC (μN) hadron data, for events selected with 22GeV > W > 10GeV, $n_F \geq 4$ forward hadrons, of which at least one has $p_T > 1.5$ GeV/c. The observed energy flow pattern is in better agreement with the $Q\bar{Q}G$ Monte Carlo (that is, with gluon bremsstrahlung included) than the $Q\bar{Q}$ Monte Carlo. Fig.46 shows corresponding results for CERN BEBC νN data, with essentially the same cuts (W > 10GeV, $p_T^{max} > 1$GeV, $n_F \geq 4$). The projected energy flow in the hadron plane shows a forward dip, but so does the $Q\bar{Q}$ Monte Carlo, and the two are consistent.

Finally, Fig.47 shows the BEBC events with W > 10GeV, $n_F \geq 4$ plotted another way. The azimuthal angular distribution, about the $\vec{q}$ vector, is plotted relative to the highest p_T (forward) secondary, which is <u>not</u> included (it is at 0°). Let us call the p_T of this "leading" secondary $p_T(\max)$. If no restriction is made on $p_T(\max)$, the angular distribution of the other secondaries is fairly flat, peaking slightly at $\Phi \sim 180°$ due to momentum conservation. For $p_T(\max) > 1$GeV/c however, the distribution is peaked both at 180° and toward 0°. The statistics are poor, but the results suggest that some secondaries follow the one of highest p_T, even though momentum conservation alone would tend to push them towards $\Phi \sim 180°$ i.e. one seems to obtain 2 forward jets. A notable feature of this analysis is that no Monte Carlo comparisons are involved at all.

The BSHW collaboration, working in the Fermilab 15' chamber, have carried out a similar analysis and get quite similar results, as also do the EMC collaboration.

4.6 CONCLUSIONS

The broadening of the p_T distribution with q^2 and W^2 in e^+e^- reactions and in lepton-nucleon scattering is well established, and in my opinion, in the higher W ranges, is clear and unambiguous evidence for pointlike hard scattering processes, as predicted in QCD.

There is indeed evidence, principally in the e^+e^- data at $W \sim 30GeV$, that a proportion of events can be attributed to single hard gluon bremsstrahlung at wide angle, by one of the quarks.

Jet studies are still in their infancy, and, as the statistical weight of the data as well as experience accumulates, a much more serious confrontation of experiment with theoretical predictions will become possible.

5. PROTON LIFETIME EXPERIMENTS

Baryon instability is discussed here because it constitutes a crucial test of grand unified gauge theories. There is, at the present time, neither evidence that baryons are unstable nor any good reasons to suppose that they are not. Conservation of baryon number B or lepton number L must be associated with an invariance principle. Thus, charge conservation is associated with gauge invariance in electromagnetism and the existence of a long range field (i.e. massless photons). If B (or L) were absolutely conserved, we would expect a long-range field coupled to baryon number, and this should show up in Eötvös experiments as a different gravitational attraction for objects of the same inertial mass but different baryon number (i.e. of different elements). No such effects are observed. Several experiments - designed originally to do other things - happen to provide limits on proton stability, and we discuss these briefly before turning to the experiments dedicated to the search for nucleon decay.

5.1 EXISTING LIMITS

5.1.1 Biological Limit

As pointed out many years ago by M. Goldhaber, existence of life sets a strong limit on nucleon stability. If all the decay products produce ionization and the mean lifetime of the proton is τ years the body dose is:

$$\text{Body dose} = \frac{6.10^{18}}{\tau} \text{ rad yr}^{-1}$$

1 rad = 100ergs g^{-1} = 6.10^{7} MeV g^{-1}

Natural body dose = 0.12 rad yr^{-1} (cosmic rays + radioactivity)

Permissible body dose = 5 rad yr^{-1}

Probably 500 rads yr^{-1}, that is 100 x permissible body dose, would have serious effects, long term, so $\tau > 10^{16}$ years, already long compared with the known age of the galaxy (4.10^{10} yr).

5.1.2 Geochemical Limit

The basic idea is to try to find rare, long-lived isotopes from small underground ore samples. Such isotopes might be formed as a result of nucleon decay, an example being I^{129} from Te^{130}:-

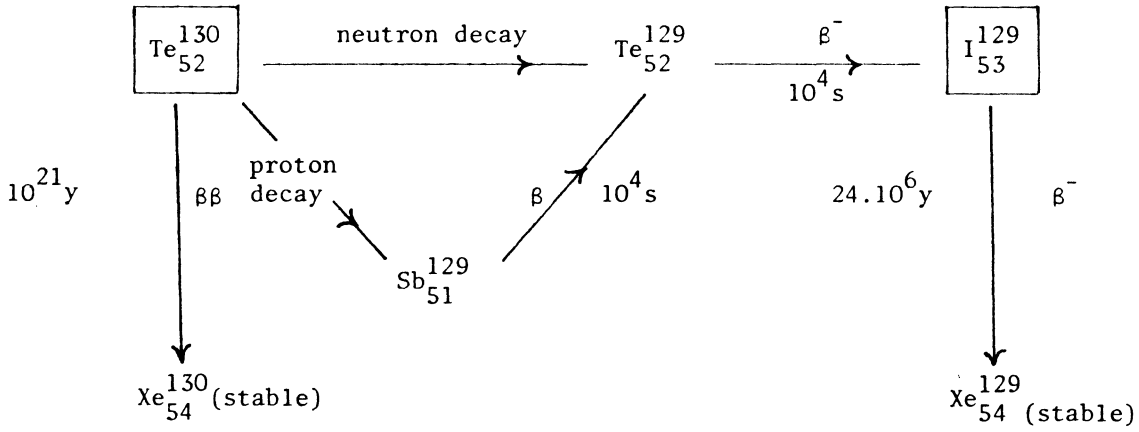

If tellurium 130 loses either a proton or neutron, and the daughter nucleus is left unexcited (the probability as computed by shell model calculations is $\sim$40%), Te^{129} decaying to I^{129} would be formed. The lifetime of I^{129} is long enough to integrate the decay of Te^{130} over a long period, yet short compared with the age of the solar system - so there is no primordial I^{129}. Existing limits using mass-spectroscopic methods of measuring the I^{129} abundance give $\tau > 10^{25}$ years (Hennecke et al (1975)). Possibly in the future one can extract, accelerate and detect single iodine ions, using stripping techniques to remove organic molecules of mass 129, and magnet spectrograph and time of flight methods to get the precision required. For $\tau = 10^{30}$ yrs, 1Kg Te^{130} will provide 10^3 atoms I^{129}. A weakness of this technique is that it depends on geological evolution over $\sim 10^6$ years, for example in comparing samples from different depths, subjected to different cosmic ray backgrounds.

5.1.3 Radiochemical Limit

A different approach is to detect the decay of a short-lived radioisotope produced as a result of baryon decay. Since the isotope is chosen to have a short lifetime, a large sample of ore is required to give any effect. An example is nucleon decay in K^{39} followed by p or n emission, resulting in Ar^{37} which decays by K-capture to Cl^{37}. Again, shell plus evaporation model calculations give ∿20% for the probability

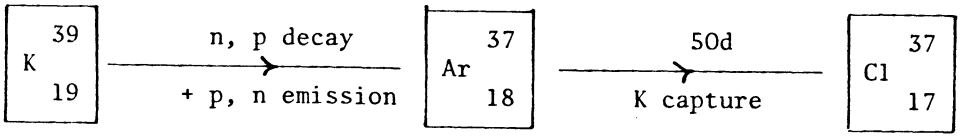

that nucleon decay will be followed by the clean removal of just one nucleon. Using 1.7 ton KAc, Evans Fireman and Steinberg (1977) working at 400mwe ((Homestake Mine) found a production rate of <1 Ar^{37} atom/day and hence $\tau > 2.10^{26}$ yr. These authors have proposed an experiment with 450 tons KAc at 9000mwe depth, where the cosmic background will be <0.1 Ar^{37} atoms/day, so that they expect to reach a limit $\tau > 5.10^{29}$ years.

In summary, radiochemical and geochemical methods have placed limits on the nucleon lifetime of $\tau > 10^{26}$ years and can probably attain a sensitivity up to $\tau \curvearrowsim 10^{30}$ years. However, there is no way they can prove that nucleons decay, since what is observed is an "excess" of a rare isotope, but this excess could have arisen in many other ways. This drawback more than offsets the advantage that the "signal" is independent of the nucleon decay mode.

5.1.4 Cosmic Ray limit

The most sensitive limit on baryon stability derives from an experiment deep underground in a South African gold mine (9000mwe), designed to detect the interactions of atmospheric neutrinos. The apparatus (Learned, Reines and Soni (1979)), consisted of flash tubes and liquid scintillator and could detect a stopping μ^+ by its decay with 2μs lifetime. 6 $\mu^+ \rightarrow e^+$ decays were observed in the detector; all could be attributed to neutrino reactions in the surrounding rock, $\nu_\mu + N \rightarrow \mu^+ + X$. If however, they are attributed to proton decay, they yield the limit

$$\tau_p > 10^{30} \text{ yrs.} \qquad (94)$$

This limit depends on assumptions about p (or n) decay modes, namely that μ^+ arise as products in $\sim$15% of decays. For the SU5 models to be discussed below, μ^+ will be produced at this rate because π^+ are important products (50% of proton decays) and half the π^+ will decay to μ^+. The limit (94) holds also for the Pati-Salam model, where decay modes involving neutrinos (e.g. $p \rightarrow \pi^+ + 3\nu$) and pions dominate. However, the above result is not generally model independent.

5.2 THEORETICAL PREJUDICE

There is no question that the present spate of experimental activity, searching for nucleon decay, neutron oscillations etc. stems from the theoretical work on grand unification schemes for the fundamental interactions, over the last few years.

Fig. 48 shows the dependence on q, the 4-momentum transfer, of the running coupling constants g and g' of the SU2 and U1 gauge groups of the electroweak interaction and that, g_s, of the colour SU3 strong interaction. g and g' represent the coupling of leptons to the gauge bosons W^+, W^-, Z° and γ of the SU2 x U1 model, g_s the coupling of quarks to the gauge bosons (gluons) of the strong interactions. The Abelian coupling g' increases with

q, while the non-Abelian g and g_s couplings decrease. To within the experimental errors, the three couplings coincide at a unification mass $M_x \curvearrowright 10^{14}$ GeV. If the three interactions are unified at this energy, then most of the distinction between quarks and leptons disappears, and indeed the "lepto-quark" bosons X and Y of charge 4/3 and 1/3, can mediate proton decay (Fig. 49), transforming a quark to a lepton or quark to antiquark and giving, for example $p(=duu) \to e^+\pi^\circ(=e^+u\bar{u})$. From this diagram of X (or Y) exchange between quarks, one can see that the matrix element contains a propagator term $(q^2 + M_x^2)^{-1}$ which at the low q^2 of proton decay gives a rate factor $\propto M_x^{-4}$. Thus, on dimensional grounds the proton lifetime can be written

$$\tau_p = c \cdot \frac{M_x^4}{M_p^5} \qquad (95)$$

where c is a dimensionless constant containing numerous factors (integrals over quark wavefunctions etc.), with a value of order unity (i.e. 10^{-2} to 10^{+2}). If we take $c = 1$, $M_x = 3.10^{14}$ GeV one finds $\tau \curvearrowright 10^{32}$ yrs. The "best" lifetime estimate available gives (Ellis et al 1980)

$$\tau_p = 10^{31\pm2} \text{ yrs} \qquad (96)$$

However, we should recognise that it depends on numbers, the values of which are not well known and which can change very dramatically. As an example, the unification mass M_x is determined mostly by the rate of decrease of $\alpha_s(=g_s^2)$, the strong coupling, with q^2. In leading order QCD $\alpha_s = 12/(33-2f)\ell nq^2/\Lambda^2$ where f is the number of quark flavours, and the parameter Λ sets the scale of strong interactions. The result (96) assumed $\Lambda = 400$ MeV, before the most recent results from the CERN EMC muon scattering experiment gave $\Lambda \curvearrowright 100$ MeV. Obviously $M_x \propto \Lambda$, hence if Λ

changes by a factor 4, τ_p changes by $4^4 = 256$. So theoretical estimates - even if the theory is right - need experimental input which leaves very large uncertainties.

The actual decay modes expected are of course of absolutely crucial importance to any detection system.

Table 5.1 gives a list of typical branching ratios based on SU5 as the symmetry of the unified (SU3 x SU2 x U1) interaction. According to this model, u and d quarks appear in the same SU5 generation as ν_e and e, while s and c quarks are partnered with ν_μ and μ. Thus a nucleon consisting of u and d quarks is expected to decay to e^+ + hadrons, not μ^+ + hadrons. The expected dominance of the decays $p \to \pi^0 e^+$, $n \to \pi^- e^+$ had dictated the design of water Cerenkov detectors tailored to detection of electromagnetic showers.

TABLE 5.1

Typical Nucleon Decay Branching Ratios (SU5)

$p \to \pi^0 e^+$	34%	$n \to \pi^- e^+$	51%
$p \to \rho^0 e^+$	16%	$n \to \rho^- e^+$	26%
$p \to y\, e^+$	12%		
$p \to \omega\, e^+$	21%		
$p \to \bar{\nu}_e X_{NS}$	13%	$n \to \bar{\nu}_e X_{NS}$	20%
$p \to \bar{\nu}_e X_S$ $\to \bar{\nu}_\mu X$ $\to e^+ X_S$ $\to \mu^+ X$	4%	$n \to \bar{\nu}_e X_S$ $\to \bar{\nu}_\mu X$ $\to e^+ X_S$ $\to \mu^+ X$	3%

5.3 BACKGROUND CONSIDERATIONS

A 1000 ton detector contains 6.10^{32} nucleons, and if $\tau \sim 10^{32}$ years, only 6 nucleon decays will occur in a whole year, some by virtually undetectable modes. In contrast, at the earth's surface, nearly 10^{12} cosmic

ray muons cross the detector, and these will produce background processes which can completely swamp any signal.

To reduce background as far as possible, experiments must be carried out underground. Fig. 50 shows the total muon flux per year through a 10 x 10 x 10m cubic detector, as a function of depth, obtained by numerically integrating the measured differential muon spectrum (Menon, 1976). Depth is quoted in metres of water equivalent (mwe): since "standard rock" has density $\sim$3, the depth in mwe is about equal to the actual depth in feet. The muon flux varies from $\sim$1 per second in the shallow mine experiments (1600mwe) to $\sim 10^{-3}$ per second in the Mont Blanc road tunnel (5000mwe).

5.3.1 Neutron Background

The muons themselves produce tracks traversing the entire detector and can hardly be mistaken for nucleon decays. The important background is contributed by energetic neutrons generated in nuclear cascades produced in inelastic muon-nucleon scattering.

First we observe from Fig. 50 that the muon absorption length is about 700 times the nuclear mean free path (100gm cm^{-2}) so that hadrons are in equilibrium with, and proportional to, the muon flux at any particular depth. An estimate of neutron production has been made by A. Grant (1979) using a Monte Carlo program to generate hadron cascades originating from muon interactions. These calculations give numbers for the energy spectrum of neutrons, either accompanied by a muon or other hadrons, or isolated in the sense that no other particle crosses the detector (again, a 10 x 10 x 10m cube). They also provide a spectrum of pions produced in hadron cascades. Whereas there are no useful measurements of fast neutron rates deep underground, there are measurements of the rate of stopping (and decaying) μ^+. For h > 1000mwe, the π^+ stop rate comes mainly from decay of π^+, the production rate of which can therefore be deduced and used to check

the Monte Carlo predictions.

The results show that: (i) the total number of neutrons of E > 100 MeV and the total number of $\pi^{\pm}$ are about equal, at $1.5.10^{-2}$ particles per crossing muon, per 100g cm^{-2} of material traversed (ii) the number of isolated neutrons of E > 1 GeV is 2.10^{-5} per muon per 100g cm^{-2}. Thus one can estimate that the number of isolated neutrons capable of giving relativistic secondaries, with a visible energy of 0.9 ± 0.2 GeV is <<0.25 of the neutrino background rate (see below) for depths h > 1600mwe. Hence, provided one goes deep, neutron interactions are much less important than neutrino background.

This result depends on making sure that the neutron is isolated. If one misses an accompanying muon, the rate goes up by a factor 15. If one misses both the muon and any accompanying hadron, the rate will go up by a factor 120. The result also depends somewhat on detector size. Although the results are quoted for a 10 x 10 x 10m cube, they apply for almost any detector with a linear dimension large compared with the nuclear mean free path.

5.3.2 Neutrino Background

This background is irreducible (except by going to the Moon and thus eliminating cosmic ray production of pions in the atmosphere) and the principal limitation on baryon decay experiments.

The magnitude of the neutrino flux is quite well known; the pions (and kaons) produced in the stratosphere decay to muons and neutrinos, so that the measured muon flux is directly related to that of neutrinos. The neutrino spectrum can be approximated by a power law:-

$$\phi_{(42n_{\mu}+\bar{\nu}_{\mu})} = 0.05\ E^{-2\cdot74} cm^{-2} st^{-1} s^{-1}\ GeV^{-1} \qquad (E > 1\ Gev) \qquad (97)$$

$$\phi_{(\nu_e+\bar{\nu}_e)} \simeq 0.5\ \phi_{(\nu_m+\bar{\nu}_m)}$$

and can be considered known to ±30%. The ν_e, $\bar{\nu}_e$ component originates from Ke3 and μ decay in the atmosphere.

From these fluxes and the known charged (CC) and neutral current (NC) cross-sections one obtains the following rate estimates:-

TABLE 5.2

Neutrino Background Rates

		Rate per 10^3 ton per year
CC $\nu_\mu + \bar{\nu}_\mu$	$E = 0.9 \pm 0.2$ GeV	27
CC $\nu_e + \nu_e$	$E = 0.9 \pm 0.2$ GeV	13
NC $\nu_\mu + \bar{\nu}_\mu$	$E_{hadron} = 0.9 \pm 0.2$ GeV	4
NC $\nu_e + \bar{\nu}_e$	$E_{hadron} = 0.9 \pm 0.2$ GeV	2
	Total	46

A total of about 50 events have visible energy 0.9 ± 0.2 GeV, for a 1000 ton detector in one year's run. (The total number of neutrino events of $E_{vis} > 1$ GeV is about 3 times this figure.) If all these events simulated proton decay, it follows that the maximum detectable lifetime would be $\tau(max) \sim 10^{31}$ years and indeed a 30 ton detector, providing 2 neutrino and 2 proton decay events per year, which could not be distinguished, would be big enough. Clearly, the only justification for building a larger detector is that one hopes to cut down the background by a substantial factor, either by:

(a) improving the energy resolution - very difficult in practice, since very massive detectors with very high resolution are extremely expensive, or

(b) identifying the decay configuration, e.g. $n \rightarrow e^+\pi^-$ by having good track pattern recognition in the detector. This can in principle reduce background by a large factor, even 100, so that lifetimes as large as 10^{33} years might be measurable.

As an example of what might be achieved, Fig. 51 shows a plot from the Irvine-Michigan-BNL proposal (1979). From events in the Gargamelle PS neutrino experiment, those compatible with $\nu_\mu + N \rightarrow \mu^- + \pi^+ + N$ were selected, and the energy ratio $E_\pi/(E_\pi + E_\mu)$ plotted against the angle $\theta_{\pi\mu}$ between μ^- and π^+. We would expect a similar plot for the neutron decay ($n \rightarrow e^+\pi^-$) background reaction $\bar{\nu}_e + N \rightarrow e^+ + \pi^- + N$, since the PS neutrino spectrum is rather similar to the cosmic ray neutrino spectrum. Fig. 51 shows the number of events expected in a 2 year run of their proposed detector. Nucleon decays (e.g. $n \rightarrow e^+\pi^-$) should exhibit a back-to-back configuration of the two secondaries, modified by Fermi motion of the neutron in the nucleus, and should be contained inside the dotted semi-circle. Out of 100 background events none actually falls into this allowed region, justifying - at least on paper - the factor 100 mentioned above.

5.4 FUTURE EXPERIMENTS

The requirements of a detector for nucleon decay can be summarised as follows:-

(1) It must be large enough to contain the decay products. For water Cerenkov detectors, oriented to the decay mode $p \rightarrow e^{+}\pi^{o}$, the electromagnetic showers must be contained inside the fiducial volume, and their spatial extent will be several radiation lengths, i.e. several metres of water. Hence, a detector of linear dimension 5-10 metres is required.

(2) It must be massive. 3000 tons for 1 year would produce 1 event for lifetime 10^{33} years.

(3) It should be deep underground, h > 1500mwe to eliminate neutron background.

(4) It should have good energy resolution, good particle identification and track recognition.

Fig. 5.2 summarises the timescales and rates involved. New experiments are aiming at the so far unexplored interval $10^{30} < \tau < 10^{33}$ years. For $\tau > 10^{33}$ years, background will be a major problem, and one would be reduced to comparing observed numbers of events with the predicted background with various cuts on the data. Eventually one will reach the point where one is taking differences of two large numbers (observed - predicted) with the signal/noise increasing only as $M^{0.5}$, so that a factor 10 on the lifetime implies a 100-fold increase in detector mass. This "neutrino brick wall" presumably occurs in the region of $\tau > 10^{33}$ years.

5.4.1 Water Cerenkov Devices

The Irvine-Michigan-BNL group and the Harvard-Wisconsin-Purdue group have proposed large water Cerenkov detectors, with useful (fiducial) masses on the order of 1000-4000 tons, or more.

In water, relativistic secondaries - and particularly electrons in electromagnetic showers from the decay modes $n \to e^+\pi^-$ and $p \to e^+\pi^\circ$ - will produce Cerenkov light at the Cerenkov angle in water (42°), which is transmitted in a cone about the particle trajectory and reaches the surface of the water as a ring of light. Fig. 53 shows examples from the IMB proposal. The light is detected by a photomultiplier array placed at the surface (IMB) or in the water volume (HWP). Since the typical time jitter over the photocathode area of a 5" tube is $\sim$2ns, timing can also be used to estimate the direction of the light cone and thus, the track orientation.

Some of the factors involved in the water Cerenkov method are illustrated in Fig. 54. The Cerenkov spectrum has the form $d\lambda/\lambda^2$, but the photoelectron yield depends on this, the quantum efficiency of the photocathode and attenuation of light in water. Even for pure (reverse osmosis) water, the number of photoelectrons is at least a factor 10 smaller than the number of Cerenkov photons in the visible region. The photoelectron yield has to be multiplied by the effective fractional surface area covered by photocathode, which is of order 4%. The resultant number of "hits" for a 20 x 20 x 20m cube with a surface array of 2400 5" photomultipliers is given in Table 5.3. The resolution could be improved by a factor 2, with 4 times the number of PM's, but this would treble the cost of the experiment.

TABLE 5.3

Photomultiplier Hits for Various Decays
20 x 20 x 20m Cube with 2400 5" PM's on Surface

Decay Mode	# Hits	Energy Resolution (rms)
$p \rightarrow e^+\pi^\circ$	210	±16%
$n \rightarrow e^+\pi^-$	150	±19%
$p \rightarrow \mu^+\pi^\circ$	160	±18%
$n \rightarrow \mu^+\pi^-$	90	±24%

The analysis of the data from the water Cerenkov devices involves reconstruction of light cones, tracks and vertices and has to be done on-line by computer.

5.4.2 Calorimeter Devices

The other types of device proposed for detecting nucleon decay are solid calorimeters, in which it is planned to record the tracks of the charged secondary products by means of proportional wire or drift chambers, streamer chambers or flash tubes, arranged in planar arrays separated by iron plates. The main advantages of a solid calorimeter device is that the radiation length is short, a few cms rather than a metre, so that a decay event is spread over less than one metre linear dimension, and tracks can be easily reconstructed.

I mention as examples, two calorimeter devices. The Minnesota group has built a 30 ton prototype calorimeter consisting of proportional tubes embedded in taconite (iron ore + cement) - see Fig. 55. The density is $\sim 2.7 gcc^{-1}$, radiation length 6.7cm and nuclear mean free path 50 cm. The

energy resolution for this device is rather poor (±30%) and the granularity is rather coarse, but it will serve to give experience for construction of a full-scale device. It is operating in the Soudan iron mine, N. Minnesota.

The Milano-Torino-Frascati (1979) group are building a 150-ton calorimeter consisting of extruded plastic tubes operated in the streamer mode, with cathode strip read out in two orthogonal directions (Fig. 56), layers of plastic tubes being separated by 1cm iron plates. A computer simulation of a $p \to e^+\pi^0$ decay is shown in Fig. 57. It will be operated in the Mont-Blanc road tunnel (h = 5000mwe).

One of the significant advantages of calorimeters is that test modules can be built small ($\sim$1m dimension) and tested in accelerator neutrino beams, so that background problems can be studied in great detail. Compared with the water detectors, the mass one can achieve for a given sum of money is about a factor 10 smaller. Obviously, it is most important to build and operate both types of detector and to learn by experience of the different techniques which is more suitable. Unfortunately, this learning process will take years.

Even if the detectors now being constructed do not find evidence for nucleon decay, it is important to emphasize that totally unexpected new phenomena might turn up. This is the first time that physicists have operated detectors of 100's or 1000's of tons capable of observing very rare phenomena in conditions of very low background.

5.5 NEUTRON-ANTINEUTRON OSCILLATIONS

In the SU(5) grand unification scheme, baryon decay obeys the selection rule $\Delta B = \Delta L(=1)$. It is also possible to consider the process $\Delta B = 2$, that is, neutrons transforming to antineutrons via a 6 quark coupling (see, for example, Marshak & Mohapatra (1980). The rate of this spontaneous transition $\Gamma(n\bar{n}) < 10^{-22}$ eV, by the arguments leading to $\tau(\text{proton}) \sim 10^{32}$ years. If neutrons were free and in remote space, the $N\bar{N}$ transitions would

be like those in the $K^{\circ}\bar{K}^{\circ}$ system. In real life, N, $\bar{N}$ states are not degenerate, because of the effects of magnetic fields, etc. which split the degeneracy by $\Delta E >> \Gamma$ ($\Delta E \sim 10^{-11}$ eV for free N, $\bar{N}$ in the earth's field). Thus, in practice the mixing angles are small. For a short observation time $t << \Gamma^{-1} = 10^{5}$ sec, the antineutron intensity in a free neutron beam has the simple form

$$I(\bar{N}) = I(N).(\Gamma/\Delta E)^{2} \qquad (98)$$

By using magentic shielding to reduce ΔE, and assuming cooled thermal neutrons from a reactor observed over a 10m length, rates of a few events per year are calculated for a free oscillation time $\Gamma^{-1} = 10^{5}$ secs. An experiment is now being carried out at ILL, Grenoble (Baldo-Ceolin 1980). The signal due to $\bar{N}$ annihilation after dumping the beam in a target is large ($\sim$2 GeV energy release). The main background comes from cosmic rays. Of course, $\Delta B = 2$ transitions are not predicted in the sense that proton decay is predicted, and the question of their existence is an experimental one.

6. NEUTRINO MASS AND NEUTRINO OSCILLATIONS

6.1 NEUTRINO MASS MEASUREMENTS

The most sensitive way to determine the ν_e mass is to observe the end-point of tritium β-decay, an allowed transition with a maximum electron energy E_o of only 18.6 keV. The spectrum has the form

$$N(p) = \text{const. } f(z,E)\ p^2(E_o-E)\ \sqrt{(E_o-E)^2-m_\nu^2} \qquad (99)$$

where p,E are the momentum and kinetic energy of the electron, f(z,E) is the nuclear Coulomb factor which can be calculated exactly. If we plot $[N(p)/p^2f(z,E)]^{\frac{1}{2}}$ against E, a straight line should result (Kurie plot) as in Fig.58(a). For $m_\nu = 0$, the plot cuts the axis at $E=E_o$, while for finite m_ν, the plot turns over and cuts the axis vertically at $E=E_o-m_\nu$. So, in principle, the shape of the spectrum at the end-point provides a measure of m_ν. In practice, one has to fold in experimental resolution of the magnetic spectrometer, etc. which introduces a tail and makes the shape for $m_\nu=0$ and finite m_ν not so very different (Fig.58(b)).

Everything hinges on (i) counting rate (statistics) and (ii) resolution. Suppose one aims at a resolution ΔE, so one is concerned with the shape in the region $E_o-\Delta E$. Furthermore, to achieve a resolution of ΔE, the source size and thickness, magnet apertures etc. have to be matched and this introduces a further factor $(\Delta E)^2$ or $(\Delta E)^3$, so that the count rate varies as $(\Delta E)^5$ or $(\Delta E)^6$.

To try to combat the low rate near the end point, Bergkvist (1972) developed a long source with a potential difference down it, so that β particles emitted with the same energy will be accelerated by different potentials from different points on the source, and traverse different path lengths in the magnetic field, such that they will reach the same momentum slit (see Fig.59). The required potential distribution along the source is determined experimentally by use of an electron gun. The calibration and resolution of the spectrometer was determined by use of Tm^{170} γ-source, giving K-conversion electrons of unique energy (22.9 keV). From the Tm^{170} profile (determined by measuring the counting rate as a function of the Helmholtz coil current) the energy resolution was found to be ±0.12% (40eV). The source used by Bergkvist consisted of tritium gas absorbed in an aluminium substrate, and energy loss fluctuations of the electrons leaving the surface were measured to be 14 ± 5 eV,

yielding a total resolution of 55 eV.

There were many other complications in the interpretation of the experiment. For example, in the β-decay

$$H^3 \rightarrow (He^3)^+ + e^- + \nu_e \qquad (100)$$

the He^+ ion can be left in the ground (1s) state or an excited (2s) state, with an energy difference of 40.5 eV. Calculations showed that ~70% of the ions are found in the ground state. When this fact is taken into account, the effective line width is increase to 70 eV.

The ITEP experiment of Lyubimov et al (1980) the first results of which were reported in 1976 by Tretyakov et al, used a similar technique to that of Bergkvist, but the source consisted of an organic material (valine) with H^3 replacing H atoms. One of the problems with this source is that, when one triton in the valine molecule decays, the molecule breaks up and tritium atoms are released and form a background of decays in the spectrometer, proportional to the time. The resolution of the Moscow experiments was comparable with that of Bergkvist, but the source strength employed and observation time were much greater.

The Kurie plots for these two experiments are shown in Fig.60. Figs.60(a) and 60(b) are the results of Bergkvist et al and Tretyakov et al, both consistent with $m_\nu = 0$. The more recent data of Lyubimov et al is given in (c) and (d). Fig.60(c) shows the combined result of 8 out of a total of 16 runs, indicating a finite mass. For each of the 16 runs, a most probable neutrino mass was computed, and the distribution is given in Fig.60(d), together with that expected for $m_\nu = 0$ and $m_\nu = 34$ eV. These latest results appear to prove that the neutrino mass is finite and of order 40 eV.

Improvements in these experiments seems possible. For example, it is feasible to design spectrometers with intrinsic resolution of 10^{-4} (=2 eV for tritium). With such precision, gas scattering in the spectrometer becomes a problem and thus, high vacuum is needed, and this suggests the use of solid tritium sources at low temperature (2.5°K) and with correspondingly low vapour pressure. Electrostatic methods are also being investigated. But such experiments are bound to be very

difficult and to take a long time to give results.

The importance of the neutrino mass problem is not restricted to particle physics. It has profound cosmological significance. For years, it has been known that the motional kinetic energy of visible matter in the universe is an order of magnitude larger than the gravitational binding energy. However, if galaxies possess large neutrino haloes, these can correct the above mismatch if the neutrino mass is finite. Presumably in the "big bang", neutrinos were produced with similar number density to photons (the 3°K background radiation today). The observed ratio of baryons to photons is $B/\gamma \sim 10^{-9}$. So, a mass of $10^{-9} \times 1$ GeV = 1 eV for a neutrino would appreciably increase the gravitational energy from the halo. Indeed, $m_\nu \sim 40$ eV is what astrophysicists estimate is required to close the universe, converting it from one which expands indefinitely to one that may even oscillate. By the same argument values of $m_\nu > 60$ eV are ruled out because that would conflict with the fact that the universe has expanded to the present scale.

The theoretically expected values of neutrino mass or mass differences are unknown and one can only make guesses. In the electroweak SU(2) × U(1) theory, neutrinos are exclusively LH and thus, $m_\nu = 0$. This is also true in the SU(5) model of unification with minimal Higgs structure. With more complex Higgs structure, a small neutrino mass is expected (usually estimated at $\sim 10^{-5}$ eV). For the O(10) unifying group, a finite neutrino mass is expected, with a value proportional to that of the charge 2/3 quark in the same generation. For example one could have

$$m_{\nu_e} \sim 10^{-2} \text{ eV}$$
$$m_{\nu_\mu} \sim 1 \text{ eV}$$
$$m_{\nu_\tau} \sim 30 \text{ eV}$$

compared with the observed limits of < 60 eV, 1 MeV and 250 MeV respectively. In neutrino mixing, $\nu_\mu \leftrightarrow \nu_\tau$ is favoured over $\nu_\mu \leftrightarrow \nu_e$, in analogy with quark (c,s) mixing.

6.2 NEUTRINO OSCILLATIONS

The possibility that lepton number is not conserved, and that one type of neutrino (say ν_e) could oscillate into another type (say ν_μ) was proposed long ago by Pontecorvo (1968) and Maki (1962). Considered as something of a curiousity at that time, it later received considerable impetus from the so-called solar neutrino problem. More recently, with the development of interest in gauge theories, it was realised that there were no good theoretical reasons for believing that baryon and lepton number should be conserved.

The theoretical treatment of neutrino oscillations is an almost exact analogue of the temporal development of a neutral kaon beam. Neutrino mass eigenstates with well defined proper frequency are denoted $\nu_i (i=1,2,3.....)$. The weak interaction eigenstates are denoted ν_α (where $\alpha=e,\ \mu,\ \tau.....$) and they are superpositions of the mass eigenstates. If the total lepton number $L = L_e+L_\mu+L_\tau+.....$ is conserved, the two are related by a unitary transformation

$$|\nu_\alpha\rangle = U_{\alpha i}\ |\nu_i\rangle \tag{101}$$

where $U_{\alpha i}$ is a unitary matrix, and the probability of the transformation $\nu_\alpha \leftrightarrow \nu_\beta$ is given by

$$P|\nu_\alpha \rightarrow \nu_\beta\ | = |\sum_{i=1}^{i=n} U_{\alpha i}\ U^{\dagger}_{\beta i}\ \exp(-iE_i t)|^2 \tag{102}$$

where $E_i = p + m_i^2/2p$.

If the states ν_i are to be spatially coherent, they must be eigenstates of the momentum operator, so that they have energies which are slightly different, depending on the mass m_i, and where we assume $m_i << p$.

In order to illustrate the main features of the oscillation phenomenon, let us consider the simplest case of two types of neutrino, say ν_e and ν_μ. Then U is a 2×2 matrix which can be specified by one parameter, the mixing angle

$$\begin{pmatrix} \nu_\mu \\ \nu_e \end{pmatrix} = \begin{pmatrix} \cos\Theta & \sin\Theta \\ -\sin\Theta & \cos\Theta \end{pmatrix} \begin{pmatrix} \nu_1 \\ \nu_2 \end{pmatrix} \tag{103}$$

where

$$\nu_1(t) = \nu_1(0)\ e^{-iE_1 t}$$

$$\nu_2(t) = \nu_2(0)\, e^{-iE_2 t} \tag{104}$$

$$E_{1,2} = p + \frac{m^2_{1,2}}{2p}$$

Let us start with $\nu_\mu(0)=1$ and $\nu_e(0)=0$ at t=0. So inverting (103) we get

$$\nu_2(0) = \nu_\mu(0)\ \sin\theta$$

$$\nu_1(0) = \nu_\mu(0)\ \cos\theta \tag{105}$$

and from (103) and (104)

$$\frac{\nu_\mu(t)}{\nu_\mu(0)} = \cos^2\theta\, e^{-iE_1 t} + \sin^2\theta\, e^{-iE_2 t}$$

$$\frac{I_\mu(t)}{I_\mu(0)} = \left|\frac{\nu_\mu(t)}{\nu_\mu(0)}\right|^2 = \cos^4\theta + \sin^4\theta + \sin^2\theta\cos^2\theta[e^{i(E_2-E_1)t} + e^{-i(E_2-E_1)t}]$$

$$= 1 - \frac{\sin^2 2\theta}{2}\,[1 - \cos(E_2-E_1)t]$$

$$1 - \sin^2 2\theta.\sin^2\left[\frac{(E_2-E_1)t}{2}\right] \tag{106}$$

If we write $(E_2-E_1) = \Delta m^2/2p$ where $\Delta m^2 = m_2^2 - m_1^2$ is the difference in mass squared, $p=E/c$ where E is the average energy, L the distance over which the beam has evolved, then

$$P(\nu_\mu \to \nu_e) = 1 - P(\nu_\mu \to \nu_\mu)$$

$$= \sin^2 2\theta.\sin^2\left(\frac{\Delta m^2 L}{4E}\right) \tag{107}$$

$$= \sin^2 2\theta.\ \sin^2\left(\frac{1.27\ \Delta m^2 L}{E}\right) \tag{108}$$

In (108), the numerical constant is that which applies if Δm^2 is in $(eV/c^2)^2$, L

is in metres and E in MeV. Eqn.(108) shows that the relative intensity of ν_e and ν_μ oscillates with an amplitude depending on the mixing angle θ and a frequency or wavelength depending on the mass difference. This variation is shown in Fig.61. The crucial quantity is $\Delta m^2 L/E$, which must be greater than 0.25 if oscillating effects above the 10% level are to occur. In all practical experiments, one is dealing with a beam of neutrinos with an energy spread. Thus, if $\Delta m^2 L/E \gg 1$, the spectrum - averaged result in the case of 2 neutrinos would lead to an effective value $\langle P/\sin^2 2\theta \rangle = 0.5$.

The case of an arbitrary number n of neutrino states is more complicated. Usually it is assumed that one mass difference, and hence one oscillation frequency, dominates, when a formula like (108) will again hold, except that the coefficient outside the oscillating term is a product of mixing angles. In the limit $\Delta m^2 L/E \gg 1$, the spectrum - integrated intensity of any one component ν_α will have an average value 1/n, if there are n types of neutrino in total.

Oscillation experiments can in principle be done with various sources. In the following table, we list these, together with the typical observation lengths L which can be achieved, and the typical mass differences to which they are sensitive (assuming the best possible experimental conditions, small statistical errors or large mixing angles):

Table 6.1 Sensitivity for Various Neutrino Sources

Source	Mean energy	L(m)	Lower limit on Δm(eV)
Solar ν_e	100 keV	10^{11}	10^{-6}
Atmospheric ($\phi_{\nu_\mu} \sim 2\phi_{\nu_e}$)	0.5 GeV	10^7	10^{-3}
Reactors $\bar{\nu}_e$	3 MeV	10	10^{-1}
Meson Factories (ν_μ, ν_e)	30 MeV	10-100	10^{-1}
Accelerators (ν_μ)	1-30 GeV	10^2-10^4	10^{-1}

The atmospheric neutrinos are generated by cosmic rays, and as indicated previously, the reaction rate is about 0.2 $ton^{-1}\ yr^{-1}$. Using the earth's diameter as the oscillation distance, one could for example observe any asymmetry of events containing muons, upwards as compared with downwards. Even for a 1000 ton detector operated for several years, it would be difficult to establish any oscillations of amplitude <10%. It is a useful fall-back possibility for nucleon decay detectors, since no artificial sources could match the mass resolution attainable.

6.3 REACTOR EXPERIMENTS

Nuclear reactors are a prolific source of antineutrinos $\bar{\nu}_e$, and the effect of any oscillations ($\nu_e \rightarrow \nu_\mu, \nu_\tau \ldots$) would be to reduce the number of charged-current $\bar{\nu}_e$ reactions (e.g. $\bar{\nu}_e + p \rightarrow n + e^+$) but to leave the number of neutral-current reactions ($\bar{\nu}_e, \bar{\nu}_\mu, \bar{\nu}_\tau + d \rightarrow n + p + \bar{\nu}_e, \bar{\nu}_\mu, \bar{\nu}_\tau$) unchanged. Since the reactor spectrum extends only to a few MeV energy, any $\bar{\nu}_\mu$ or $\bar{\nu}_\tau$ particles will be below threshold for the charged-current process. Therefore, experimental evidence for oscillations depends on comparison of the absolute number of charged-current reactions with that expected in absence of oscillations, or on measurement of the ratio of charged to neutral current cross-sections and comparison with theory, for which all the required parameters are well known. Because of the low neutrino energy (2-6 MeV), and the source-detector distances employed (5-10m), these experiments are sensitive to mass differences $\Delta m^2 \sim 0.1 (eV/c^2)^2$.

The Irvine experiment at the Savannah River Reactor (Reines et al 1980) employed a deuterium target and He^3-filled neutron counters to detect the charged and neutral current reactions,

		$E_{(threshold)}$	
CC	$\bar{\nu}_e + d \rightarrow n + n + e^+$	4 MeV	(109)
NC	$\bar{\nu}_e + d \rightarrow n + p + \bar{\nu}_e$	2.2 MeV	(110)

Note the difference in threshold energies, and recall that the reactor spectrum peaks at ~0.5 MeV and falls off very rapidly with increasing energy. The expected

ratio of the two reaction rates must depend on the shape of the spectrum. Reines et al observed a spectrum-averaged ratio at L=11m:-

$$r_{expt} = \frac{\bar{\sigma}\ (CC)}{\sigma\ (NC)} = 0.167 \pm 0.093 \qquad (111)$$

compared with the expected numbers (in absence of oscillations)

$$r_{th} = 0.42 \quad \text{(Avignone)}$$
$$= 0.44 \quad \text{(Davis-Vogel)} \qquad (112)$$

where the two estimates correspond to slightly different forms calculated for the spectrum. Thus the ratio of ratios

$$R = \frac{r_{expt}}{r_{theory}} = 0.40 \pm 0.22 \quad \text{(Avignone)}$$
$$= 0.38 \pm 0.21 \quad \text{(Davis-Vogel)} \qquad (113)$$

significantly less than unity, and claimed as evidence in favour of oscillations, with $\Delta m^2 \sim (1eV/c^2)^2$.

Another reactor experiment has been carried out at the ILL (Grenoble) reactor (Boehm et al 1980) in which the observed rate for the reaction

$$\bar{\nu}_e + p \rightarrow n + e^+ \qquad (114)$$

was compared with that expected theoretically. In this case, the products are detected by a two-fold delayed coincidence of the γ-rays from e^+ annihilation and those from neutron capture in gadolinium. With L=8.7m they find, averaged over the spectrum

$$\frac{\sigma_{exp}}{\sigma_{th}} = 0.87 \pm 0.14 \quad \text{(Davis - Vogel)} \qquad (115)$$

consistent with the unity value expected in absence of oscillations. The ratio (115) as a function of energy is shown in Fig.62. Boehm et al deduce from these results $\Delta m^2 < 0.15 (eV/c^2)^2$, assuming maximal mixing.

The results (113) and (115) are not compatible - see Fig.63 - and it is clear that more experiments are required, and additionally better information on the spectrum. So far, spectra have all been calculated assuming a plausible model for the fission fragment distribution; recently, direct observations of the β spectrum from fission fragments have been carried out and preliminary results support the Davis - Vogel fluxes.

6.4 COSMIC AND SOLAR NEUTRINO EXPERIMENTS

Other evidence quoted in favour of neutrino oscillations comes from cosmic ray and solar neutrino observations.

In deep underground experiments, the Case-Witts-Irvine collaboration (Crouch et al 1978) and the India-Japan-Durham collaboration (Krishnaswamy et al 1971) compared the absolute rate of charged-current events produced by muon neutrinos generated by pion, kaon decay in the atmosphere with that expected from cross-sections measured at accelerators. The events occurred in rock surrounding the detectors, which only observed the secondary muons (differentiated from atmospheric muons by a zenith angle cut, $\theta > 45°$). The observed rates were somewhat smaller than expected. For example, Crouch et al found

$$\frac{\bar{\sigma}(\text{predicted})}{\bar{\sigma}(\text{observed})} = 1.60 \pm 0.4$$

However, since what is observed are muons produced in rock by a neutrino flux which is not known to better than 30%, from which atmospheric muon effects have to be subtracted, any discrepancy between the above result and the unit value can hardly be significant.

Oscillations have also been suggested to account for the discrepancy between the observed and expected solar neutrino flux (Bahcall and Frautschi 1969). The Davis experiment (Davis et al 1978) relies for detection on the reaction $\nu_e + Cl^{37} \rightarrow Ar^{37} + e^-$ which is above threshold for neutrinos from the main reaction ($p+p \rightarrow d+e^+ + \nu_e$) and relies on those from β decay of Be^7 and B^8 made in side

reactions. The standard solar model predicts a rate of 7.8 ± 1.5 SNU (solar neutrino units) compared with an observed rate of 2.2 ± 0.4 SNU. The solution to this discrepancy has to await the development of gallium and indium detectors sensitive to the pp reaction, and it is quite wrong to conclude that the "solar neutrino problem" is yet evidence for neutrino oscillations.

6.5 MESON FACTORY EXPERIMENTS

Meson factories generate intense low energy pion beams (no kaons) and produce reactions via the decays at rest

$$\pi^+ \to \mu^+ + \nu_\mu \tag{116}$$

$$\mu^+ \to e^+ + \nu_e + \bar{\nu}_\mu \tag{117}$$

The experimental approach at LAMPF (Willis et al 1980) was to use a 6 ton water Cerenkov counter to detect relativistic electrons ($e^{\pm}$) from the possible charged-current reactions

$$\left.\begin{aligned} \nu_e d &\to ppe^- \\ \bar{\nu}_e d &\to nne^+ \end{aligned}\right\} \quad D_2O \tag{118, 119}$$

$$\bar{\nu}_e p \to ne^+ \qquad H_2O \tag{120}$$

If no oscillations occur, then from (117) only the reaction (118) is allowed. Hence, one expects a signal from D_2O but none from H_2O. They measured

$$R_{H_2O} = \bar{\nu}_e/\mu^+ \text{ decay} = -0.001 \pm .061 \tag{121}$$

and put a limit $\Delta m^2 < 0.9(\text{eV})^2$ for the transition $\bar{\nu}_\mu \leftrightarrow \bar{\nu}_e$. From the heavy water they found

$$R_{D_2O} = \nu_e/\mu^+ \text{ decay} = 1.1 \pm 0.4 \tag{122}$$

Assuming CP invariance, (121) shows that $\nu_\mu \leftrightarrow \nu_e$ is excluded, so that the result (122) then sets limits on mixing $\nu_e \leftrightarrow \nu_\tau$, with $\Delta m^2 < 2.6(\text{eV})^2$. However, the errors are such that this result is only valid of the mixing is large, with $\sin^2 2\theta > 0.3$.

6.6 HIGH ENERGY ACCELERATORS

The results from high energy accelerators as well as the meson factory experiment, are summarized in Table 6.2. The beams from high energy accelerators are formed from sign-selected pion, and to a lesser extent kaon, decay in flight. They are dominantly ν_μ or $\bar{\nu}_\mu$ with a small admixture, typically 0.5%, of ν_e, $\bar{\nu}_e$ from Ke3 decay. Thus, they are very sensitive to the transition $\nu_\mu \leftrightarrow \nu_e$, since even a 1% effect would double the number of charged current ν_e events with electron secondaries.

In experiments to data - not optimized for detecting oscillations but for maximum flux - the distances L from the source to the detector have been determined by the amount of earth or steel required to absorb background muons, which is proportional to the muon energies in pion decays in flight, and hence to the neutrino beam energy. Hence L/E is practically the same in all PS, SPS or FNAL experiments. In future experiments, L/E values can be 1-2 orders of magnitude larger.

The second entry in Table 6.2 relating to Gargamelle experiments at the CERN PS several years ago, still provides the most stringent limits on the amplitude squared for the transition $\nu_\mu \leftrightarrow \nu_\tau$ or $\nu_e \leftrightarrow \nu_\tau$. Since the tau neutrinos were below threshold for the charged current reaction

$$\nu_\tau + N \rightarrow \tau^- + X \tag{123}$$

the oscillation $\nu_\mu \leftrightarrow \nu_\tau$ might be detected as a decrease in the absolute number of charged current ν_μ events. But this absolute number is determined by fluxes and structure function integrals and cannot be computed from first principles.

The 15' bubble chamber experiments at FNAL relied on a comparison of the observed ratio of charged current events containing electron and muon secondaries, with that computed from the ν_e and ν_μ fluxes in the absence of oscillations. The reaction (123) results in (almost prompt) electron secondaries through the decay

$$\tau^- \rightarrow e^- + \bar{\nu}_e + \nu_\tau \tag{124}$$

with a 15% branching ratio. The observed e^-/μ^- ratio in neutrino running then sets the limit quoted. For antineutrino reactions, a better limit can be obtained, since in the charged current reaction

$$\bar{\nu}_e + N \rightarrow e^+ + X$$

the positron retains the bulk of the energy (the distribution varies as $dN/dy \propto (1-y)^2$ where $(1-y) = E_{e^+}/E_{\bar{\nu}}$). On the other hand production of τ^+ and subsequent decay as in (124) results in lower energy positrons. Hence, the low y events are very sensitive to a small $\bar{\nu}_\tau$ admixture. These, and the CERN SPS experiments, find no evidence for the transitions $\nu_\mu \leftrightarrow \nu_\tau$, but are only sensitive to mass differences such that $\Delta m^2 > 5(eV)^2$.

Lastly, absolute calculations of ν_e charged-current rates (based on e-μ universality and the known ν_μ cross-sections) are sensitive to the transition $\nu_e \leftrightarrow \nu_\tau$. The most reliable limit is set by a BEBC SPS experiment with a narrowband neutrino beam, where the ν_e flux from Ke3 decay was known to within 7%. Based on 70 e^- events, the experiment found $P(\nu_e \rightarrow \nu_e) = 1.04 \pm 0.15$. Because of the limited statistics and the beam energy, it would be sensitive only to $\Delta m > 7$ eV and mixing amplitudes, squared, exceeding 20%.

If we, optimistically, accepted a mass of order 30eV for ν_τ as proposed by cosmologists, and smaller masses for ν_μ and ν_τ, then the Δm^2 limits of present experiments are not important for the transition $\nu_e \leftrightarrow \nu_\tau$, or $\nu_\mu \leftrightarrow \nu_\tau$ and we could conclude that the mixing angles are small ($\theta < 0.2$ radians). If we make no assumptions about masses, then it seems that future progress will depend on

i) Accelerator experiments with much higher statistics, better-measured fluxes and with larger values of L/E. However, regarding the last, only one order of magnitude could be obtained on the limiting value of Δm^2 ($<0.1(eV)^2$). Such experiments are our best hope if mixing angles are small (say of order the Cabibbo angle). A number of such experiments are planned for the future.

ii) Experiments without accelerators, using the naturally occurring solar and atmospheric neutrinos and the large base lines provided by the size of the Earth or Earth-Sun distance. These would be sensitive to very small Δm^2 values but large mixing amplitudes would be required because event rates are inevitably low.

Table 6.2 Accelerator Oscillation Experiments

Experiment	$\bar{E}$	Test	$P(\nu_\alpha \to \nu_\beta)$ 90% CL or rate	(L/E) m MeV^{-1}	Δm^2(90%CL, $\Theta=\pi/4$)
LAMPF (Willis et al 1980)	50 MeV	$\bar{\nu}_\mu \to \bar{\nu}_e$	<0.10	0.3	<0.9 (eV)^2
GGM PS (Blietschau et al 1978)	2 GeV	$\nu_\mu \to \nu_e$	<.0013	0.02	<1 (eV)^2
		$\bar{\nu}_\mu \to \bar{\nu}_e$	<.0014		<1 (eV)^2
FNAL 15' νNe (Cnops et al 1978)	30 GeV	$\nu_\mu \to \nu_\tau$	<.025	0.01	<6 (eV)^2
$\bar{\nu}$Ne (Roe 1980)	30 GeV	$\bar{\nu}_\mu \to \bar{\nu}_\tau$	<.0075	0.01	<6 (eV)^2
ν Emulsion (Kondo et al 1980)	30 GeV	$\nu_\mu \to \nu_\tau$	<.013	0.01	<3.5 (eV)^2
BEBC SPS NBB (Deden et al 1981)	80 GeV	$\nu_\mu \to \nu_e$	<.005	0.01	<55 (eV)^2
GGM SPS WBB (Armenise et al 1981)	30 GeV	$\nu_\mu \to \nu_e$	<.004	0.01	<2 (eV)^2
		$\nu_\mu \to \nu_\tau$	<.03	0.01	<10 (eV)^2
LAMPF	50 MeV	$\nu_e \to \nu_e$	1.1 $\pm$ 0.4		<2.6 (eV)^2
GGM PS	2 GeV	$\nu_e \to \nu_e$	0.92 $\pm$ 0.21		<1 (eV)^2
BEBC SPS	80 GeV	$\nu_e \to \nu_e$	1.04 $\pm$ 0.15		55 (eV)^2

REFERENCES

Altarelli G. and Parisi G. Nucl.Phys. B126, 298 (1977).

Anderson H. et al Phys.Rev.Lett. 40, 1061 (1978).

Anderson K.J. et al Proc. XIX Int. Conf. High Energy Physics, Tokyo (1978).

Armenise N. et al CERN EP/80-226 (1980).

Aubert J.J. et al Proc. XX Int. Conf. High Energy Physics, Madison, Wisc. (1980a).

Aubert J.J. et al CERN EP/81-10 (1981).

Bahcall J. and Frautschi S.C. Phys.Lett. 29B, 623 (1969).

Baldo-Ceolin M. 7th Trieste Conf. on Particle Physics, (May 1980).

Barber D.P. et al Phys.Rev.Lett. 43, 830 (1979).

Barber D.P. et al Aachen PITHA 81/07 (1981).

Bartel W. et al Phys.Lett. 99B, 281 (1981).

Bergkvist K.E. Nucl.Phys. B39, 317 (1972).

Blietschau J. et al Phys.Lett. 87B, 281 (1979).

Blietschau J. et al Nucl.Phys. B133, 205 (1978).

Boehm F. et al Phys.Lett. 97B, 310 (1980).

Bollini D. et al CERN EP/81-58 (1981).

Bosetti P. et al Nucl.Phys. B140, 1 (1978).

Brandelik R. et al Phys.Lett. 86B, 243 (1979).

Brandelik R. et al DESY 80/80 (1980).

Bures A.J. and Gaemers K.J. Nucl.Phys. B132, 249 (1978).

Callan C.G. and Gross D.G. Phys.Rev.Lett. 22, 156 (1969).

Cnops A.M. et al Phys.Rev.Lett. 40, 144 (1978).

Crouch M.F. et al Phys.Rev. D18, 2239 (1978).

Davis R. et al Phys.Rev.Lett. 20, 1205 (1968).

Davis P., Evans S.C. and Cleveland B.T., Proc. Neutrino Conf., Purdue (1978).

Deden H. et al Nucl.Phys. B149, 1 (1979).

Deden H. et al Phys.Lett. 98B, 310 (1981).

Fisele F., Proc. Neutrino Conf. '80, Erice (1980).

Ellis J., Gaillard M.K., Nanopoulos D.V. and Rudaz S., CERN TH/2833 (1980).

Ellis J. and Karliner M., Nucl.Phys. B148, 141 (1979).

Glück M. and Reya E., Nucl.Phys. B156, 456 (1979).

Grant A. CERN EP/ALG (1979).

de Groot J.G.H. et al Zeit Physik C1, 143 (1979).

Hennecke E.W. et al, Phys.Rev. C11, 1378 (1975).

Jonker M. et al Phys.Lett. 99B, 265 (1981).

Kondo T. et al FERMILAB - Conf - 80/92 - EXP.

Krishnaswamy M.R. et al Proc.Roy.Soc. A323, 489 (1971).

Langacker P. et al Proc. Neutrino Conf. '79, Bergen, p.276 (1979).

Learned J., Reines F., and Soni A. Phys.Rev.Lett. 43, 907 (1979).

Liede I. and Roos M., Nucl.Phys. B167, 397 (1980).

Lyubimov V.A. et al Phys.Lett. 94B, 266 (1980).

Marshak R.E. and Mohapatra R.N. Phys.Lett. 91B, 222 (1980); Phys.Rev.Lett. 44, 1316 (1980).

Maki Z. et al Prog.Th.Phys. 28, 870 (1962).

Menon M.G.K. Proc. Neutrino Conf., Aachen (1976).

Pontecorvo B. Sov.Phys. JETP 26, 984 (1968).

Prescott C.J. et al Phys.Lett. 77B, 347 (1978).
ibid. 84B, 524 (1979).

Reines F., Sobel H.W. and Pasierb E., Phys.Rev.Lett. 45, 1307 (1980).

Roe B.P. (FIMS collaboration) private communication (1980).

Steinberg R. and Evans J. Proc. Neutrino Conf. '77 Vol.2, 321 (1977).

Tretyakov E.F. et al Proc. Neutrino Conf. '76, Aachen (1976).

Wahl H. Proc. Int. Conf. High Energy Physics., Lisbon (1981).

Wiik B. DESY 80/124 (1980); also G. Wolf DESY 80/13 (1980) and P.Duinker DESY 81/012 (1981).

Willis S.E. et al, Phys.Rev.Lett. 44, 522 (1980).

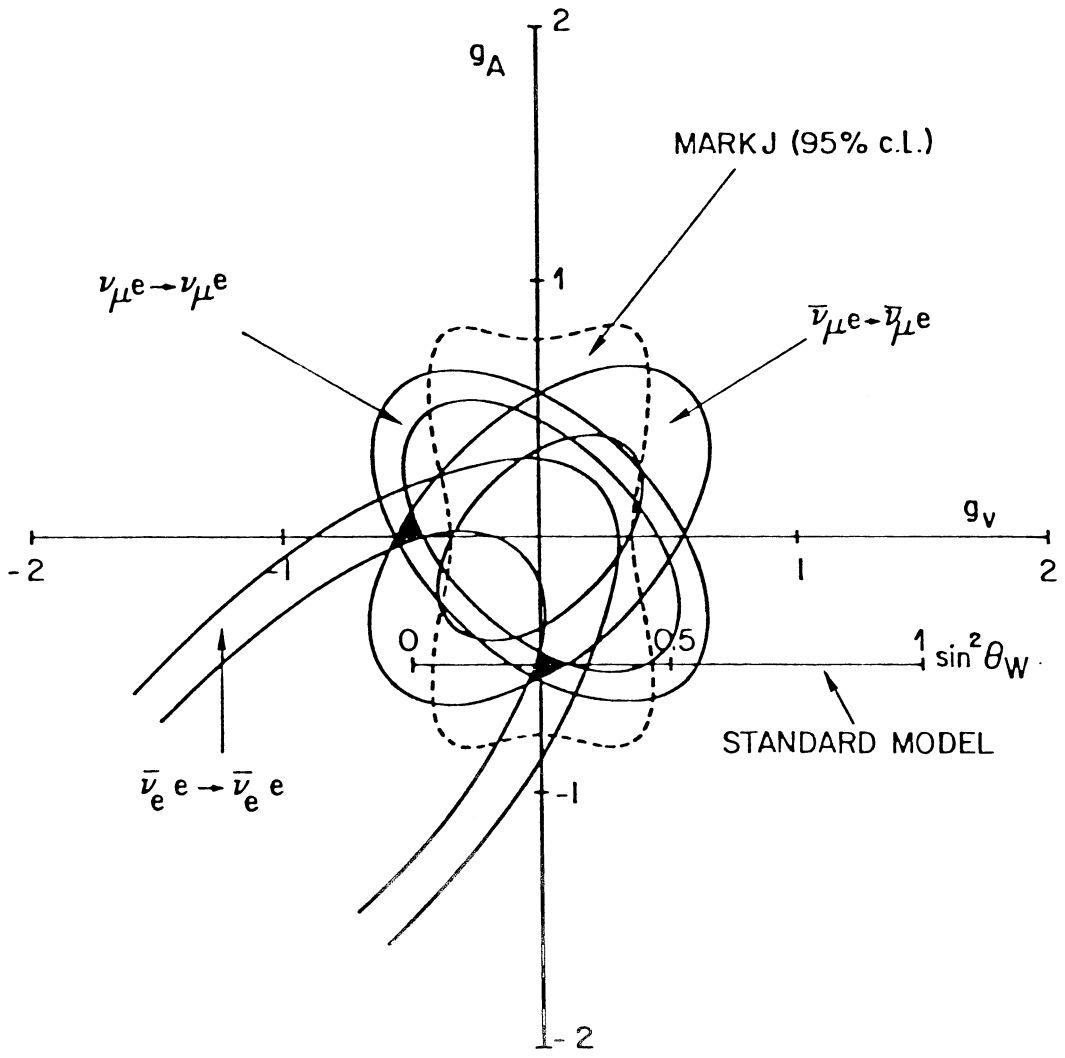

Fig.3 Elliptical contours in the g_A, g_V plane from the measured cross-sections for ν_μ, $\bar{\nu}_\mu$ and $\bar{\nu}_e$ scattering from electrons. The two possible solutions are shown by the black overlap areas. One of these is excluded by the observations of $e^+e^- \to \ell^+\ell^-$ at PETRA by the Mark J group.

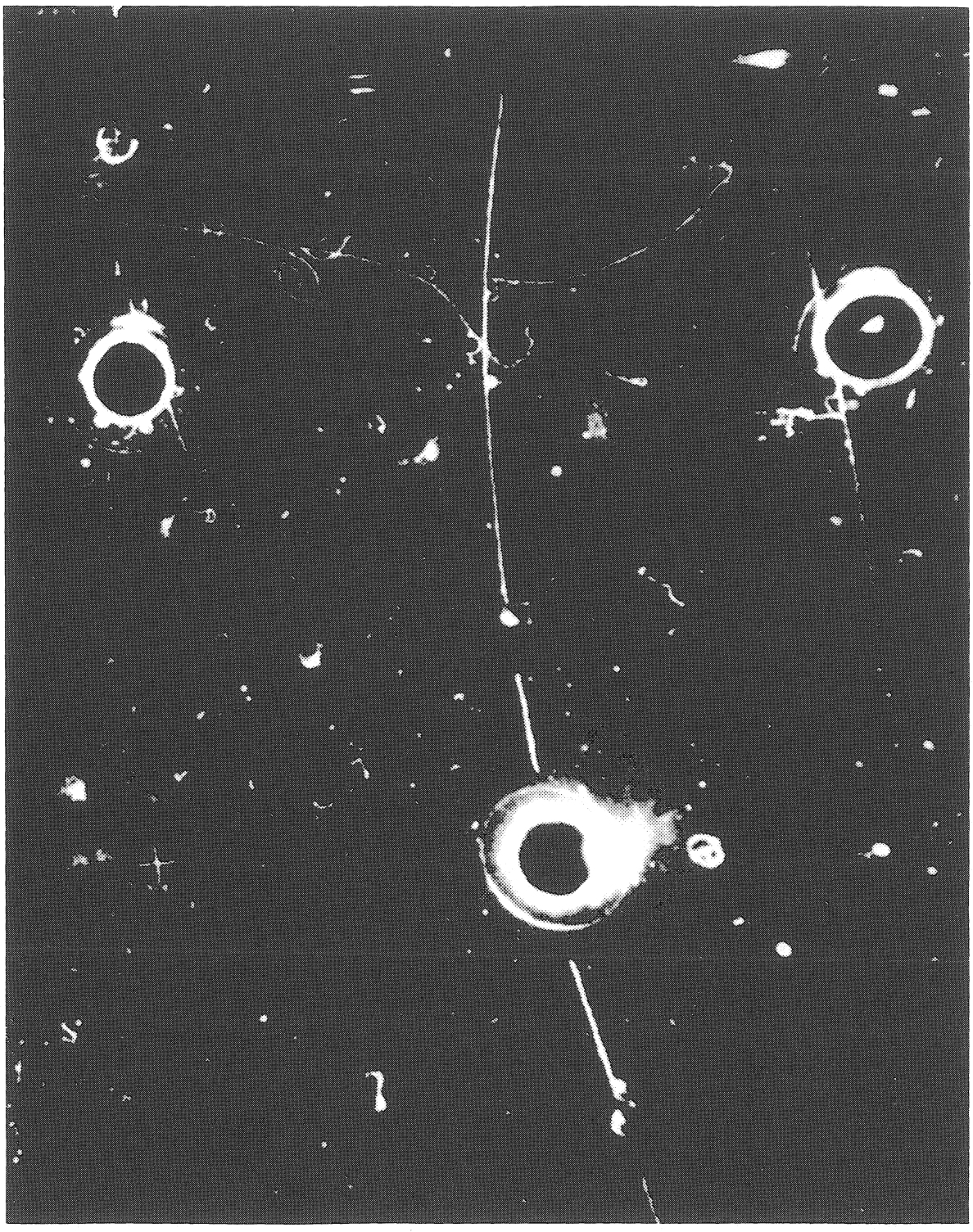

Fig.4 First historic observation (Dec. 1972) of the process $\bar{\nu}_\mu + e^- \rightarrow \bar{\nu}_\mu + e^-$ in the Gargamelle chamber in the CERN PS neutrino beam, incident from the left in the picture. The single recoil electron has energy 300 MeV and is emitted at $\theta < 3°$ to the beam.

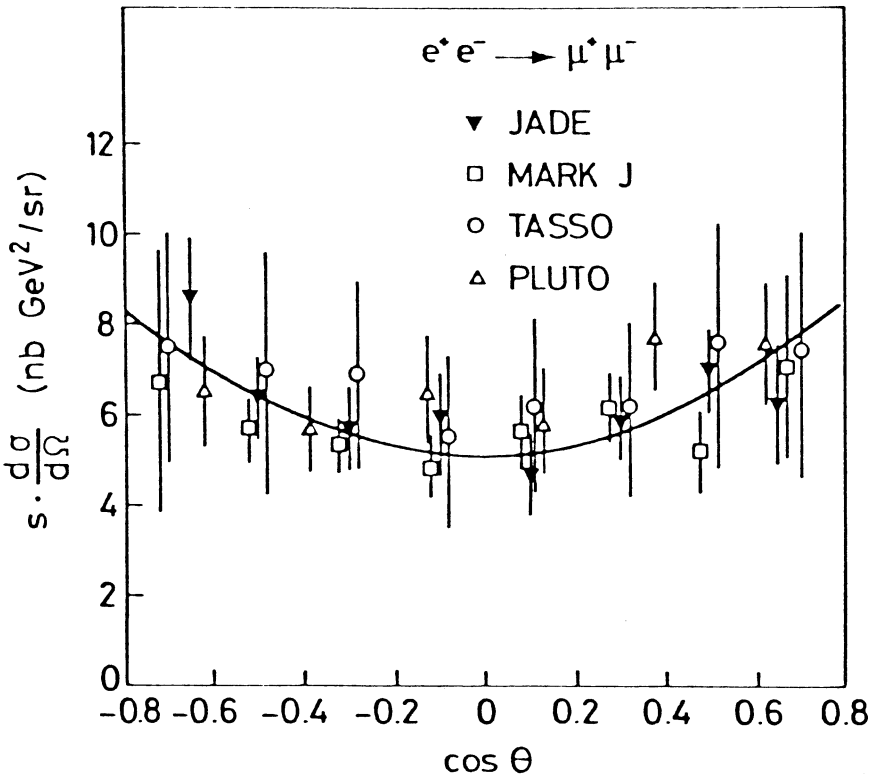

Fig.5 Data from PETRA on the angular distribution for $e^+e^- \to \mu^+\mu^-$. The curve is the pure QED prediction $(1+\cos^2\theta)$. After Wiik (1980).

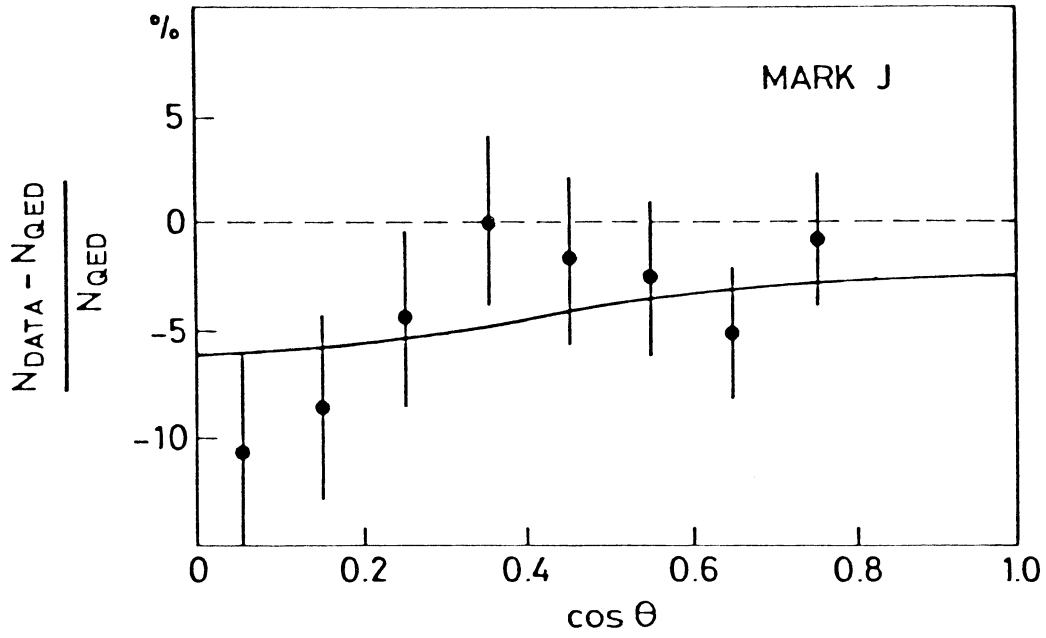

Fig.6 Mark J data on Moller $(e^+e^- \to e^+e^-)$ scattering. The curve is the electroweak prediction for $\sin^2\theta_W = 0.23$. (Barber et al 1981).

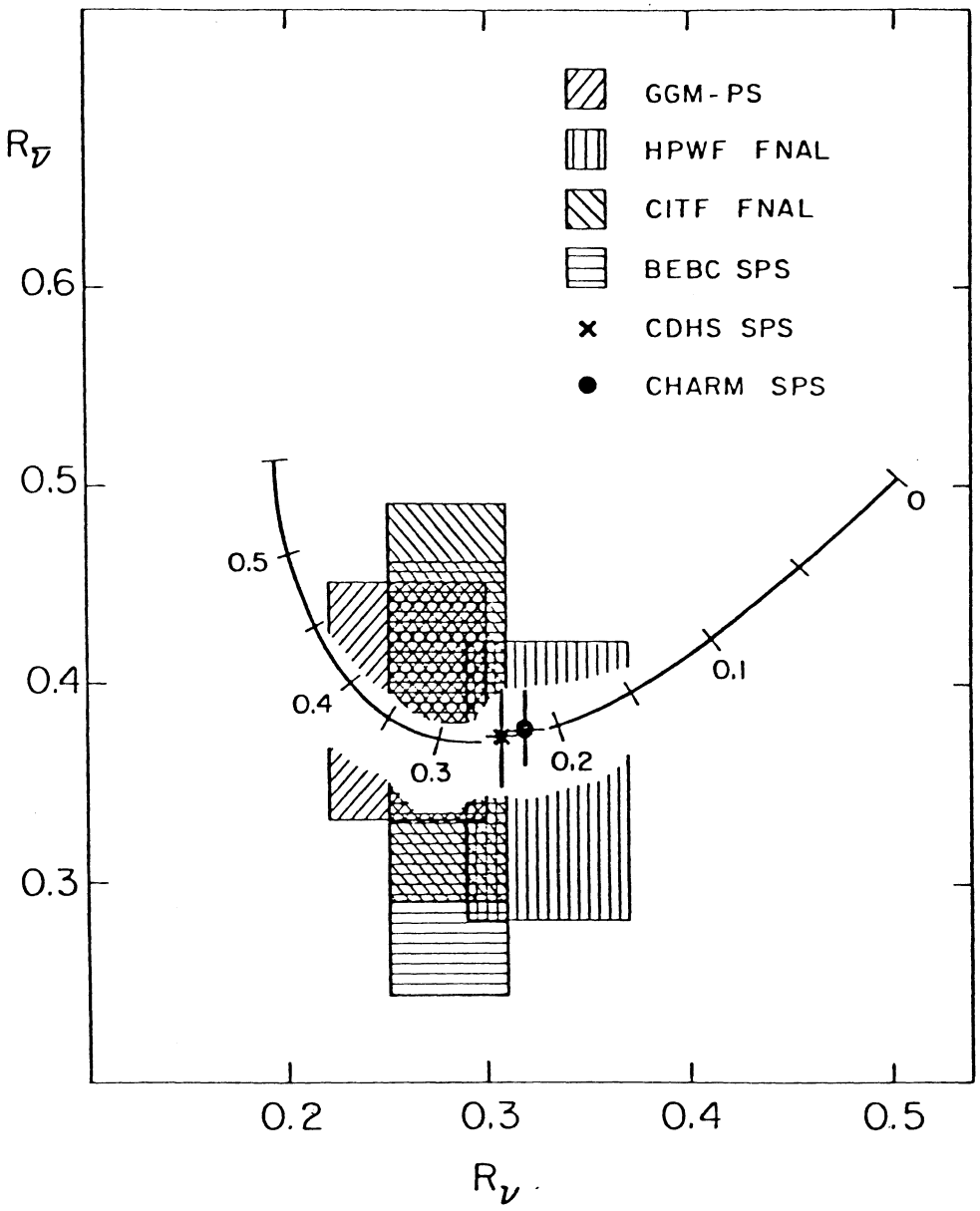

Fig.7 Results on R_ν and $R_{\bar{\nu}}$ from various neutrino experiments, together with the electroweak prediction.

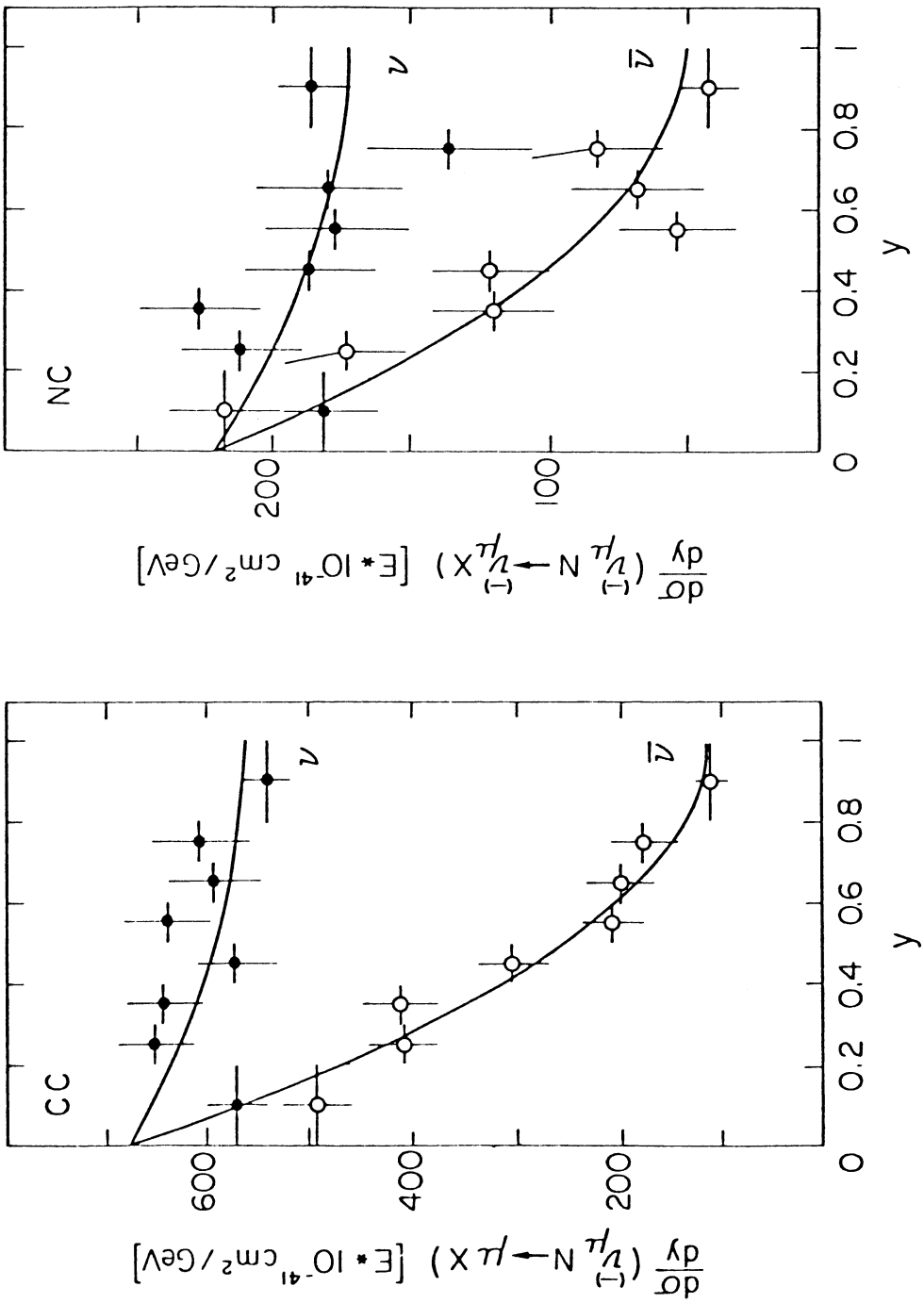

Fig.8 Charged and neutral current y-distributions from CHARM neutrino experiment at CERN SPS (Jonker et al 1981).

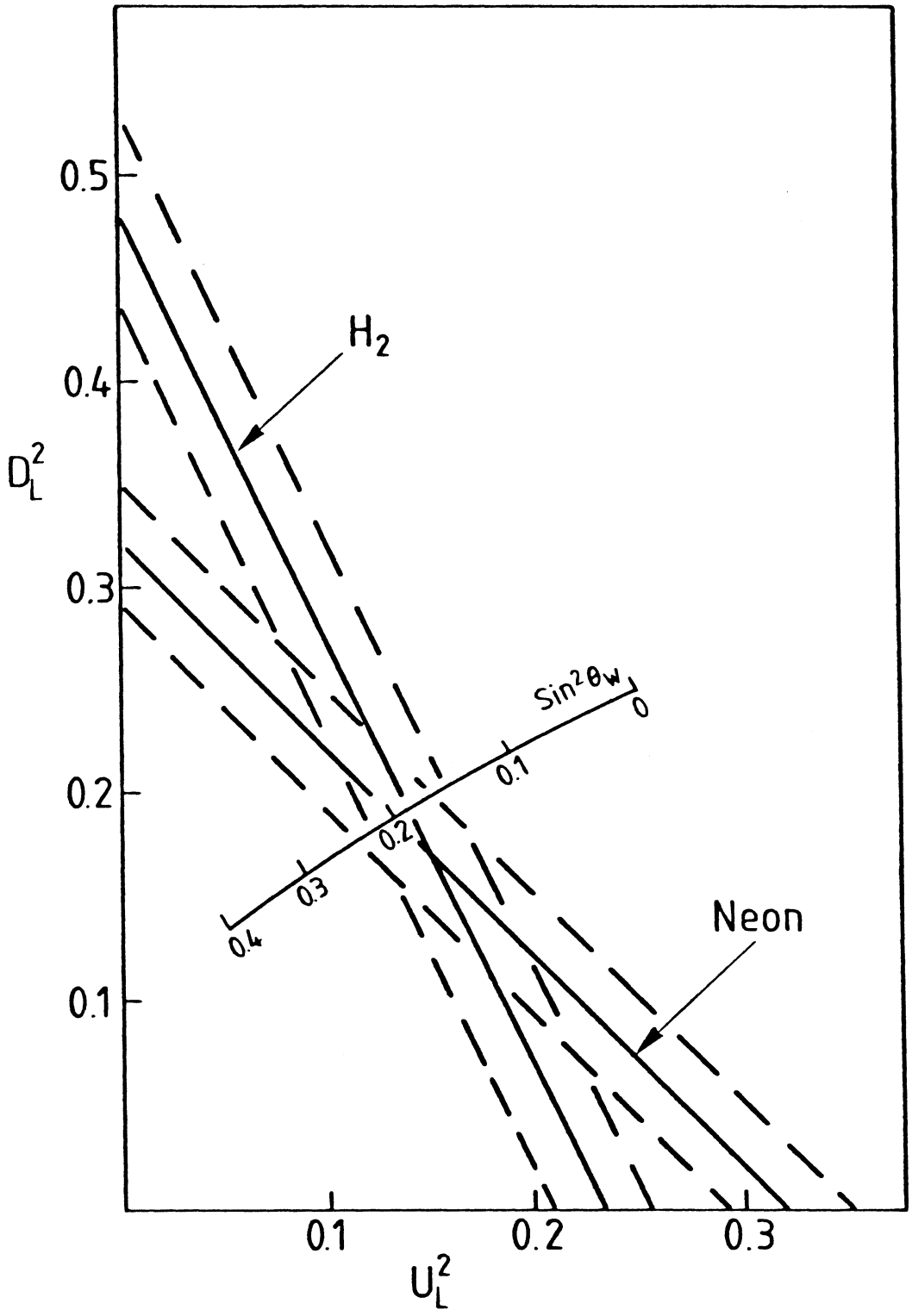

Fig.9 Relations between D_L^2 and U_L^2 from the BEBC neutrino experiments in hydrogen and neon. They yield a value $\sin^2\theta_W \simeq 0.20$. (Blietschau et al 1979).

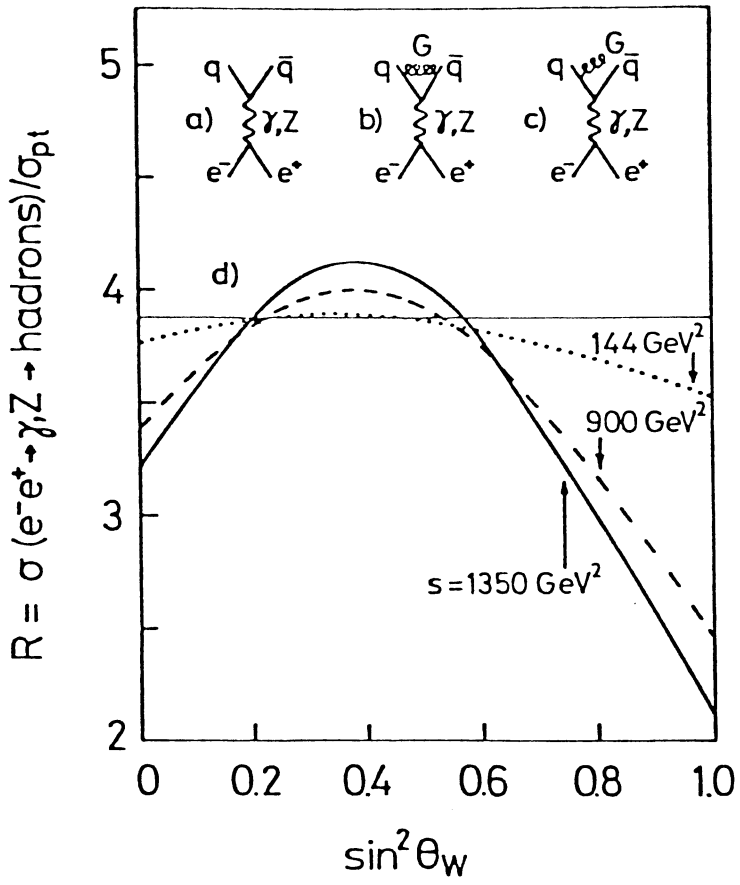

Fig.12 Variation with $\sin^2\theta_W$ of the ratio of σ ($e^+e^- \to$ hadrons) to the pointlike cross-section, as expected from the standard electroweak quark couplings, for 3 values of s. (Bartel et al 1981).

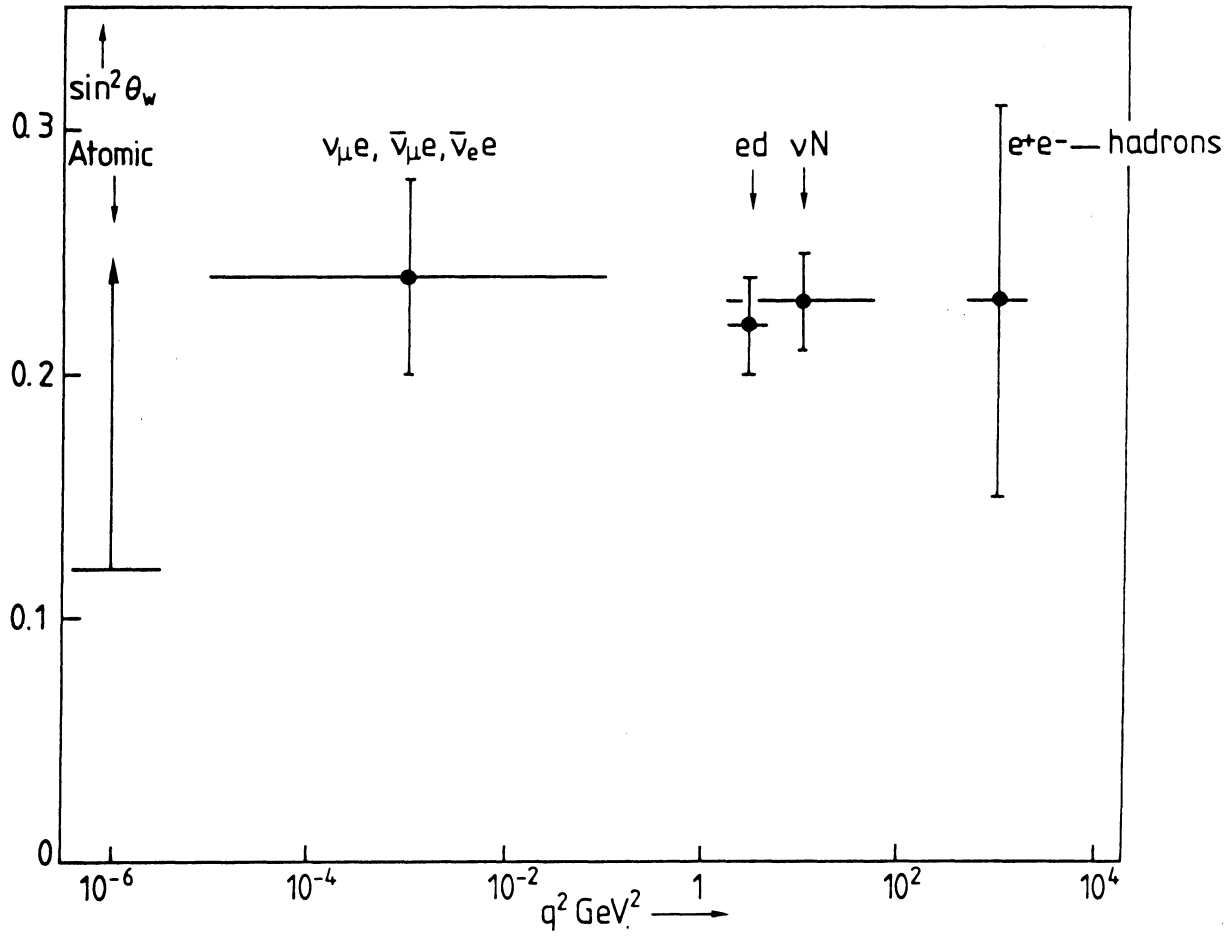

Fig.13 Summary of determinations of $\sin^2\theta_W$ as a function of $|q^2|$, from various experiments.

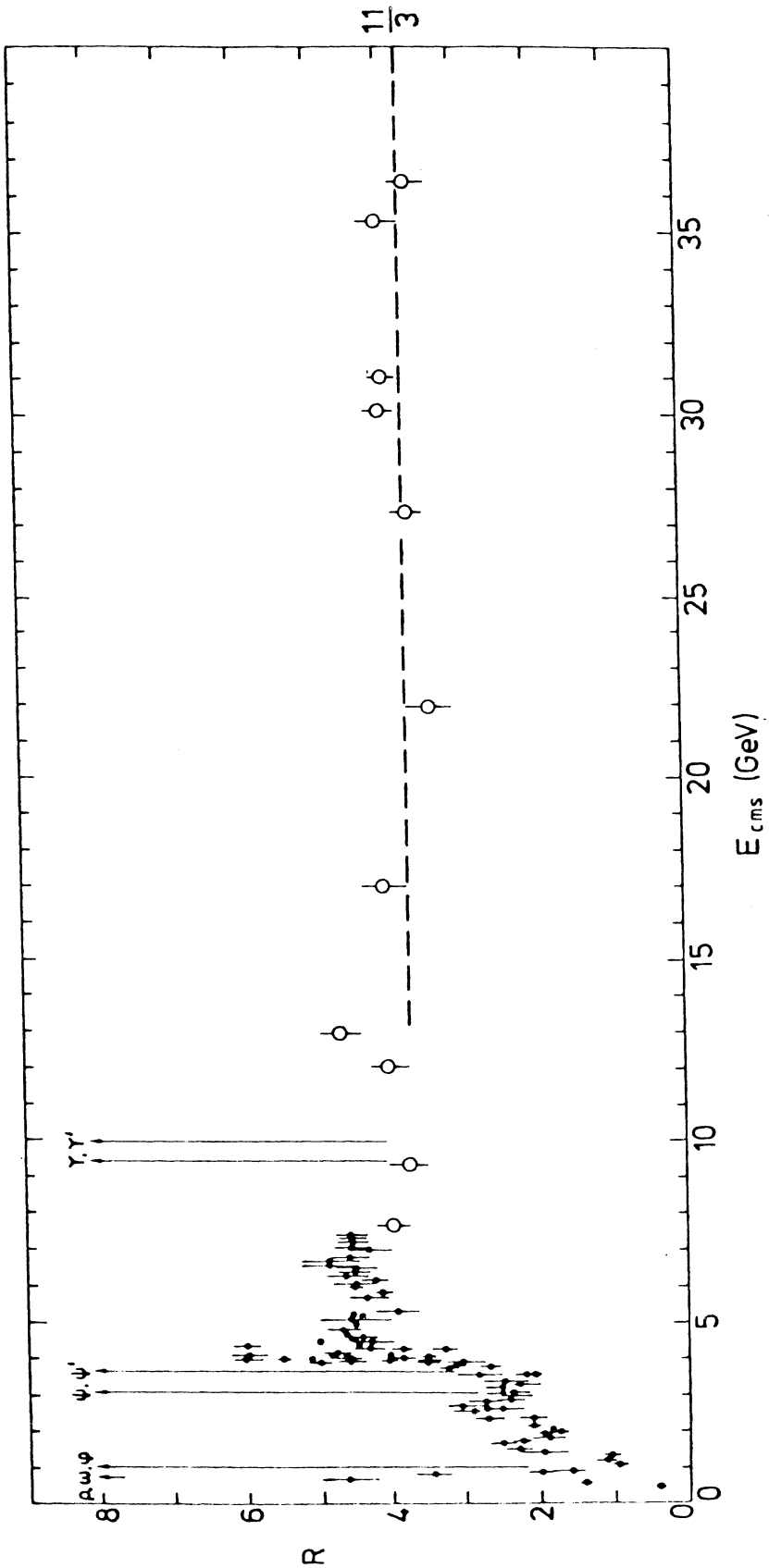

Fig.14 Ratio R=σ ($e^+e^- \to$ hadrons)/σ ($e^+e^- \to \mu^+\mu^-$) as a function of CMS energy. Above 12 GeV, all the data are from the PETRA accelerator.

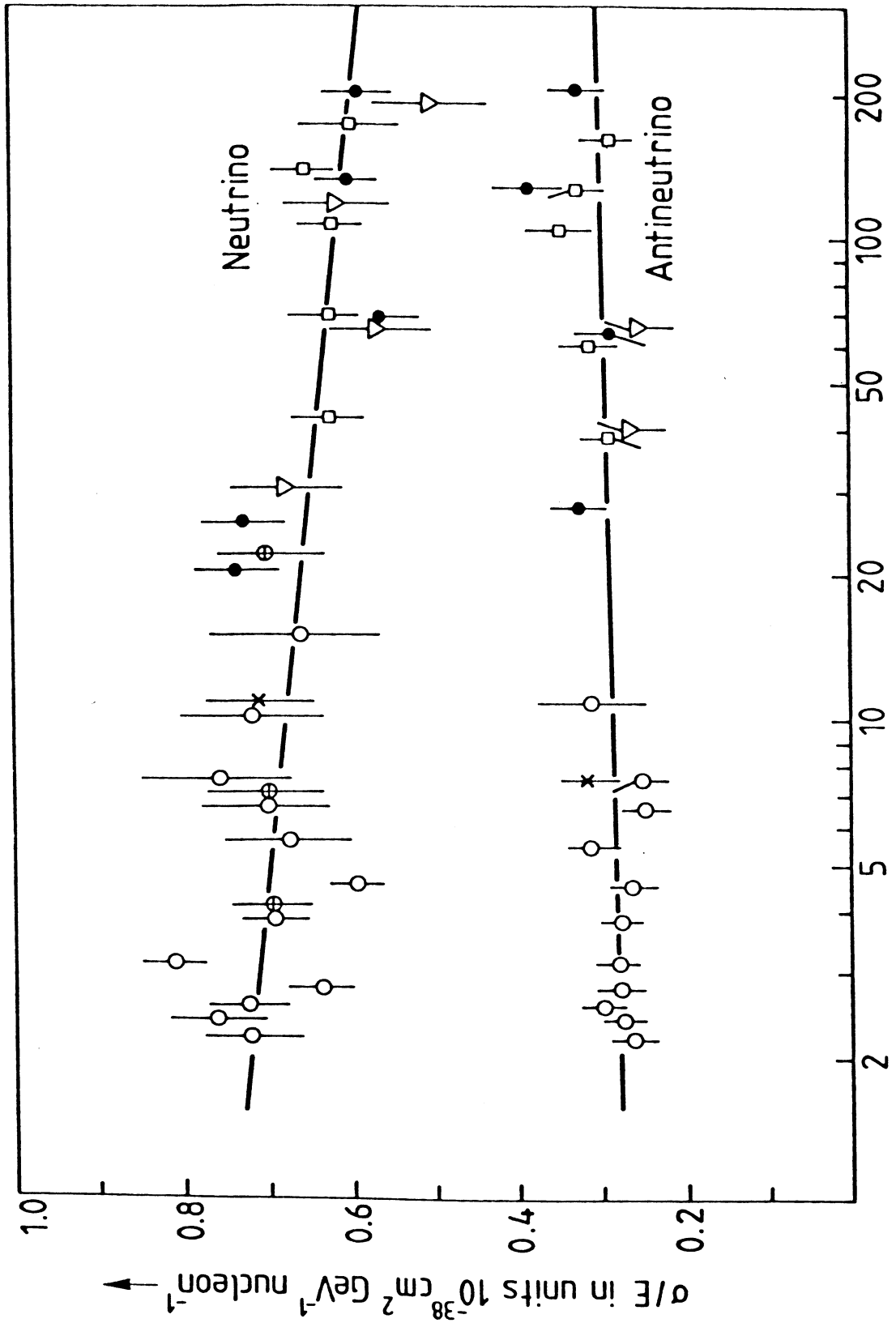

Fig.15 Neutrino and antineutrino cross-sections on nucleons.

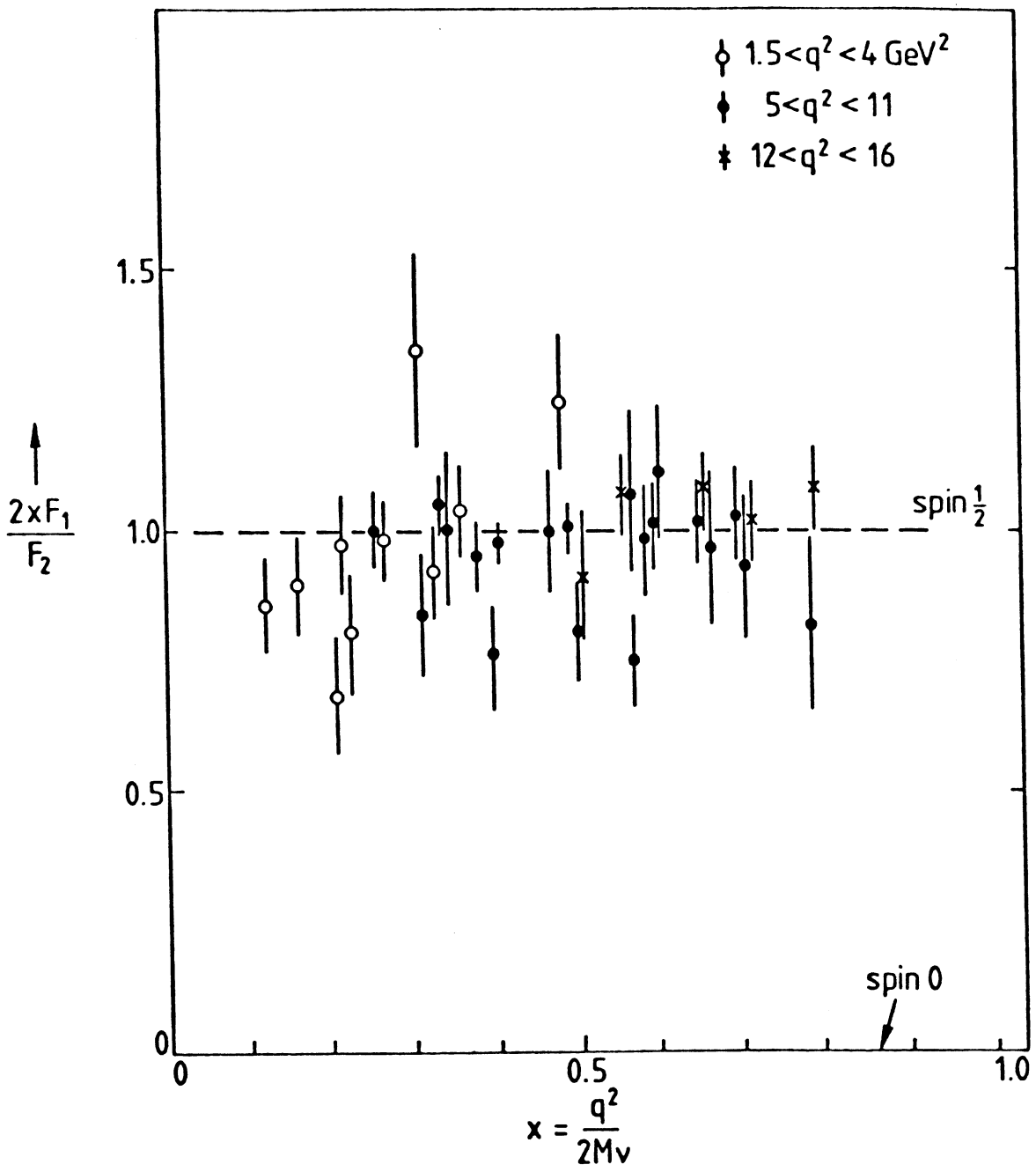

Fig.16 SLAC ep data on the ratio $2xF_1/F_2$ of magnetic to electric scattering, indicating spin ½ partons.

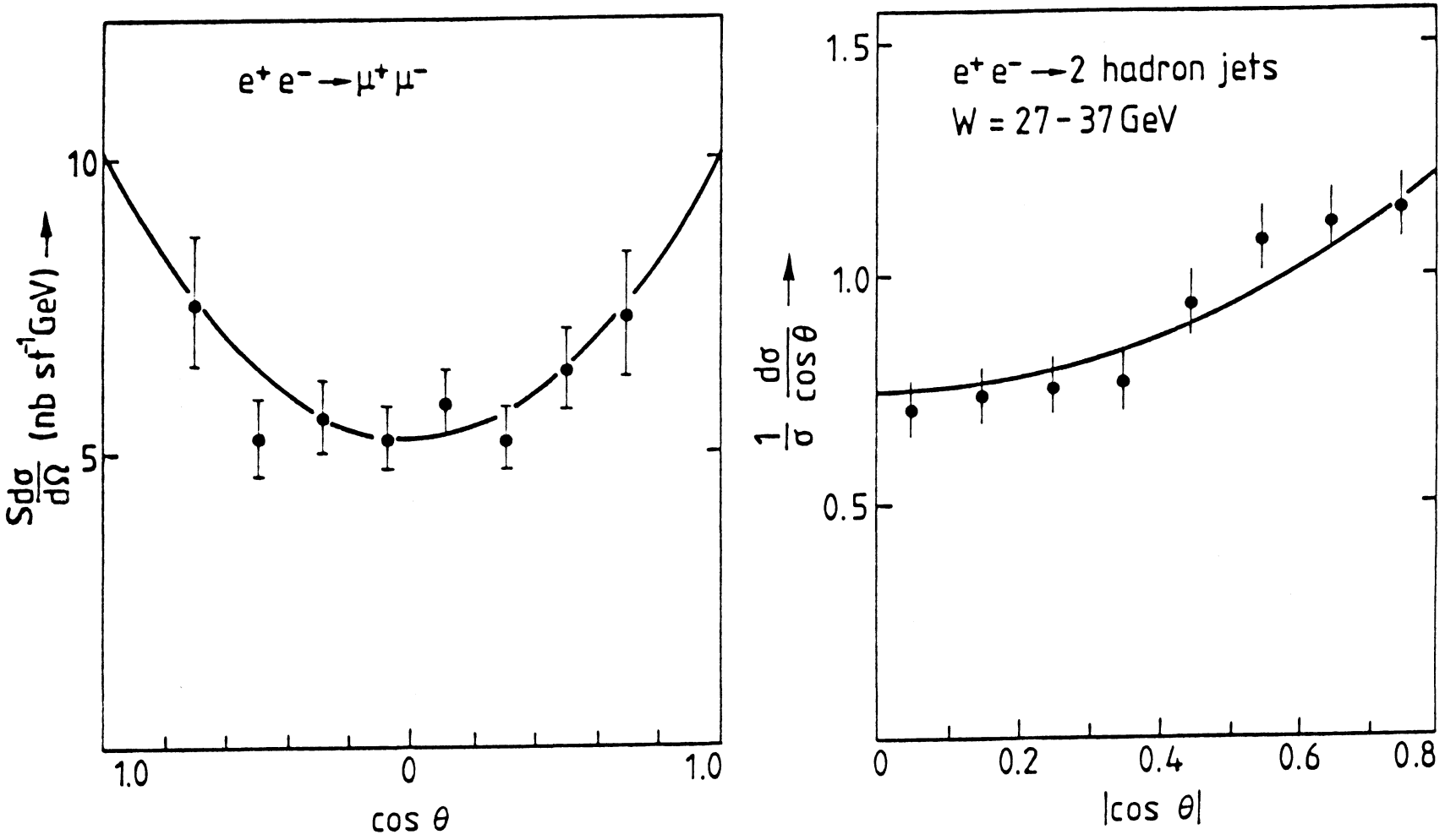

Fig.17 Angular distribution of jet axis relative to beam in $e^+e^- \to$ hadrons, compared with that for $e^+e^- \to \mu^+\mu^-$. In both cases, the distribution has the form $(1+\cos^2\theta)$ as expected for spin ½ particles ($e^+e^- \to \mu^+\mu^-$ or $Q\bar{Q}$).

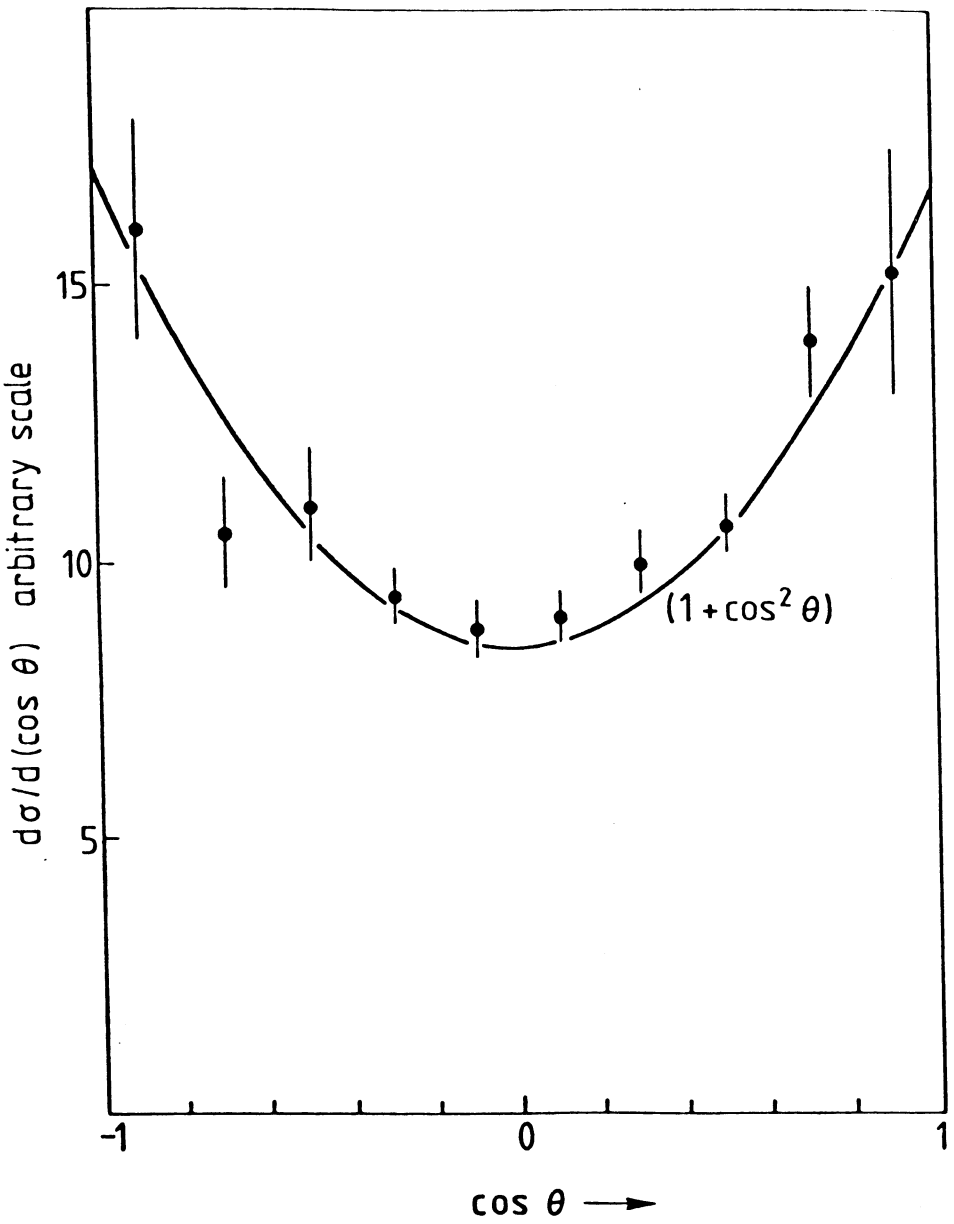

Fig.18 Angular distribution of muons in dimuon rest-frame, relative to the incident beam, in the process $p+p \rightarrow \mu^+\mu^-+X$. The $(1+\cos^2\theta)$ distribution is expected for the process $Q\bar{Q} \rightarrow \mu^+\mu^-$ involving spin ½ partons. (Anderson et al 1978).

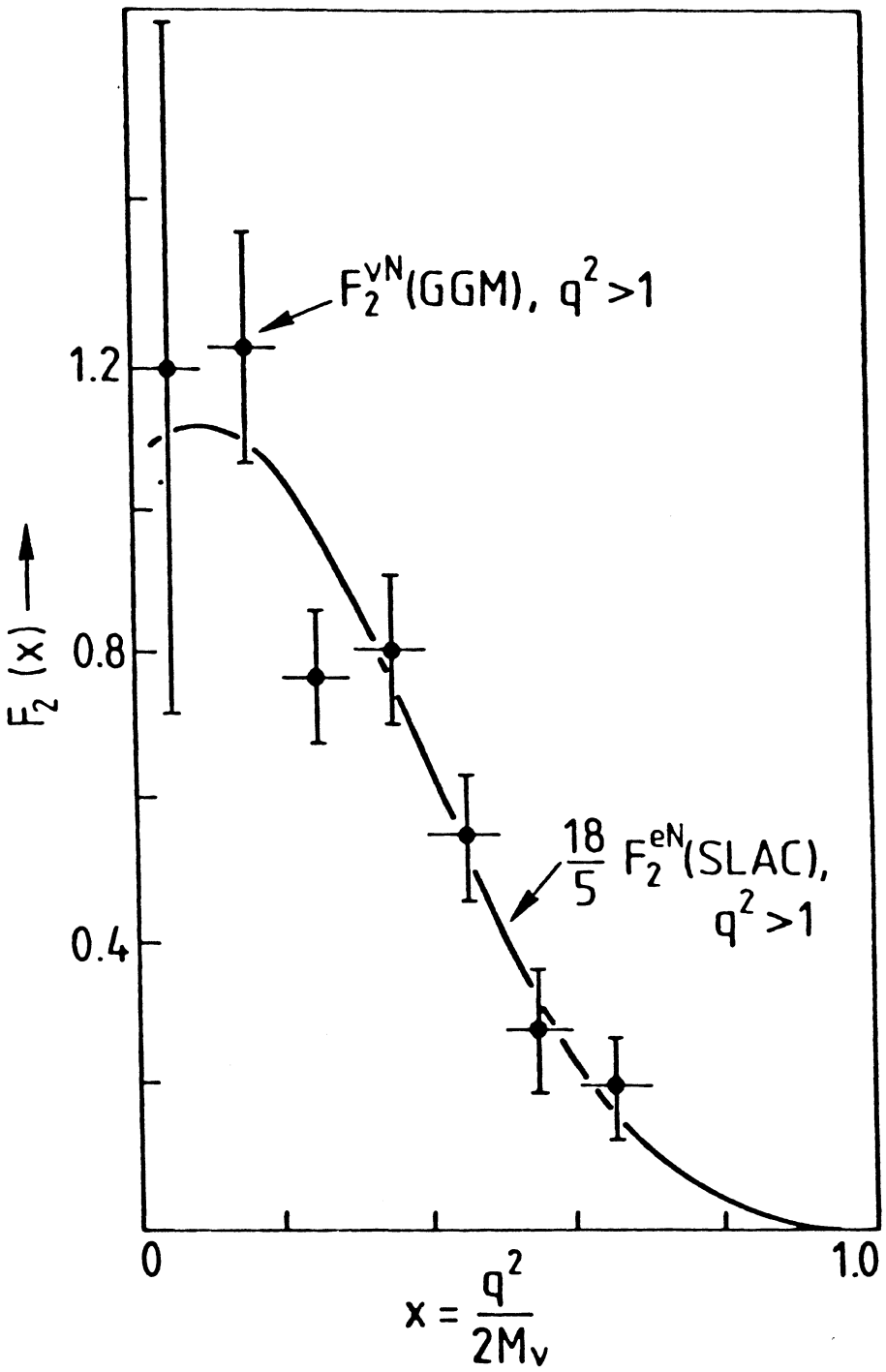

Fig.19 $F_2^{\nu N}(x)$ measured in Gargamelle PS neutrino experiments, compared with (18/5) $F_2^{eN}(x)$ measured in SLAC electron scattering experiments. These results support the fractional charge assignments for quarks.

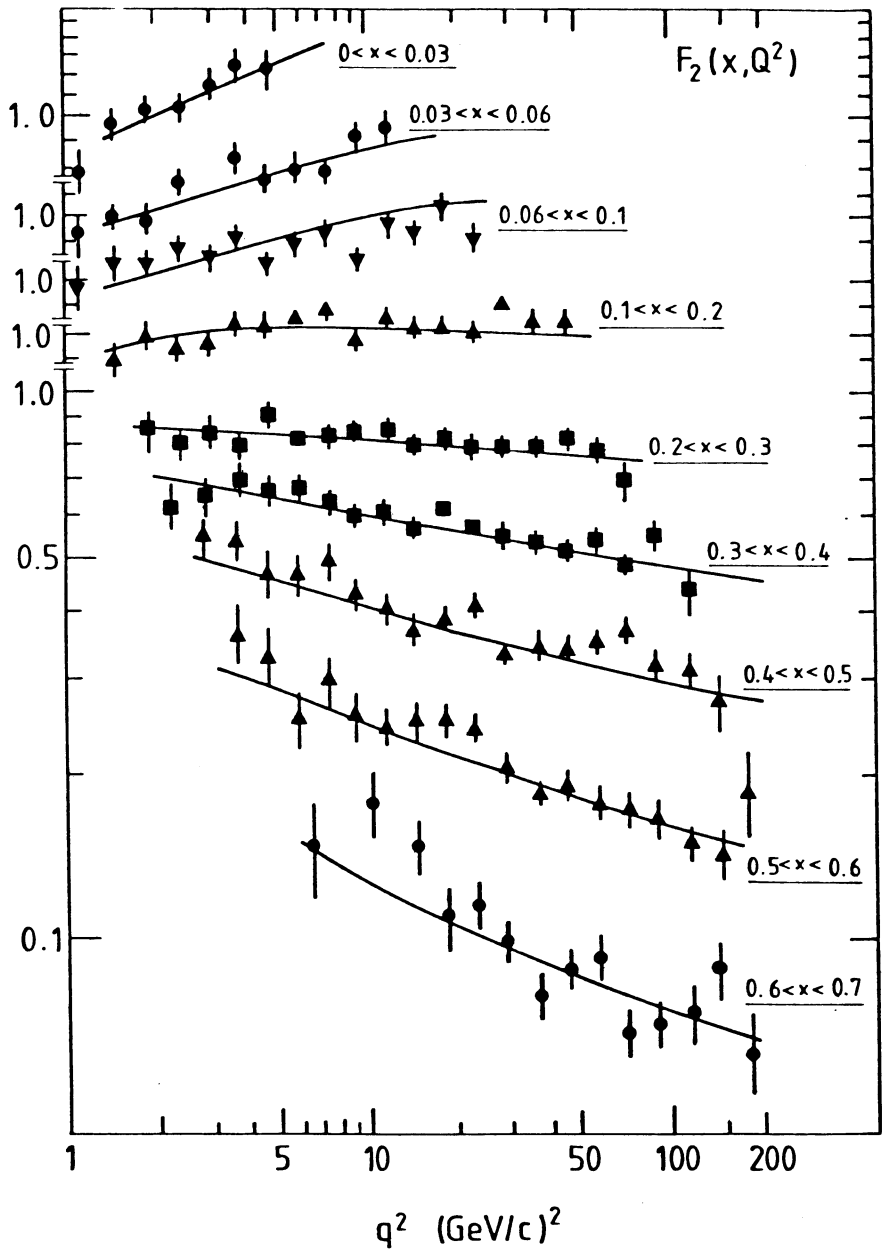

Fig.21 Recent data from CDHS neutrino group on $F_2^{\nu N}(x,q^2)$. The curves show fits from Buras-Gaemers parametrizations of the quark/gluon distributions, with Λ = 0.5 GeV. (Eisele 1980).

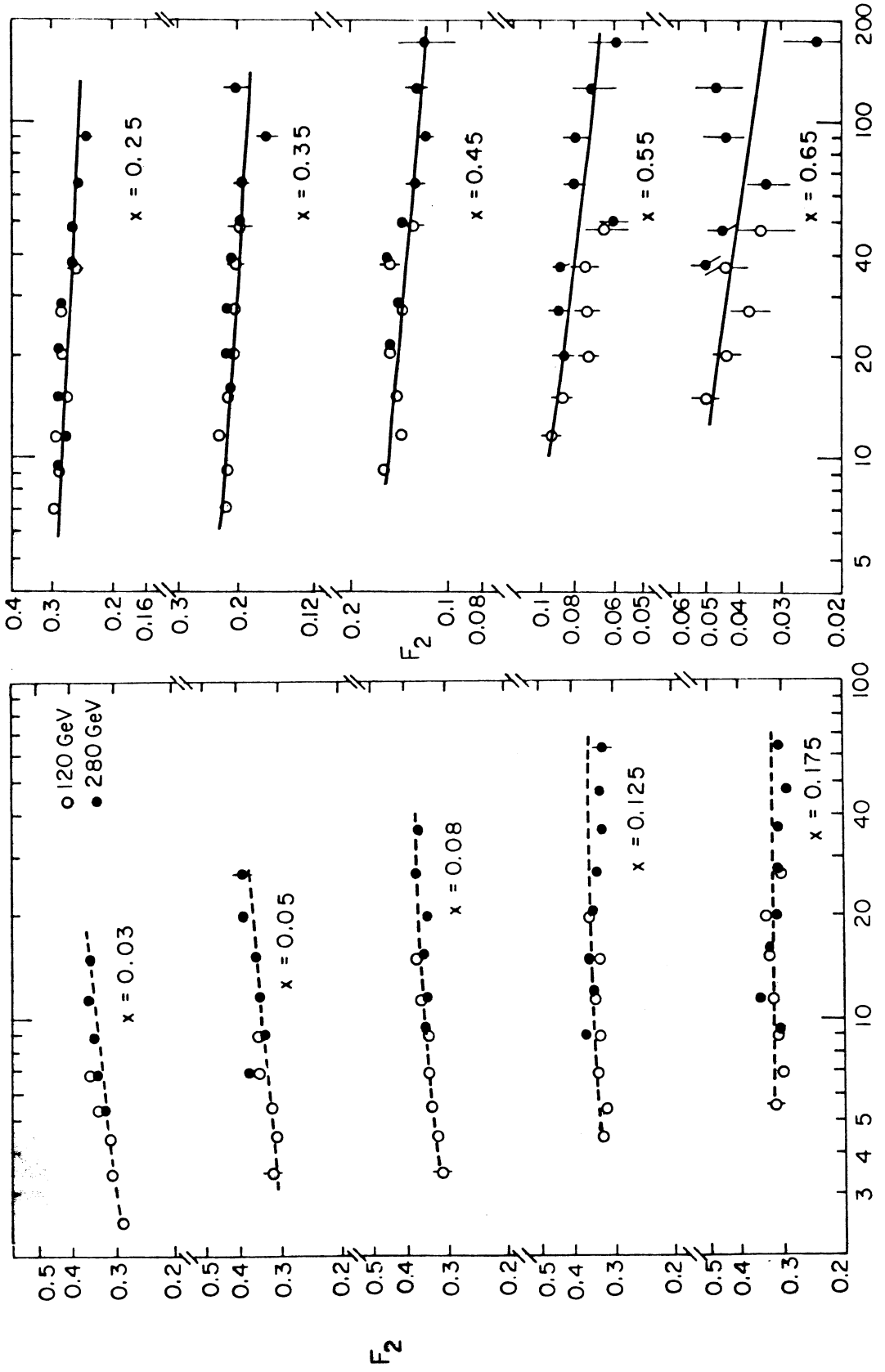

Fig.22 Data from CERN EMC (NA2) muon scattering in iron (Aubert et al 1980a).

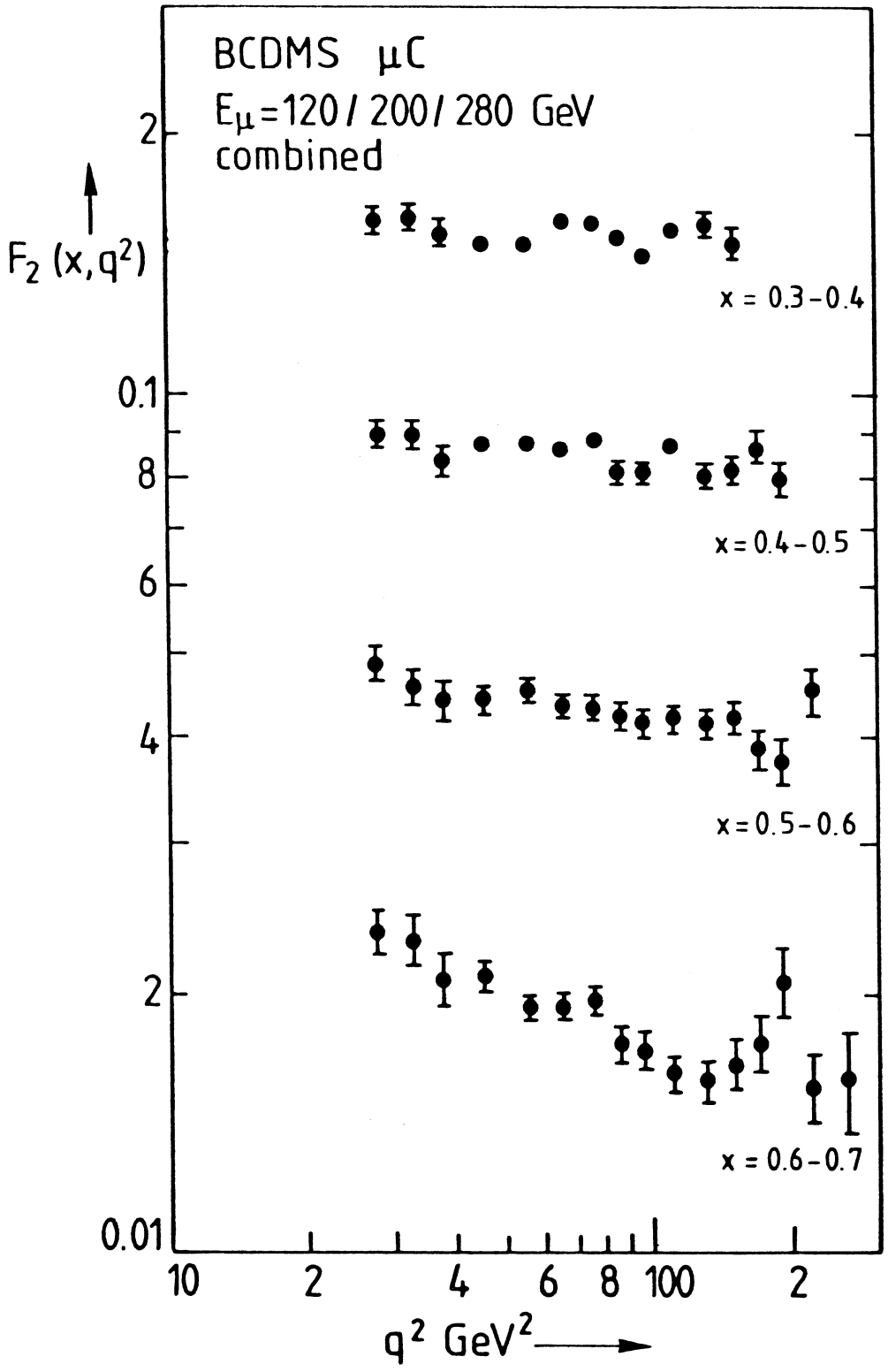

Fig.23 Data from CERN BCDMS (NA4) muon scattering in carbon. (Bollini et al 1981).

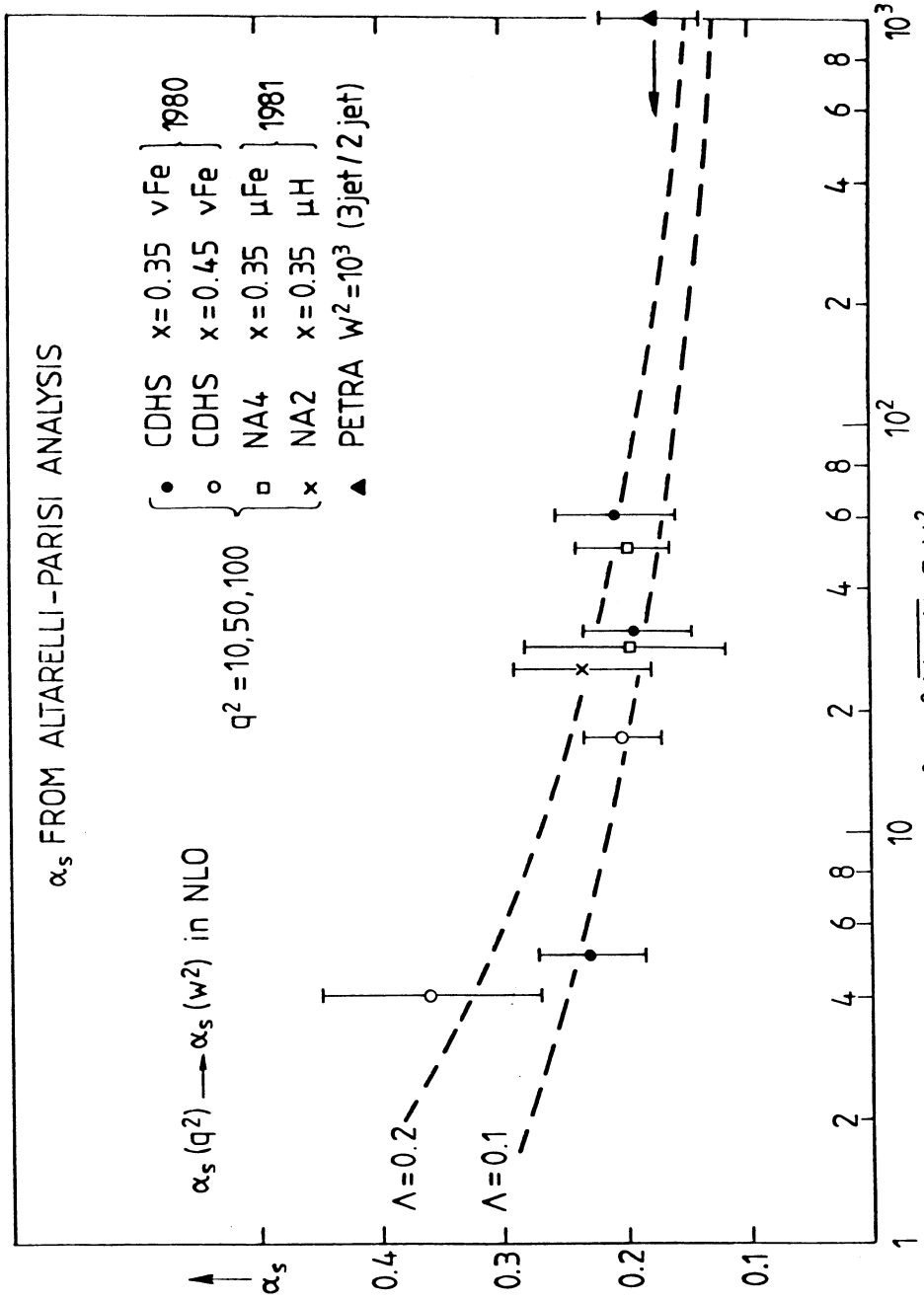

Fig.25 Calculation of α_s from the Altarelli-Parisi equation using the data shown in Figs.21, 22 and 23.

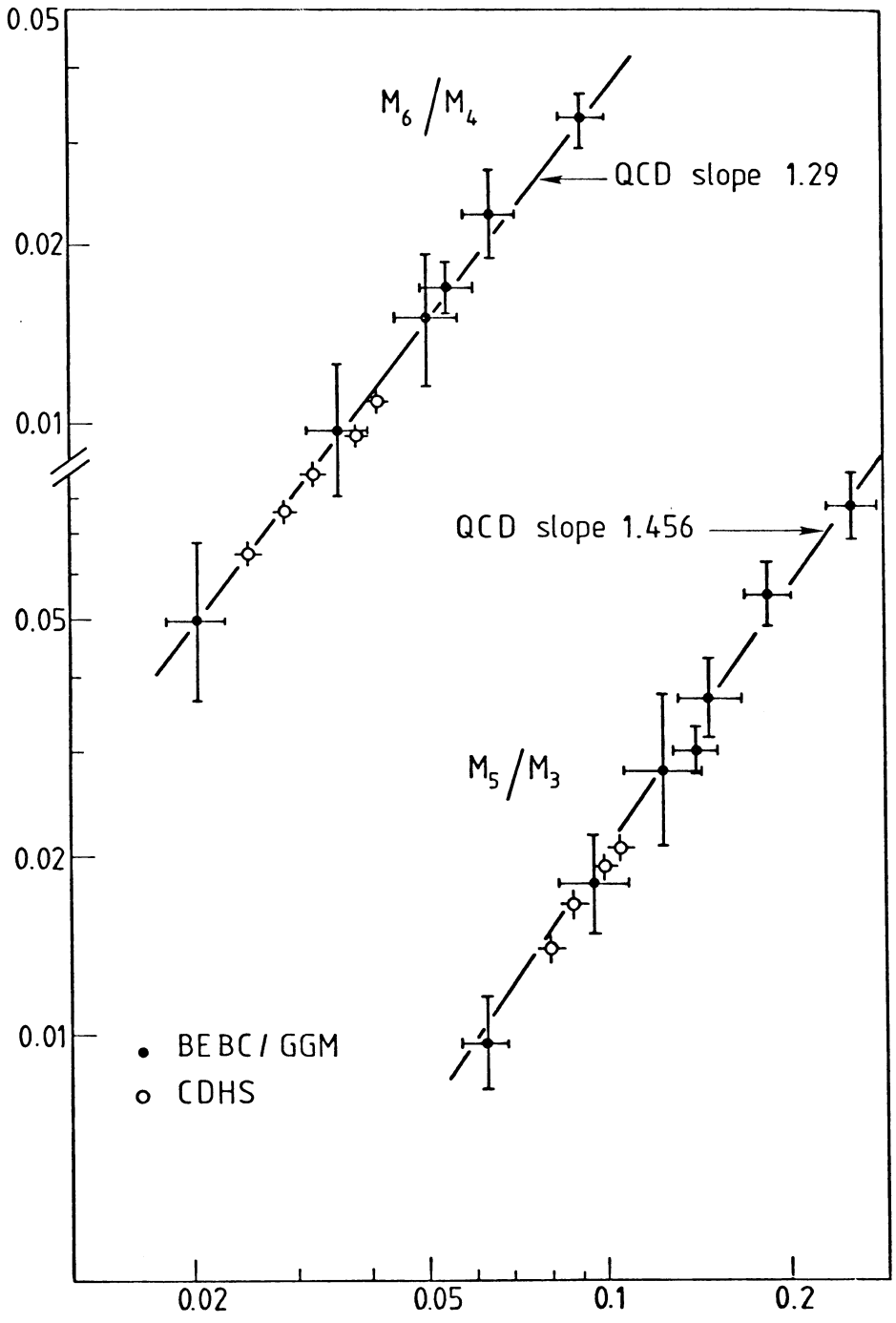

Fig.26 Logarithmic non-singlet moment/moment plots from CDHS and BEBC experiments, together with slopes predicted by QCD.

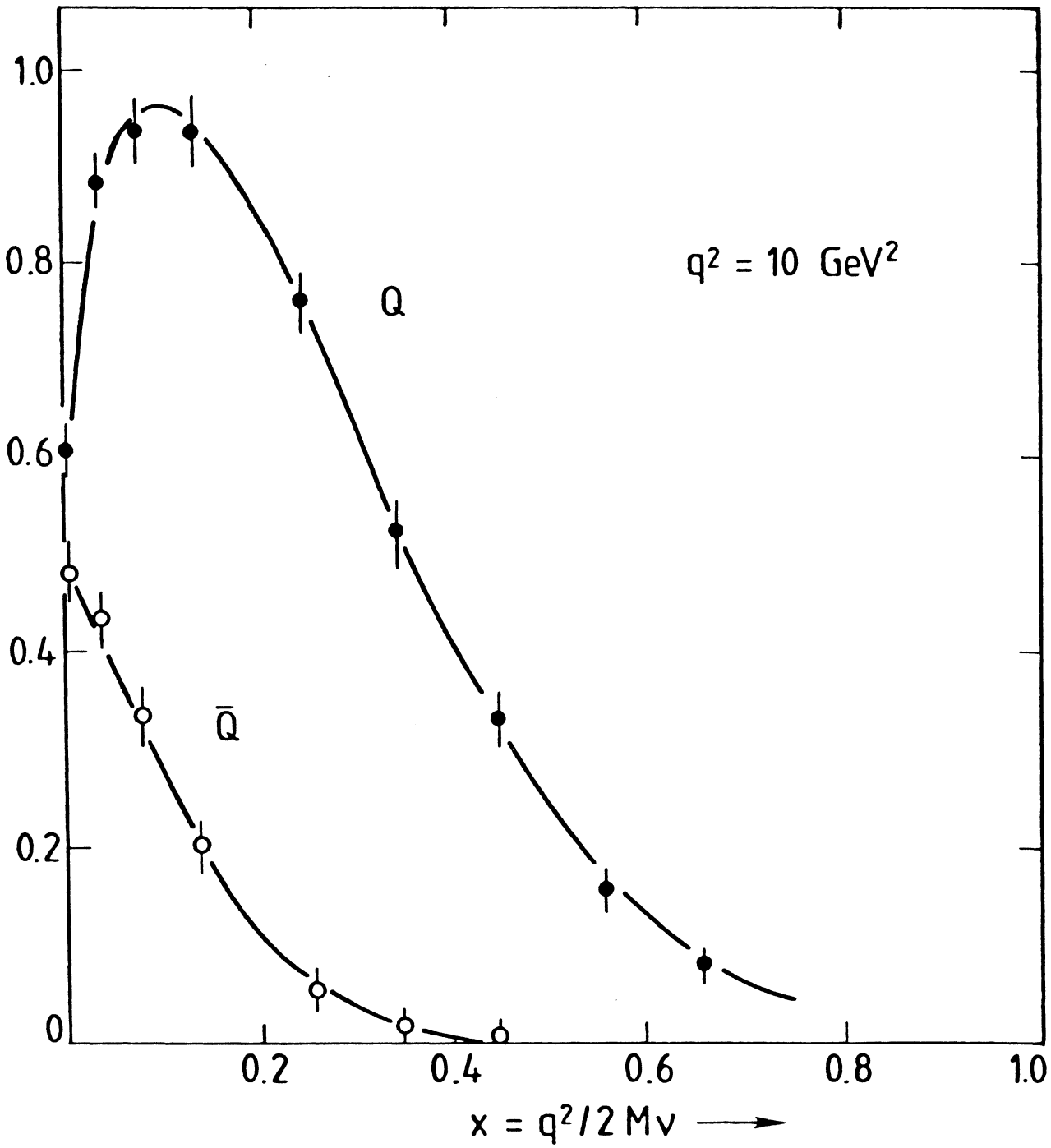

Fig.27 Quark and antiquark momentum distributions from the CDHS experiment at CERN.

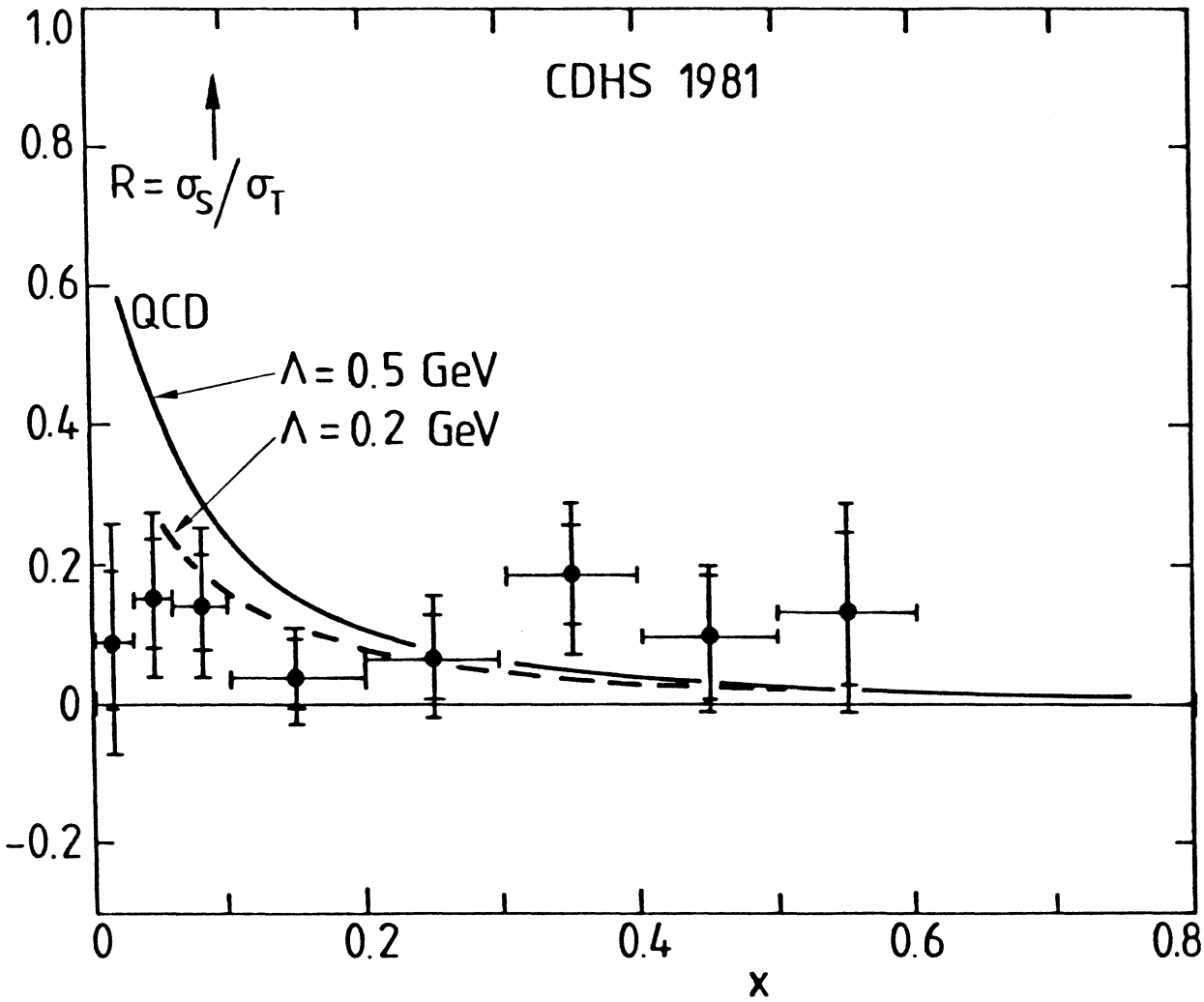

Fig.29 CDHS data (Wahl 1981) on $R = \sigma_S/\sigma_T$. The curves show the (perturbative) QCD prediction. At large x, additional (high-twist) contributions are evident.

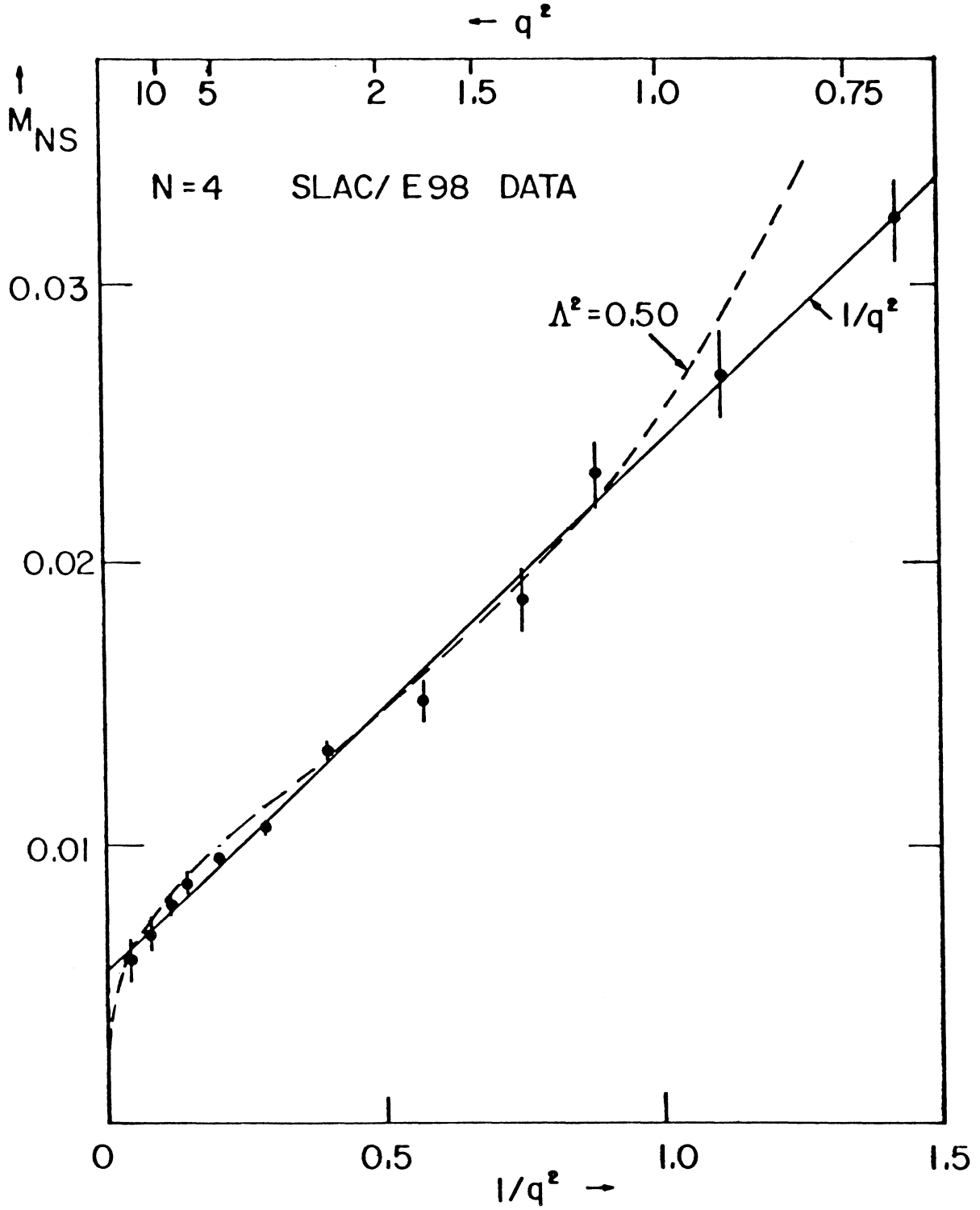

Fig.30 Data on N=4 non-singlet moments from CHIO experiments at Fermilab. They fit equally a $1/q^2$ dependence (full line) or the logarithmic variation (dashed curve) expected from QCD.

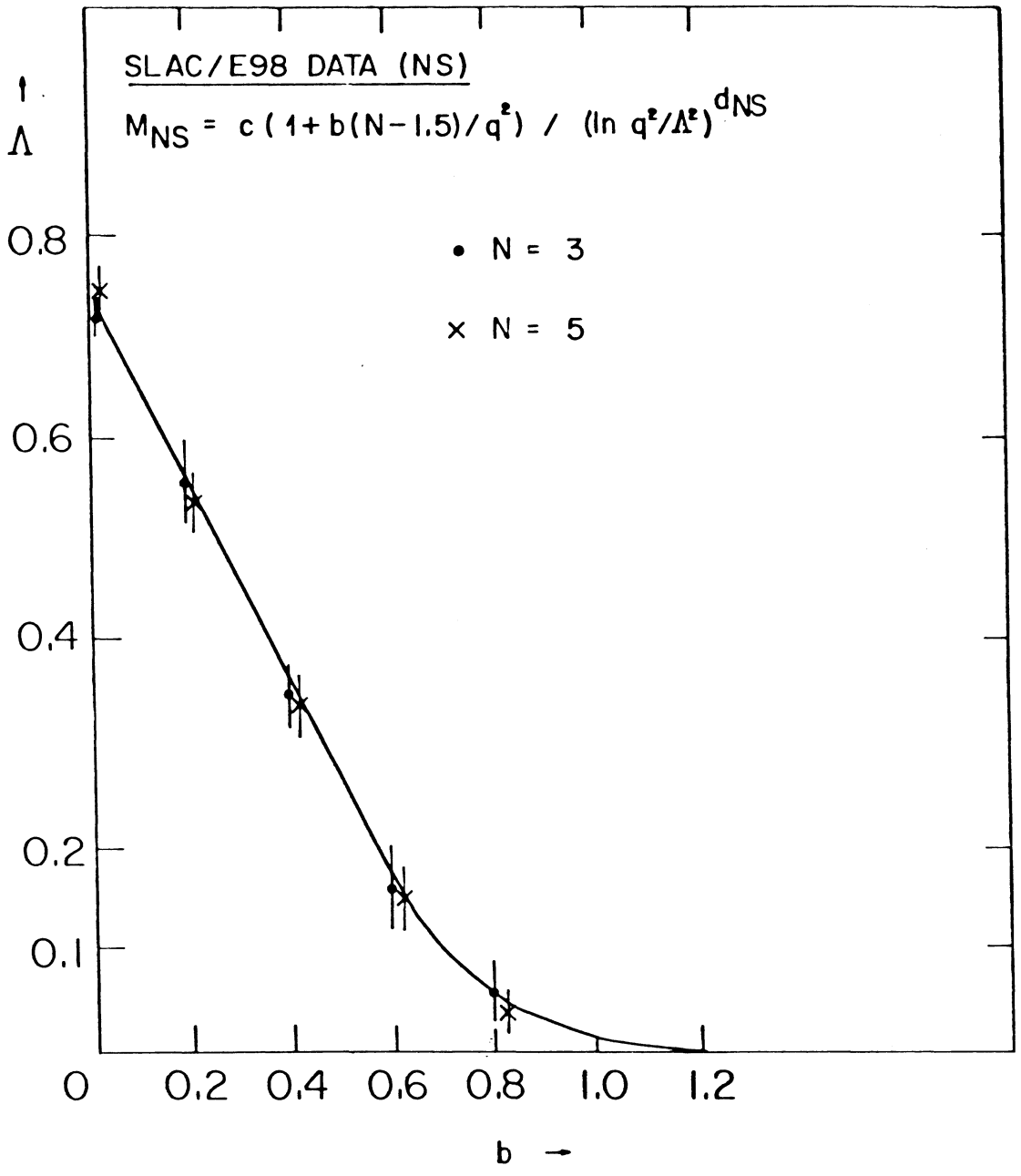

Fig.31 Relation between the parameters Λ and b from fits to N=3 and N=5 non-singlet moments using a combination of $1/q^2$ and $\ln q^2$ dependence. All pairs of values on the curve yield equally good fits.

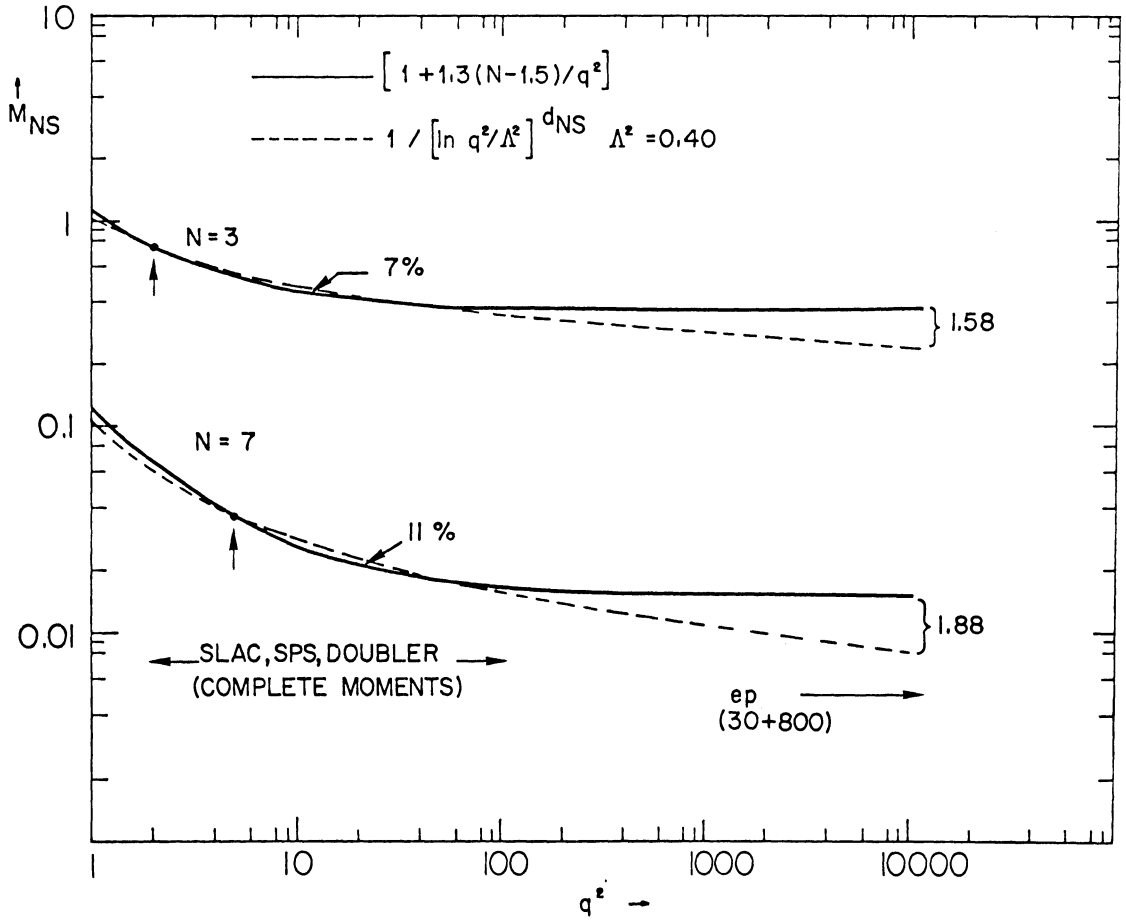

Fig.32 Variation with q^2 of the N=3 and N=7 moments, according to a $1/q^2$ or $\ln q^2$ dependence as described by the extreme values of the parameters in Fig.31. The two curves are normalized at $q^2 = 5$ GeV^2 in each case. Large differences only appear at $q^2 >> 100$ GeV^2.

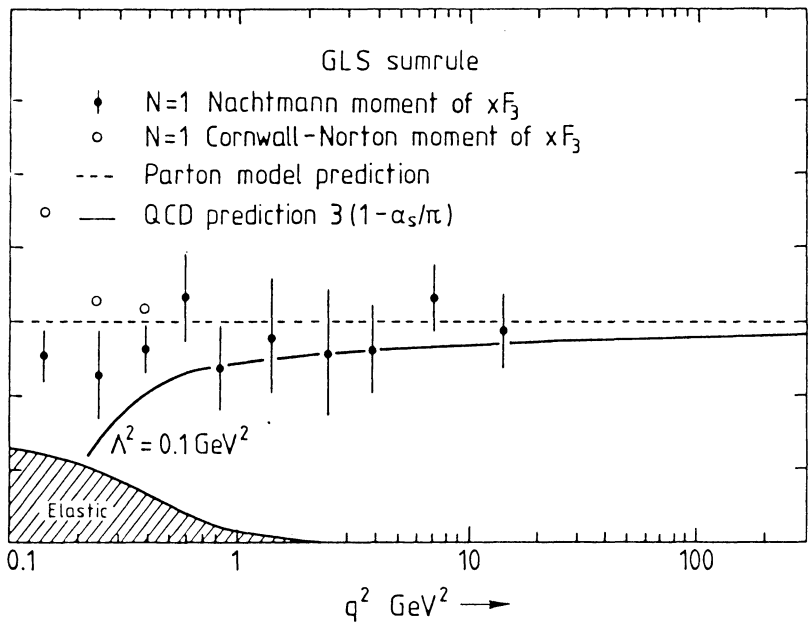

Fig.33 Data from BEBC and Gargamelle on the GLS sumrule. The QCD prediction (Λ^2 = 0.1 GeV^2) is shown by the full curve.

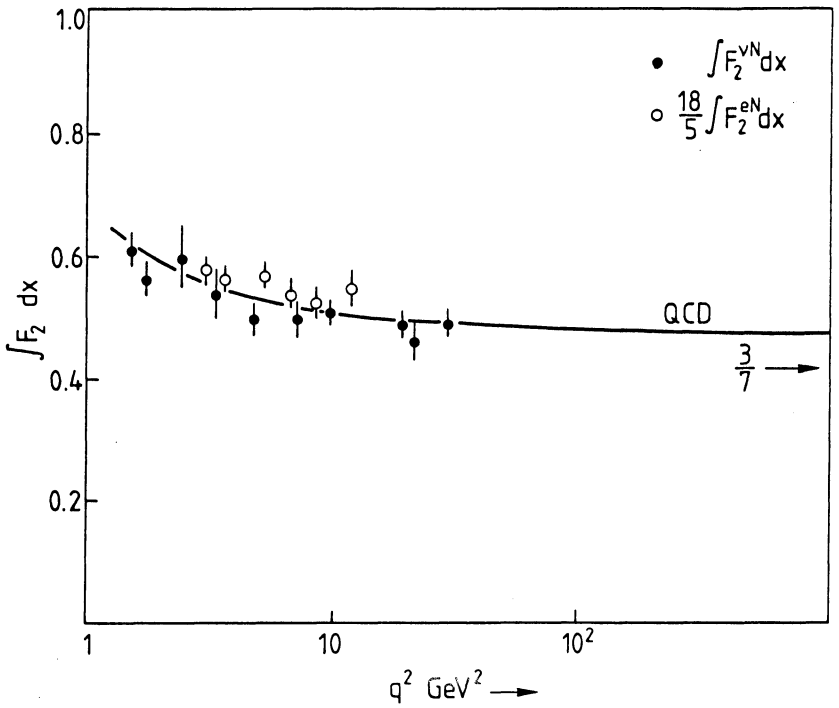

Fig.34 Variation with q^2 of the integrals of $F_2^{\nu N}(x)$ and (18/5) $F_2^{eN}(x)$ from the BEBC/Gargamelle and SLAC/MIT experiments. A decrease with increasing q^2 (assuming non-perturbative effects can be neglected) is, according to Glück and Reya (1979) clear evidence for an asymptotically-free gauge theory.

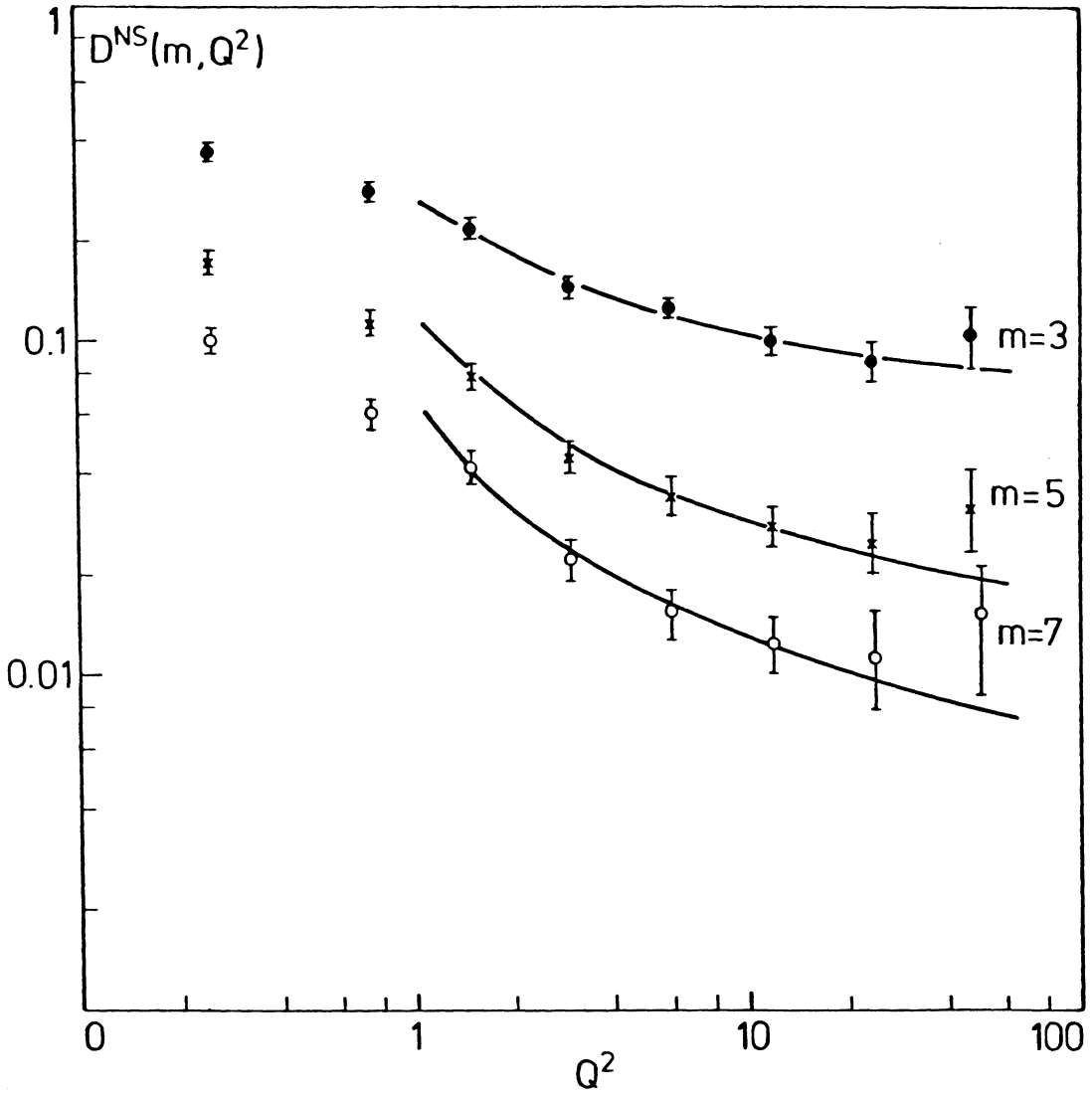

Fig.35 ABCMO results on q^2 dependence of non-singlet fragmentation function moments, measured in νH_2 collisions in BEBC (Blietschau et al 1979(a)).

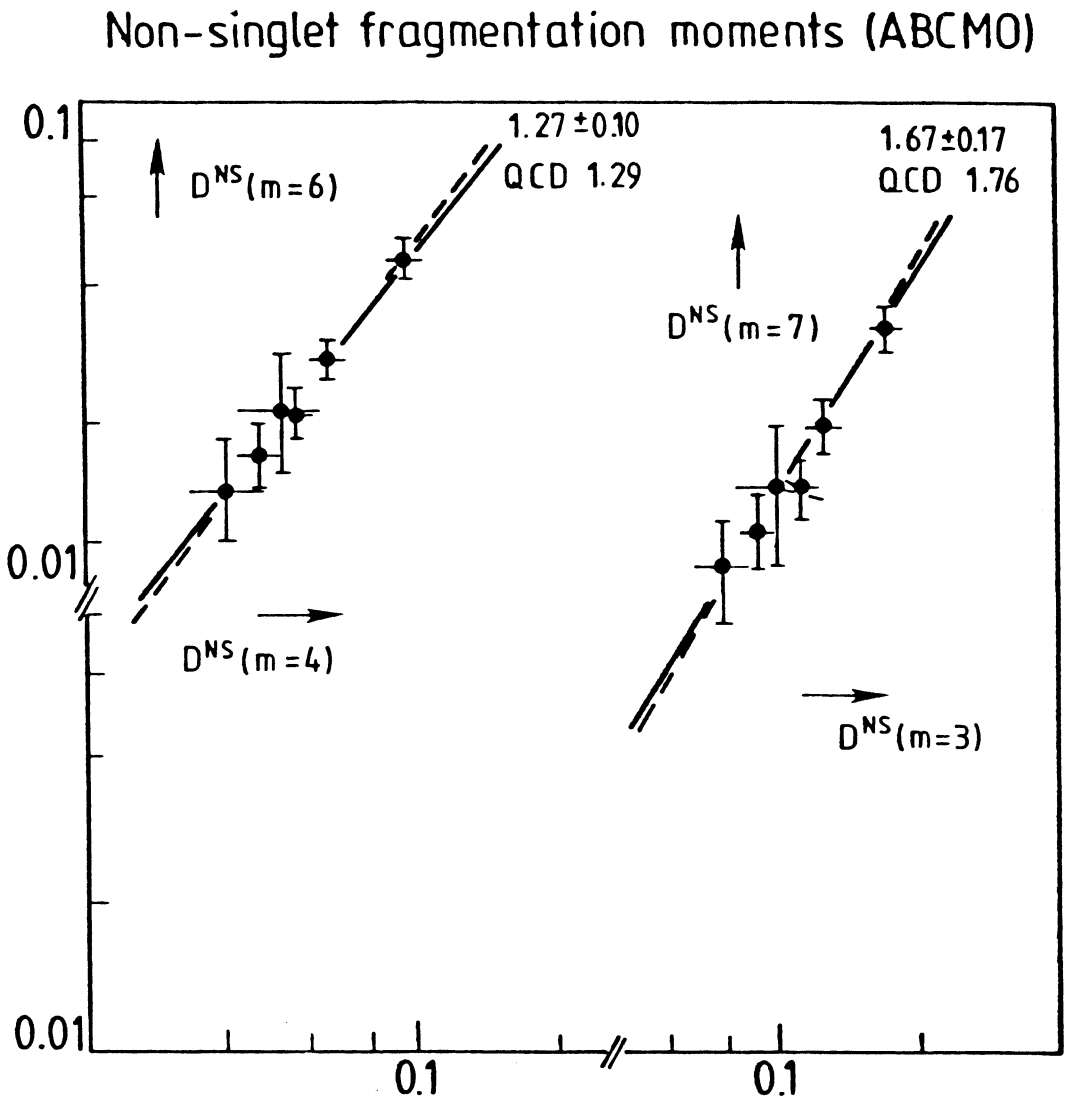

Fig.36 Moment/moment plots for data of Fig.35, with fitted slopes and QCD predictions.

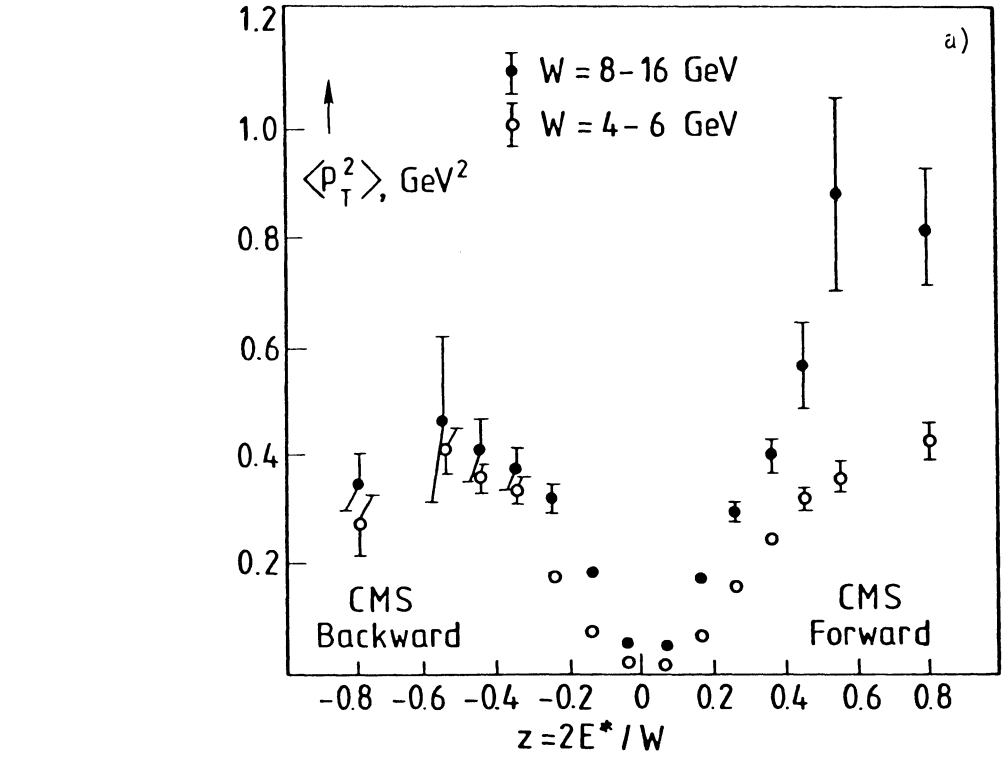

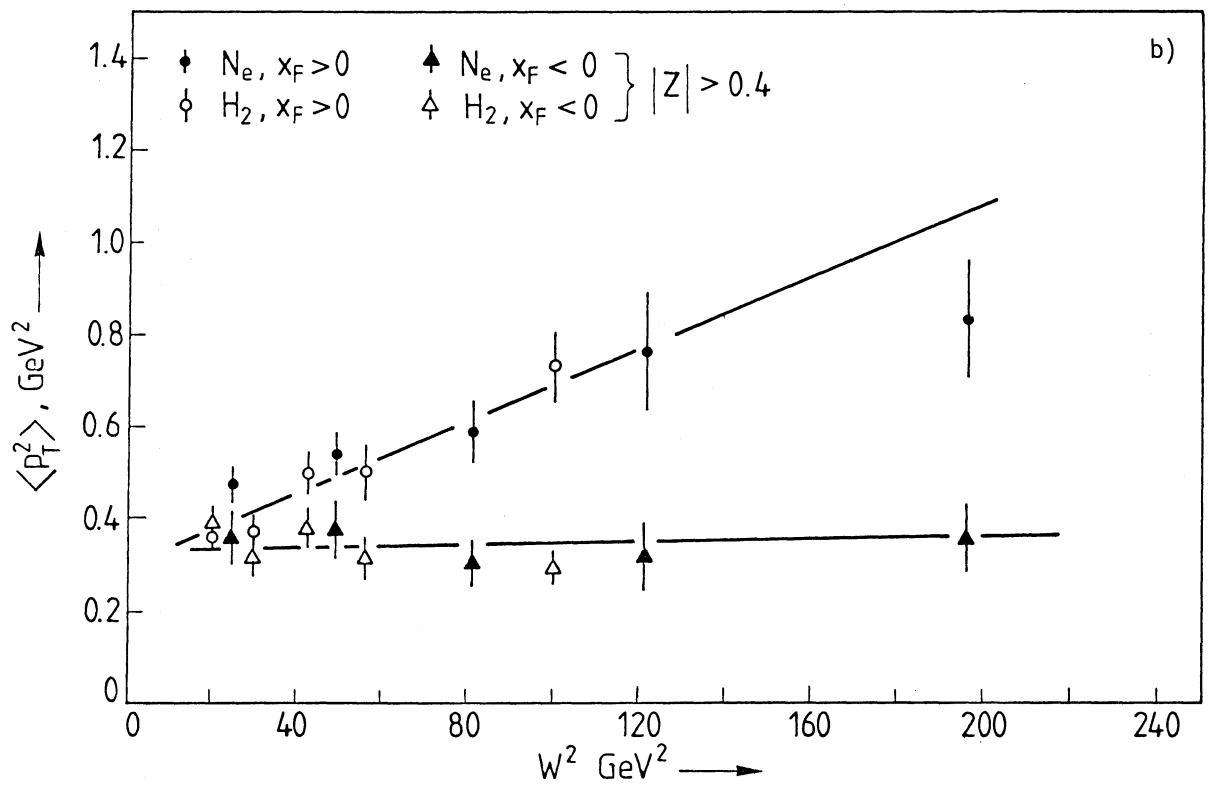

Fig.38 (a) Average values of p_T^2 of secondaries from νN collisions, relative to the q vector, as a function of z(CMS) for forward and backward particles, in 2 ranges of W (ABCMO data).

(b) As in Fig.38(a), for secondaries of $|z| \geq 0.4$.

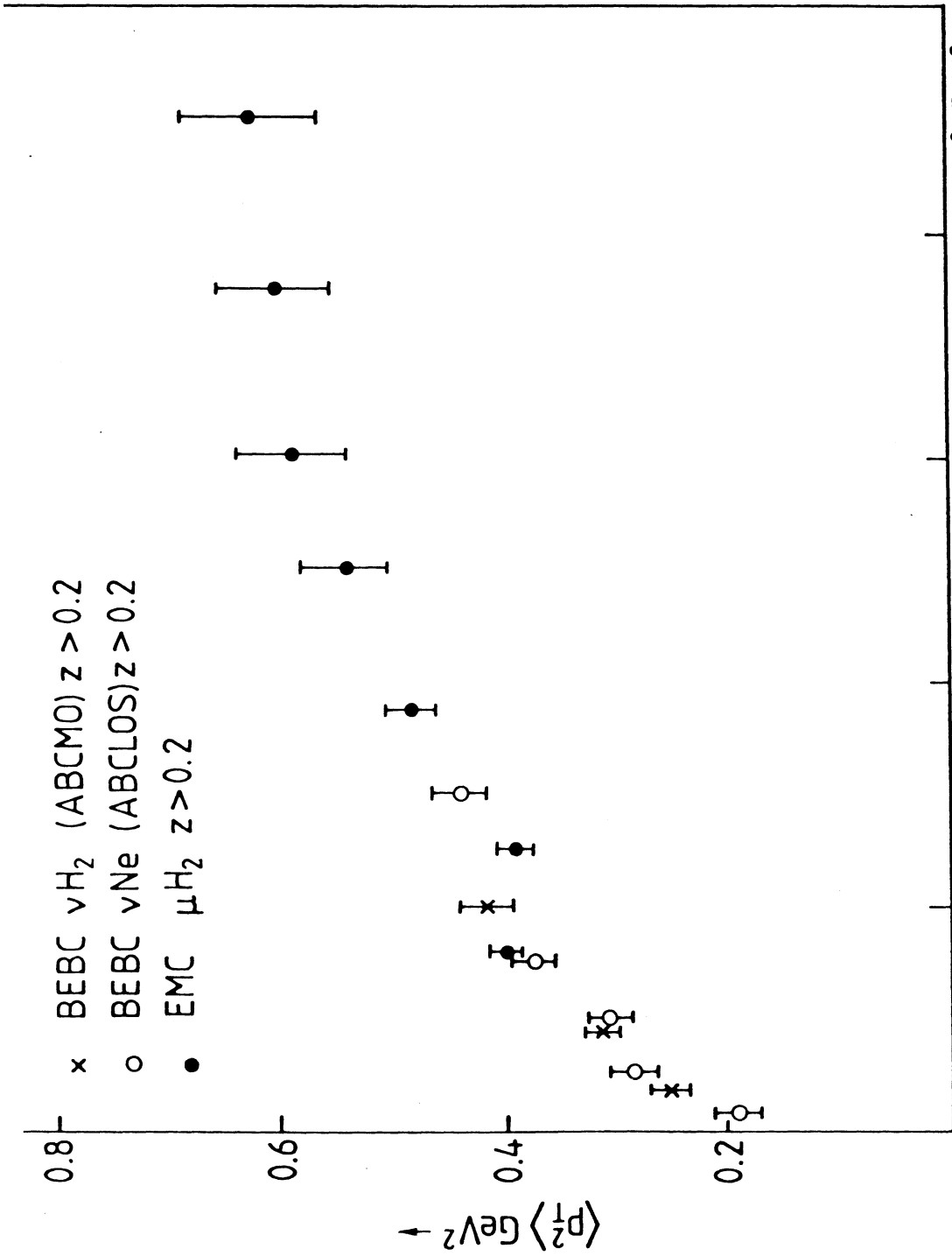

Fig.40 Average p_T^2 of forward secondaries of z(LAB) > 0.2 as a function of W^2, from neutrino and muon scattering experiments.

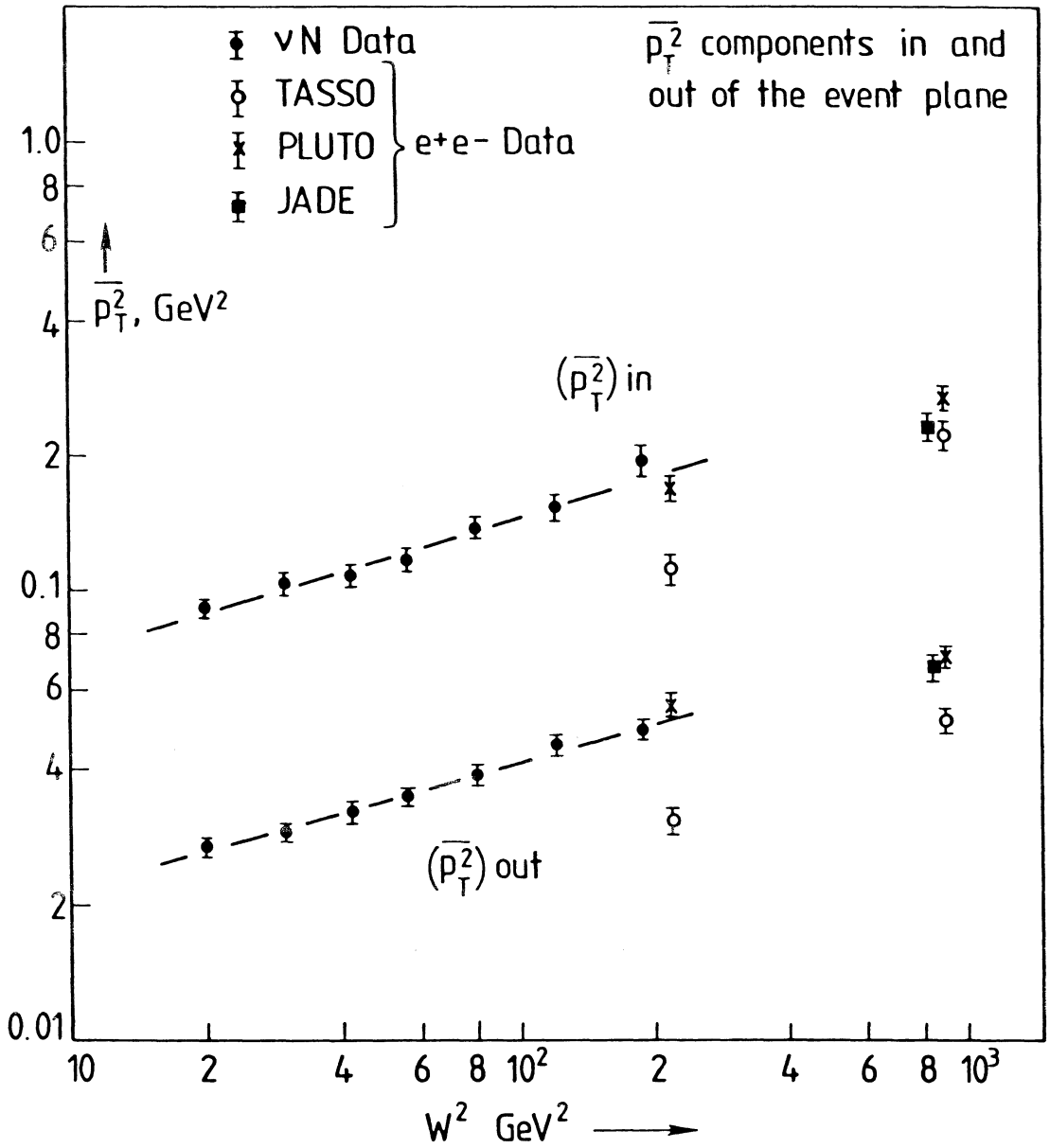

Fig.41 p_T^2 components in and out of the hadron plane, as a function of W^2, from νN and e^+e^- data.

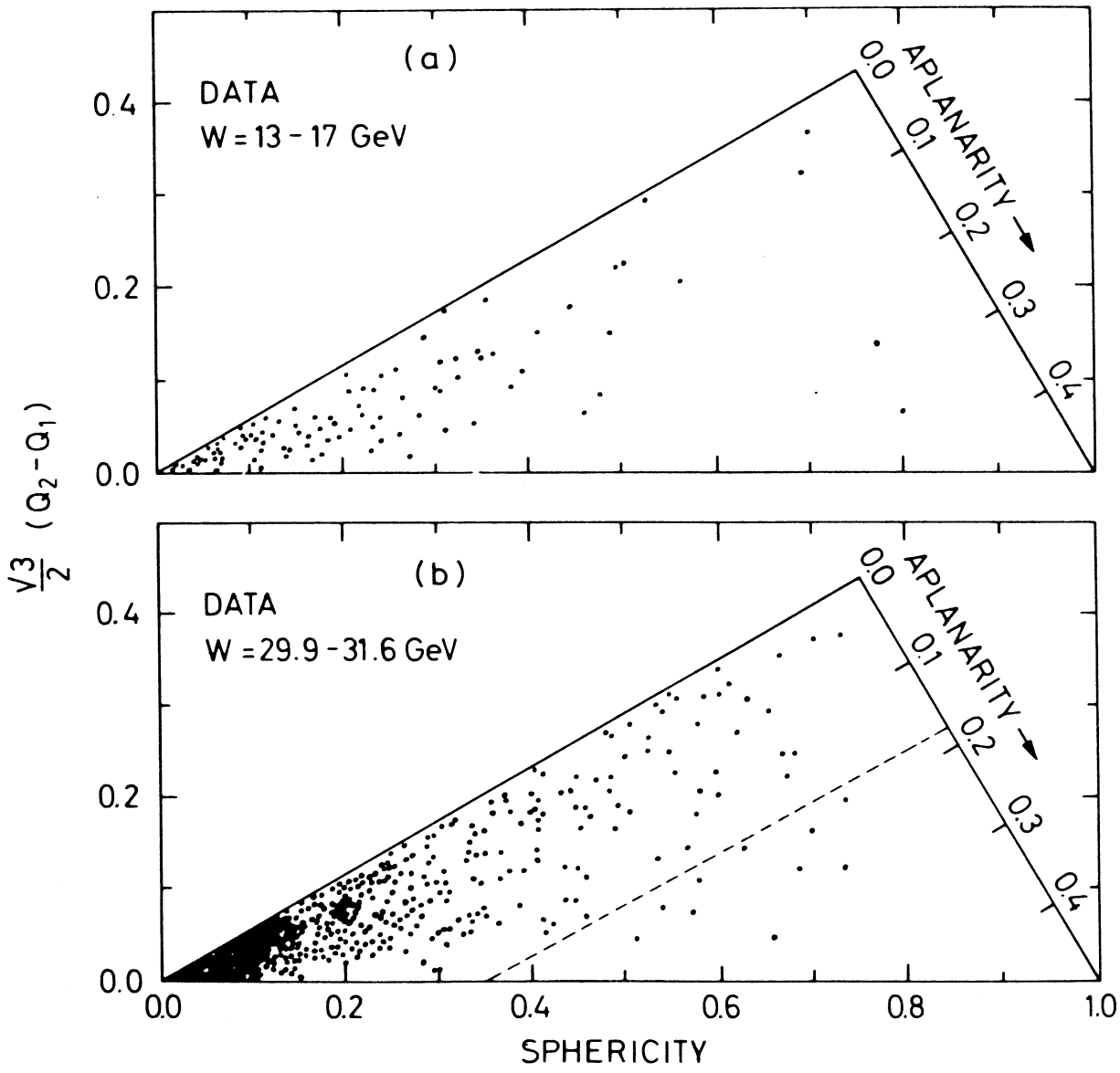

Fig.42 Dalitz plot of eigenvalues Q_1, Q_2, Q_3 in the TASSO experiment (Brandelik et al 1979). The so-called planar events are near the upper side of the triangle, defined by $S > 0.25$, $A < 0.04$. The increase in proportion of these in the higher W range is apparent.

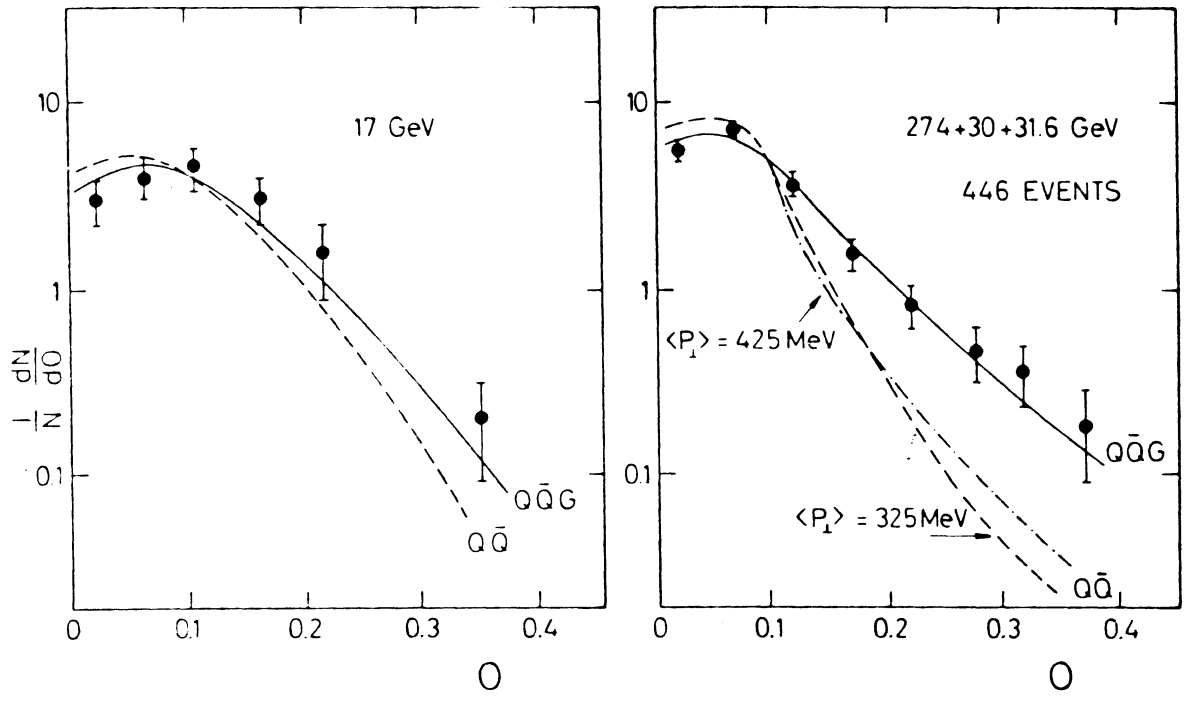

Fig.43 Oblateness distribution from the MARK J experiment (Barber et al 1979).

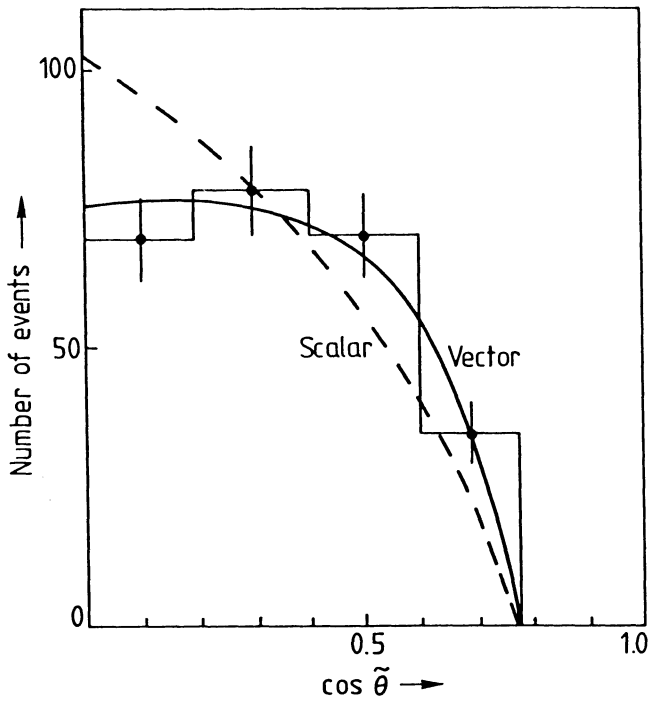

Fig.44 Distribution in angle $\tilde{\theta}$ between the momentum vector of the quark assigned to the "slim jet" and the common line of flight of quark and gluon producing the "fat jet", measured in the QG CMS system, in "planar 3 jet" events. (Brandelik et al 1980).

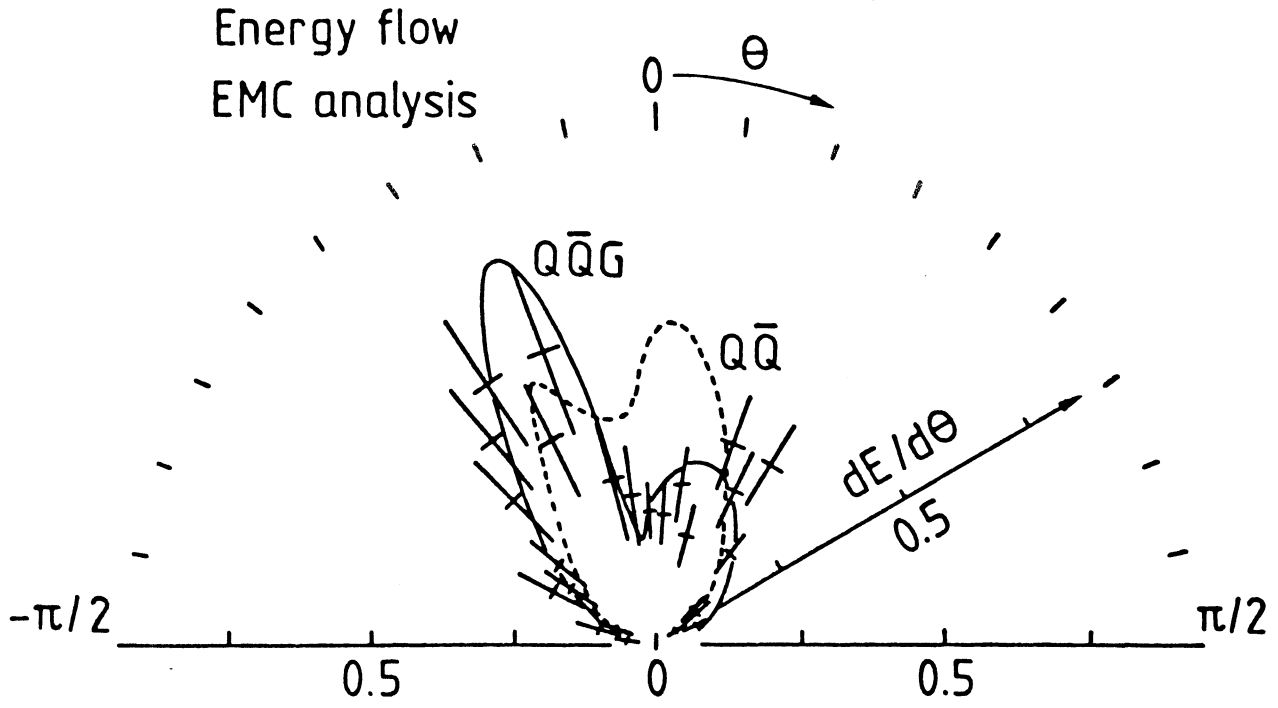

Fig.45 Polar angle distribution of energy flow relative to q vector in μp events with W = 10-20 GeV and more than 4 forward charged hadrons, with at least one of p_T > 1.5 GeV/c. The forward 2-lobe structure is in better agreement with a $Q\bar{Q}G$ Monte Carlo than the $Q\bar{Q}$ Monte Carlo (Aubert et al 1981).

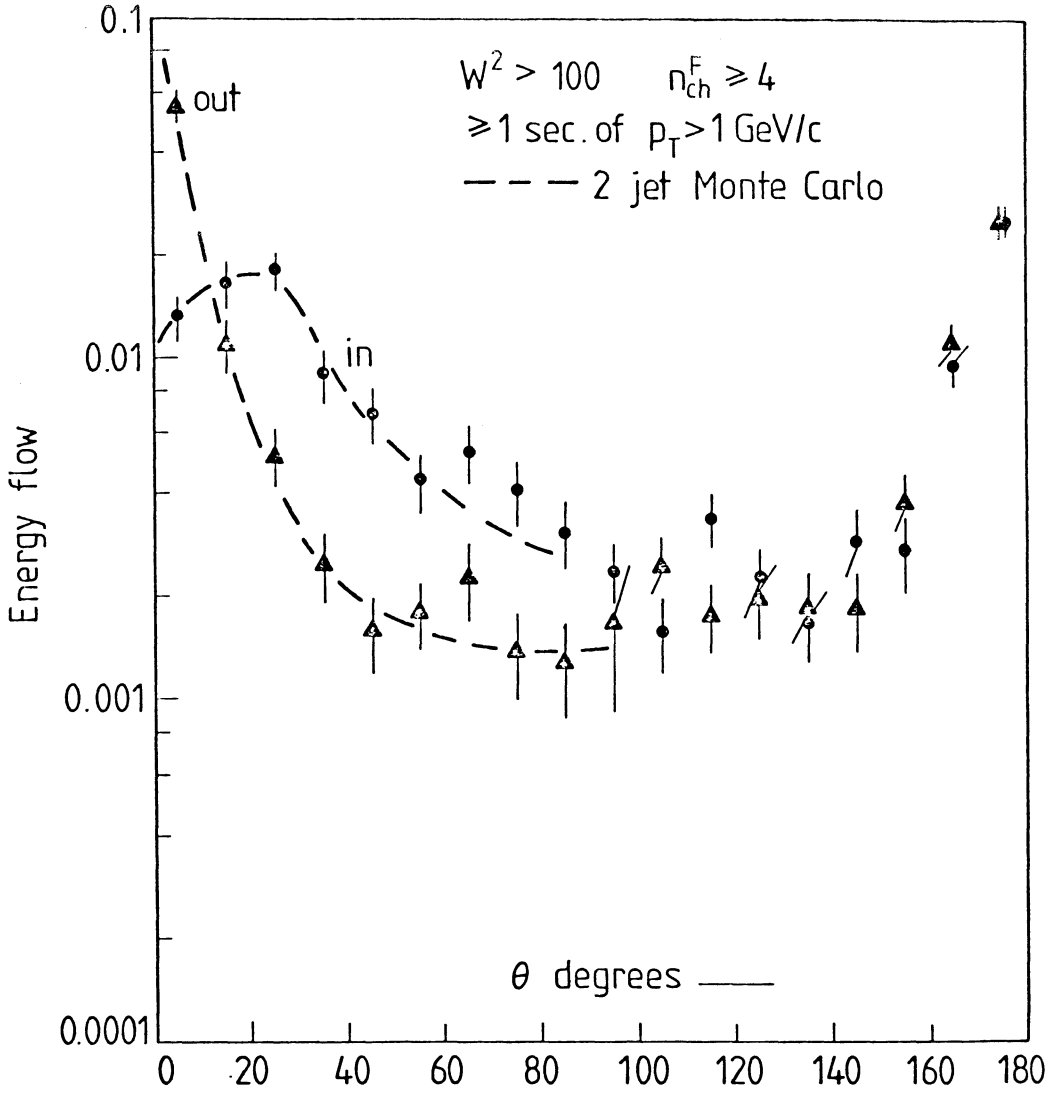

Fig.46 Projected energy flow, in and out of the hadron plane in neutrino events of $W^2 > 100$ GeV^2.

(ABCMO collaboration, private communication). The dashed lines indicate predictions of a 2-jet Monte Carlo program.

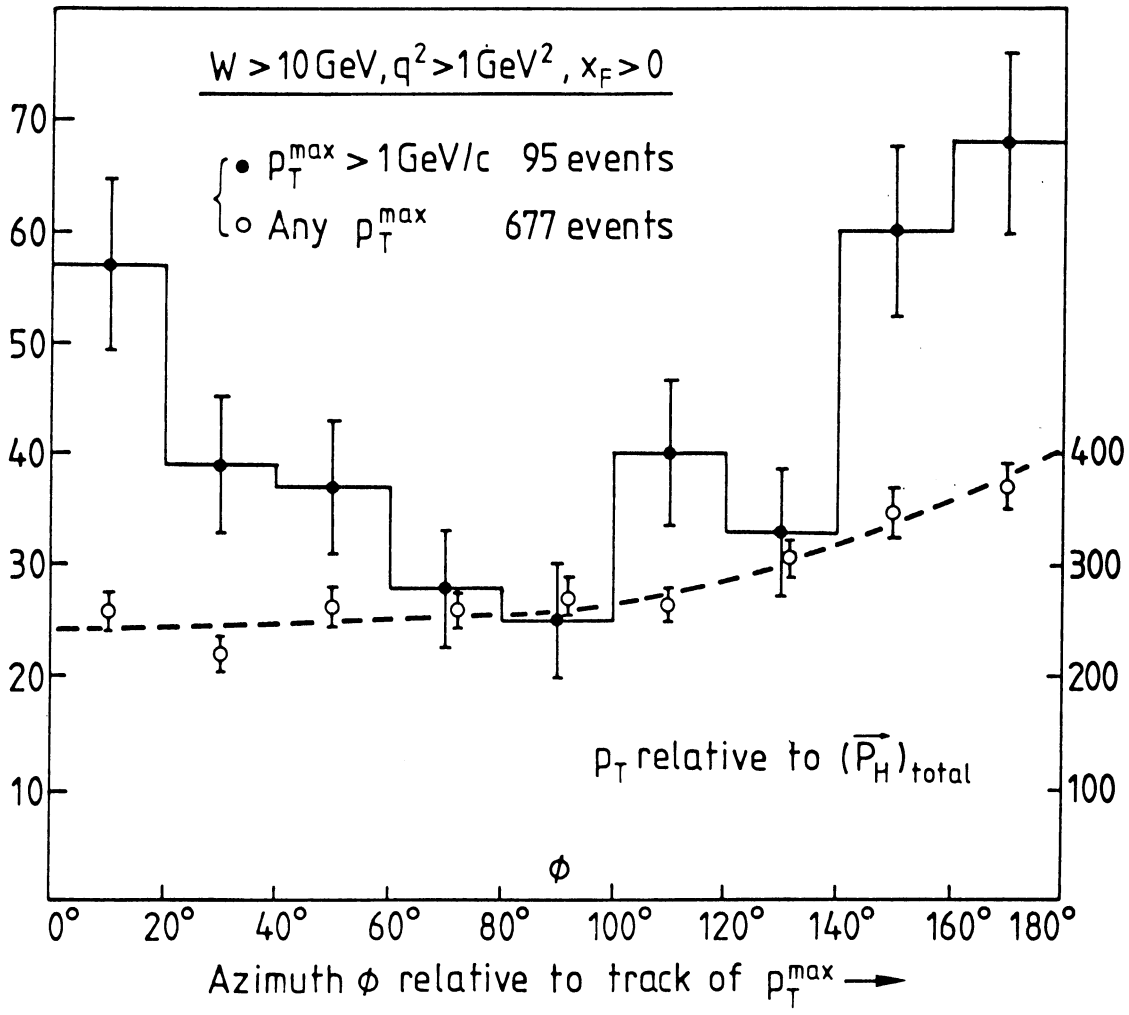

Fig.47 Azimuthal distribution of forward secondaries in events of W > 10 GeV, relative to the highest p_T secondary (p_T^{max}). With no restriction in p_T^{max}, the distribution is flat with a peak towards $\phi = 180°$ from momentum conservation. For $p_T^{max} > 1$ GeV/c, there are peakings, both towards $\phi = 180°$ and $\phi = 0°$; some secondaries "follow" the one of highest p_T (Unpublished data from BEBC νNe (ABCLOS) and νH_2 (ABCMO) experiments).

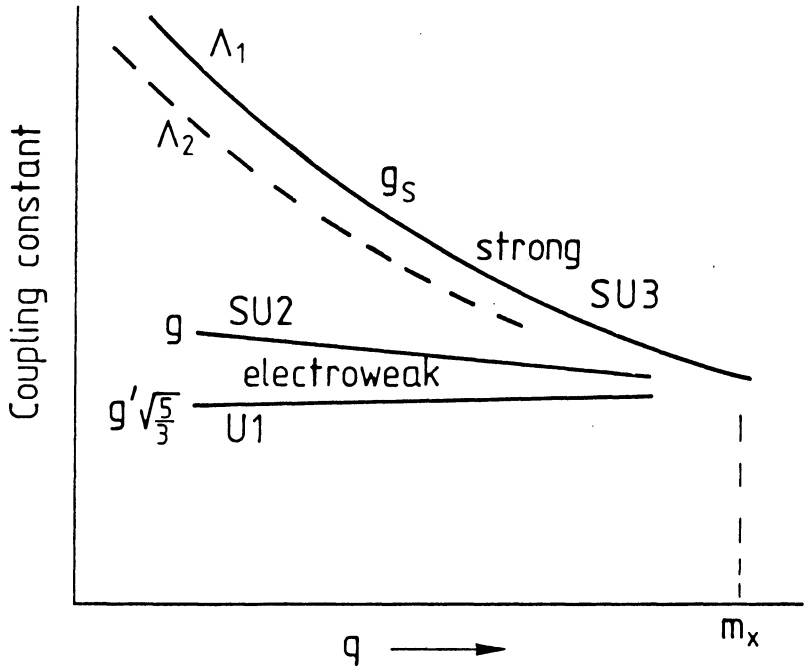

Fig.48 The q dependence of the couplings g' and g of the electroweak theory, and g_s of QCD. They appear to coincide at $q = M_X \sim 3.10^{14}$ GeV.

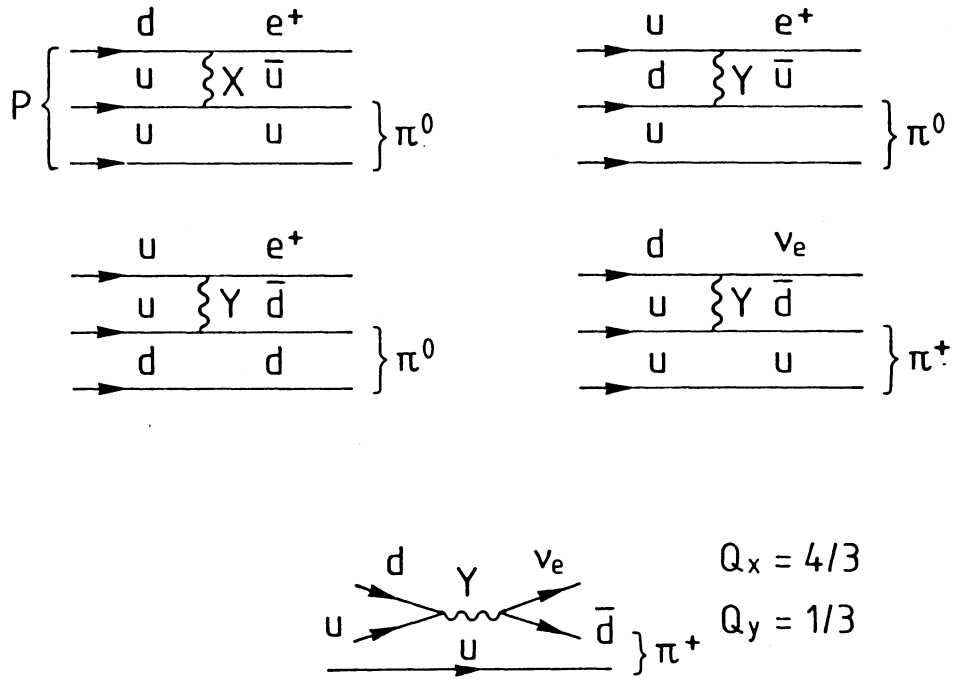

Fig.49 Possible diagrams representing nucleon decay via the leptoquark bosons X, Y of the grand unified theories.

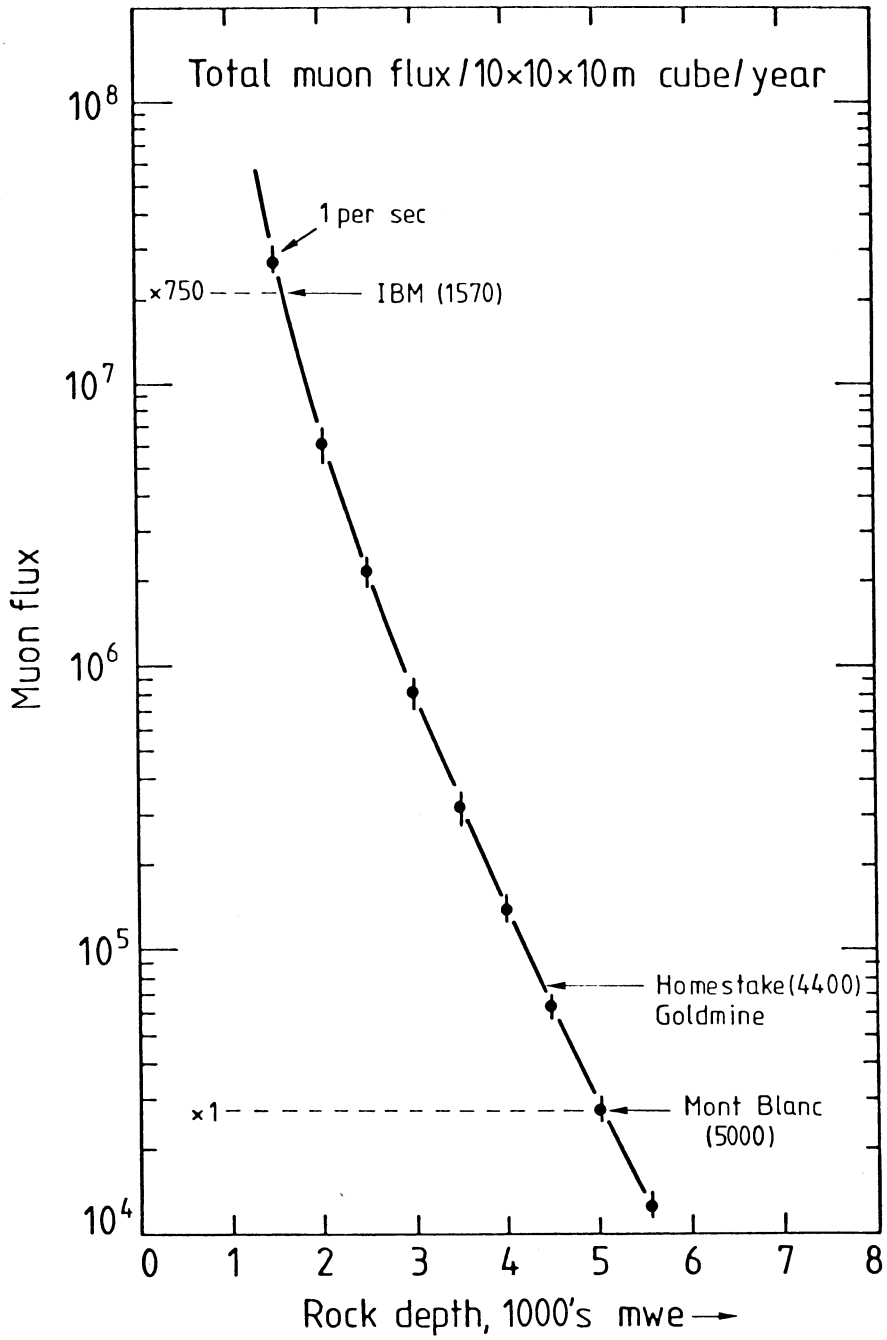

Fig.50 Cosmic ray muon flux through a 10m cube as a function of rock depth in meters of water equivalent.

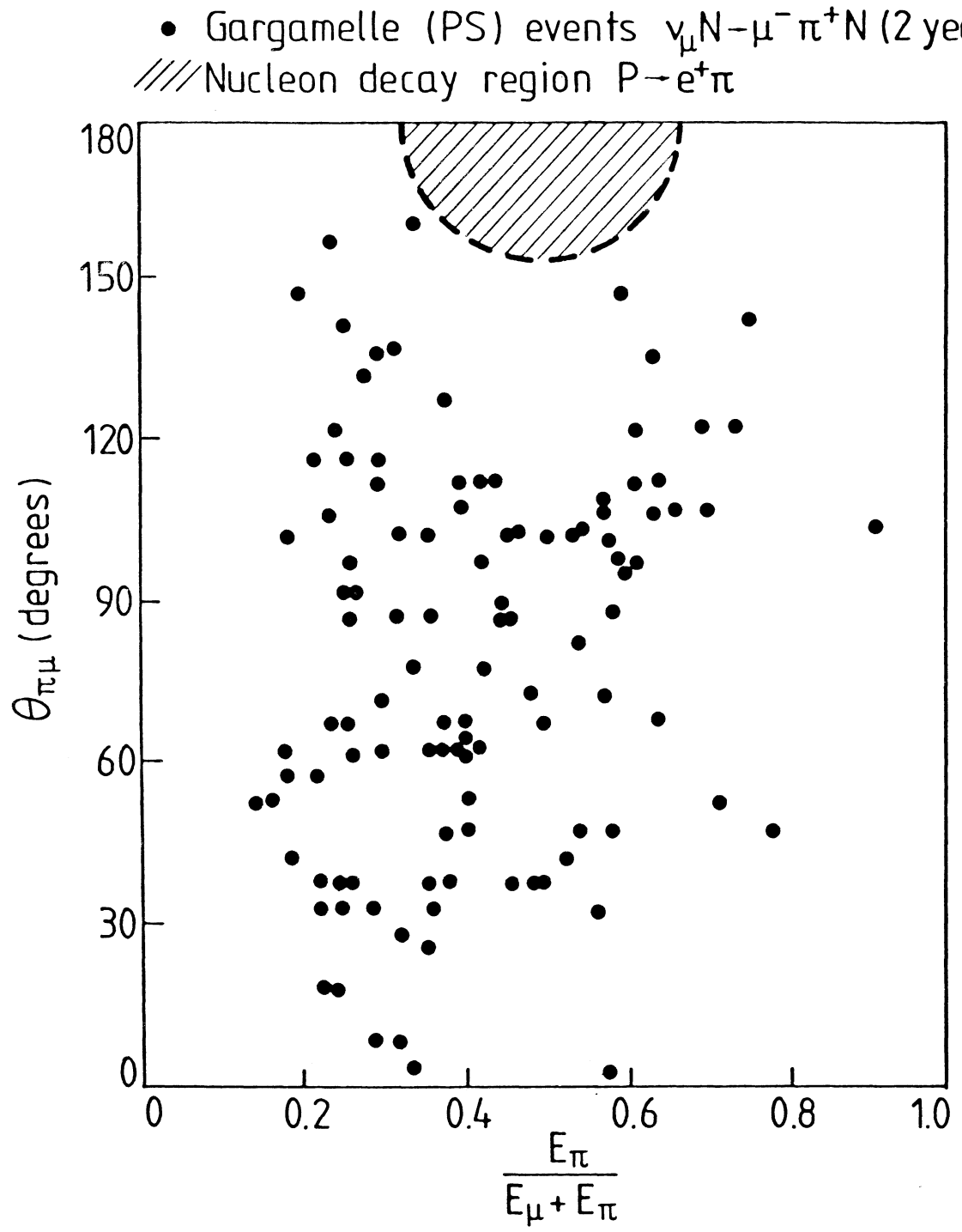

Fig.51 Division of energy and lepton-pion angle in Gargamelle (PS) neutrino events of the type $\nu_\mu N \to \mu^- \pi^+ N$. The number of events is equal to that expected as neutrino background in a 2-year run of the IMB proton decay experiment (from IMB proposal).

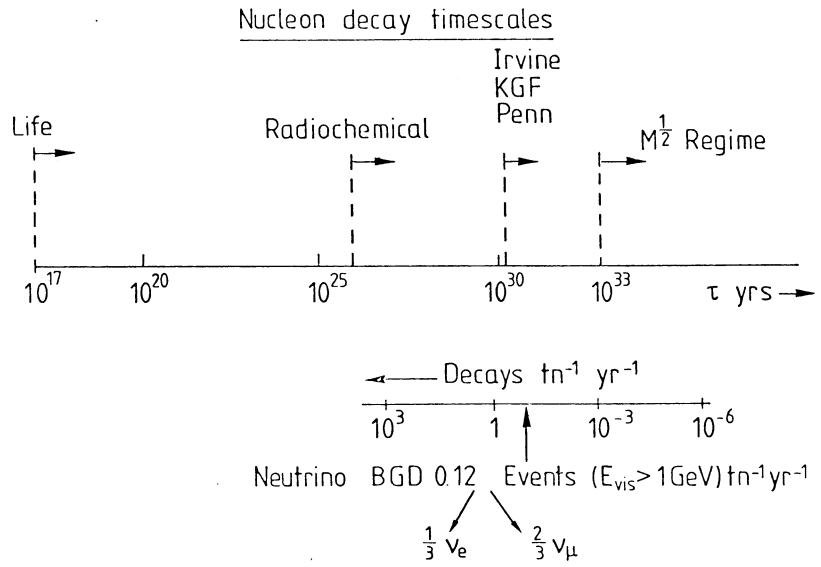

Fig.52 Timescales and backgrounds in proton decay.

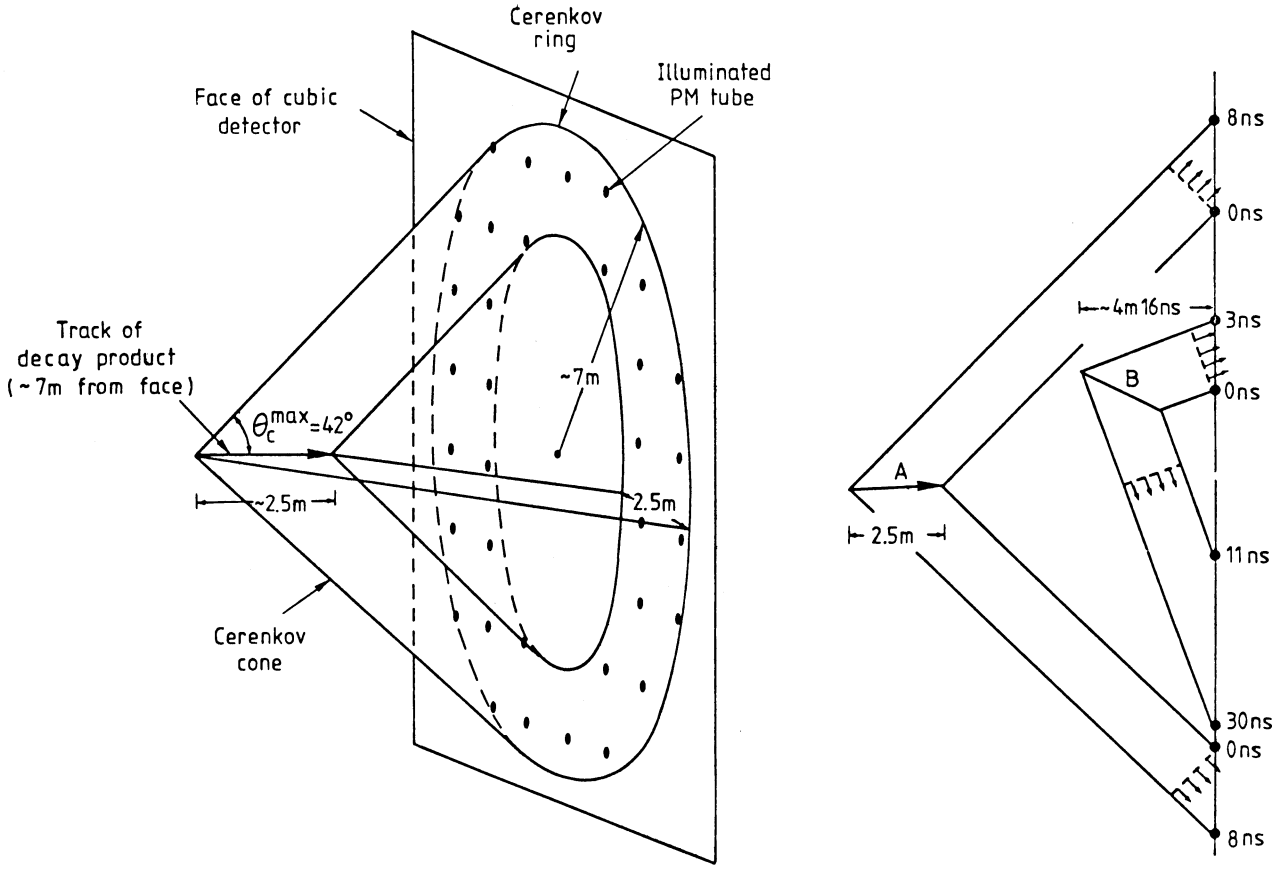

Fig.53 Tyoical Cerenkov light cones from relativistic particles in water detector (from IMB proposal).

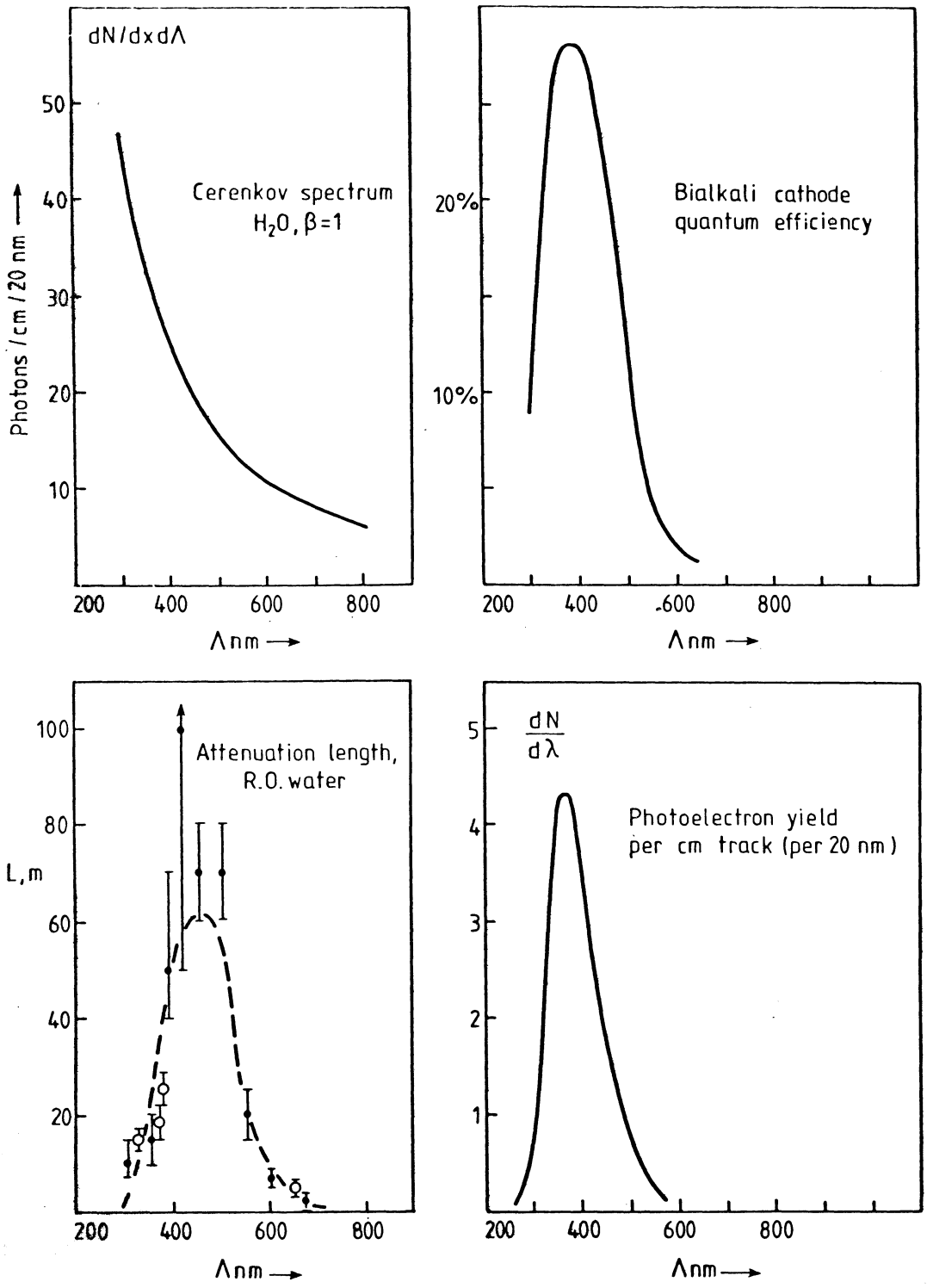

Fig.54 Cerenkov spectrum in water, photomultiplier quantum efficiency, and light attenuation as a function of wavelength. The photoelectron yield after 10m traversal of purified water is the product of factors from the preceding plots.

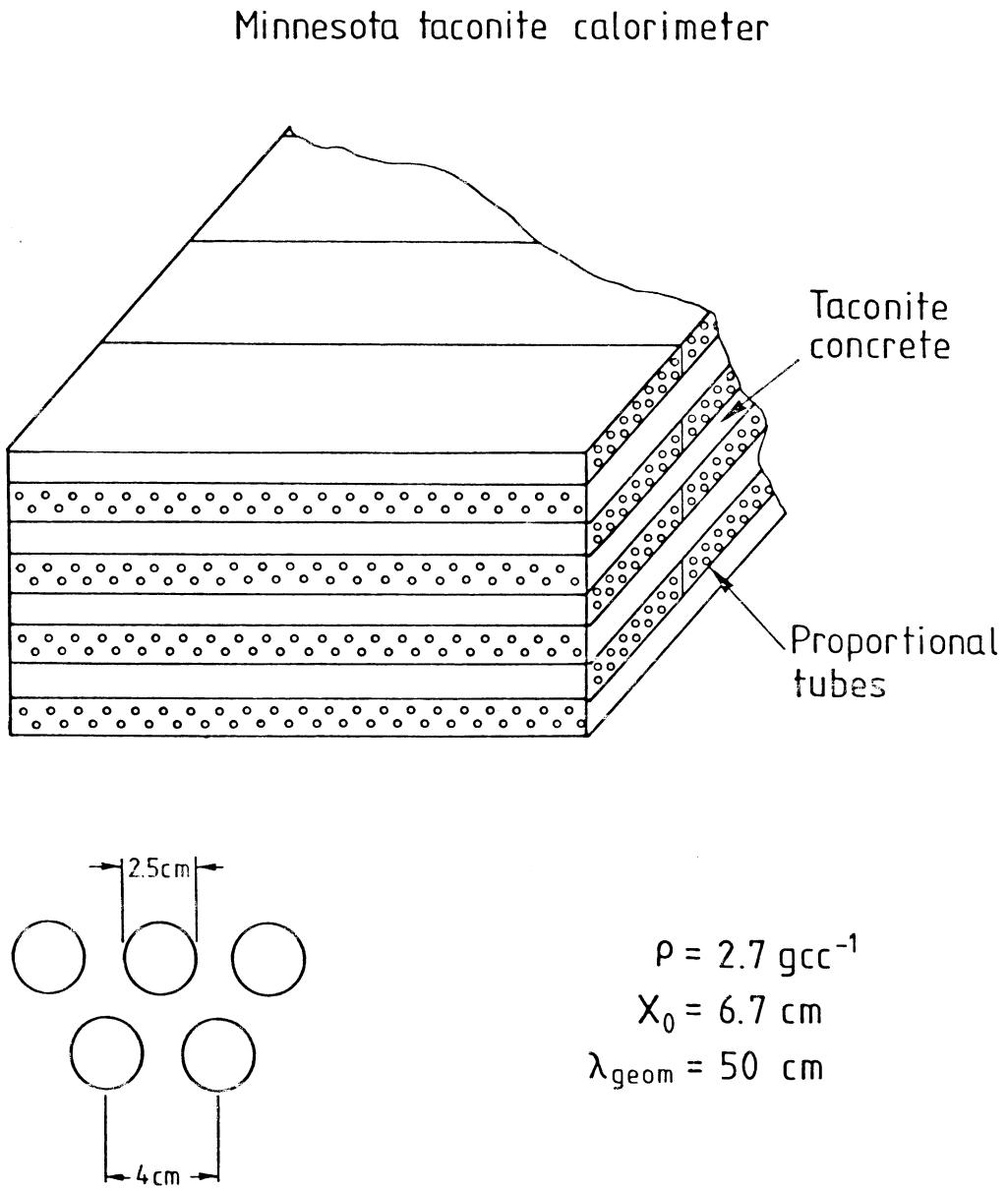

Fig.55 Taconite (iron + concrete) calorimeter of U of Minnesota experiment employing proportional tube detectors.

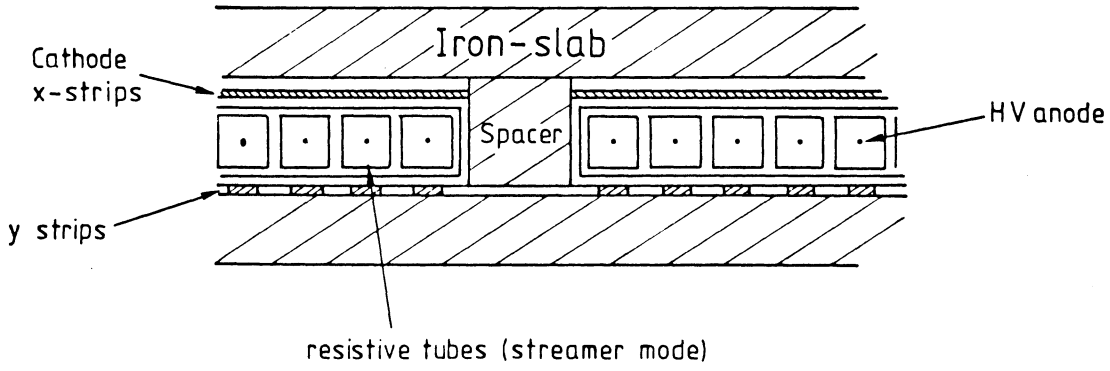

Fig.56 Design of the NUSEX (Milano - Frascati - Torino) nucleon decay calorimeter. It consists of 1cm iron slabs with resistive tubes operated in the streamer mode. The ion pulse from a streamer is recorded on orthogonal layers of cathode strips.

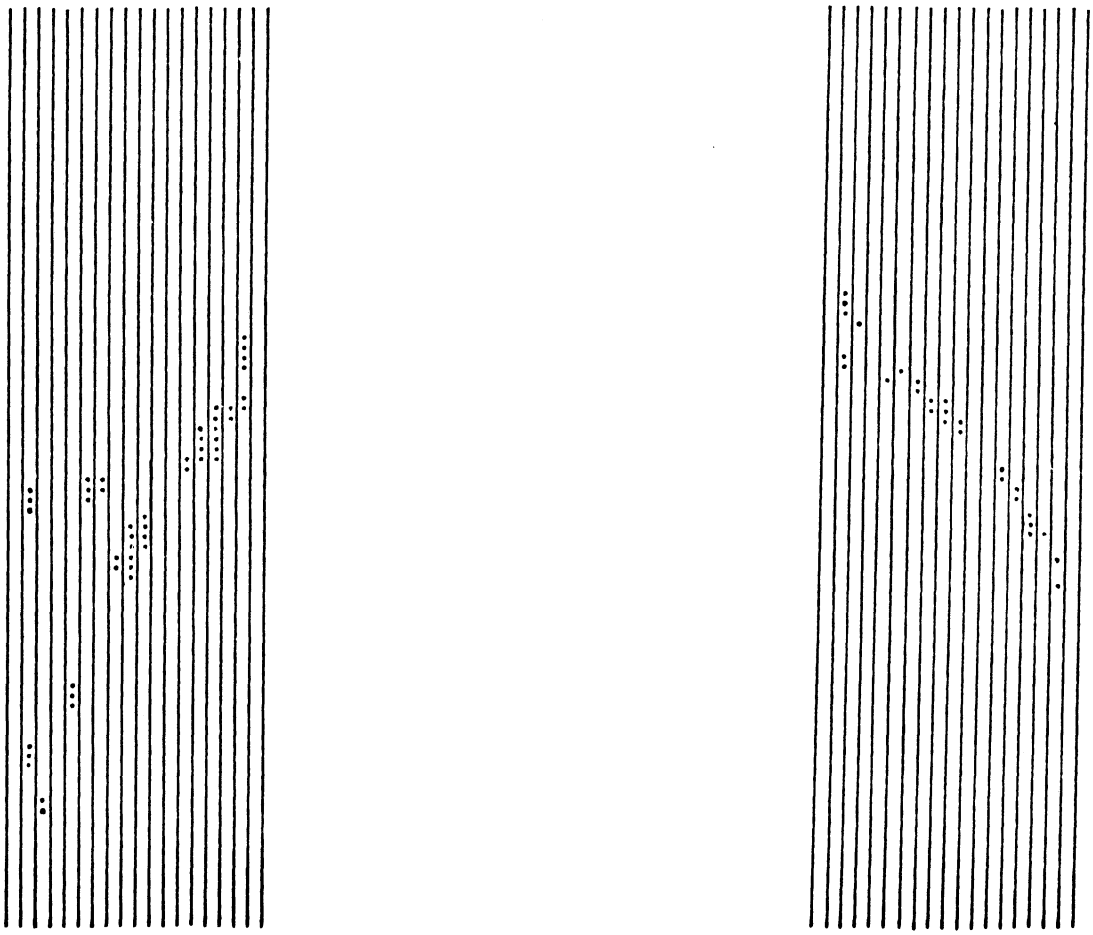

Fig.57 Simulation of $p \to e^{+}\pi^{\circ}$ decay in NUSEX calorimeter.

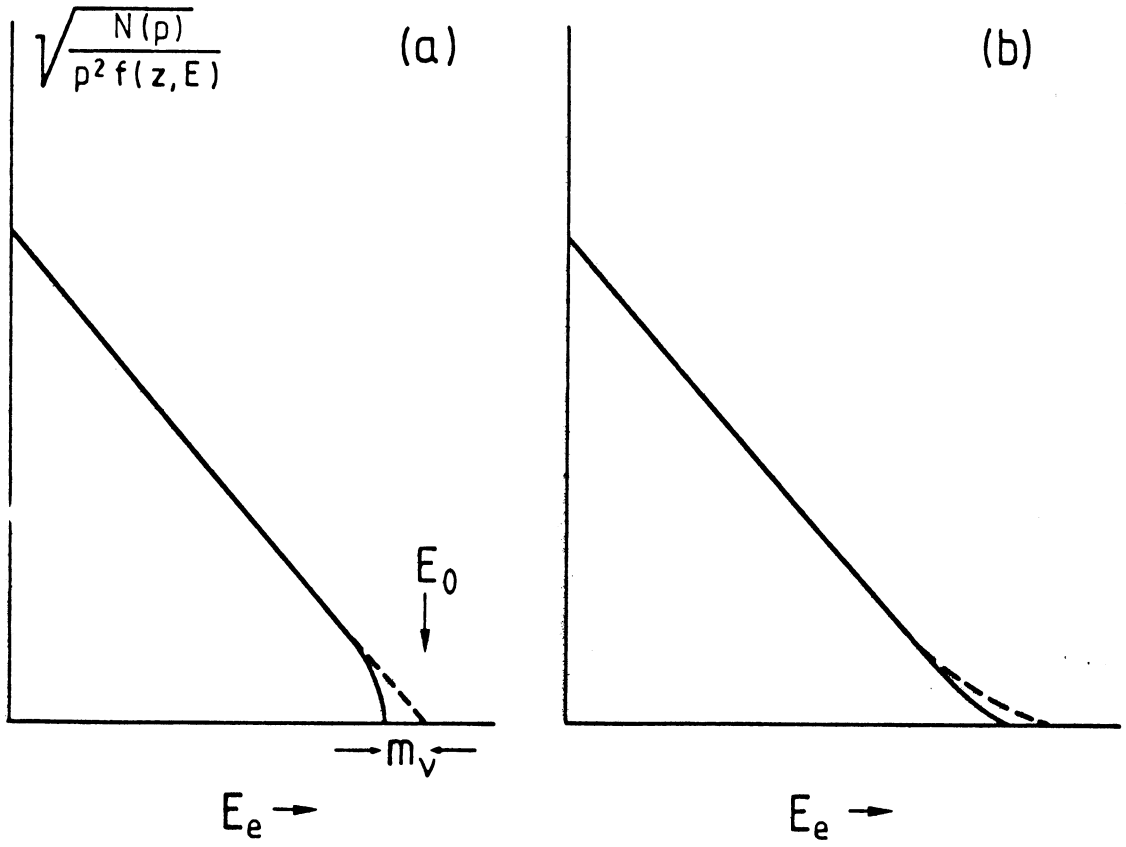

Fig.58 (a) Kurie plot of tritium β-decay, showing the effect of finite neutrino mass.
(b) Actual shape of plot when experimental resolution is folded in.

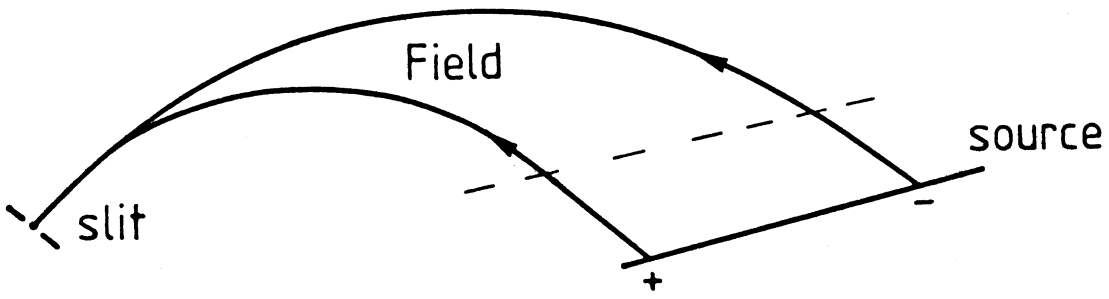

Fig.59 The acceptance of the β-source can be improved by extending it over a line and applying a suitable potential gradient, so that electrons emitted with the same energy from different points arrive at the momentum slit.

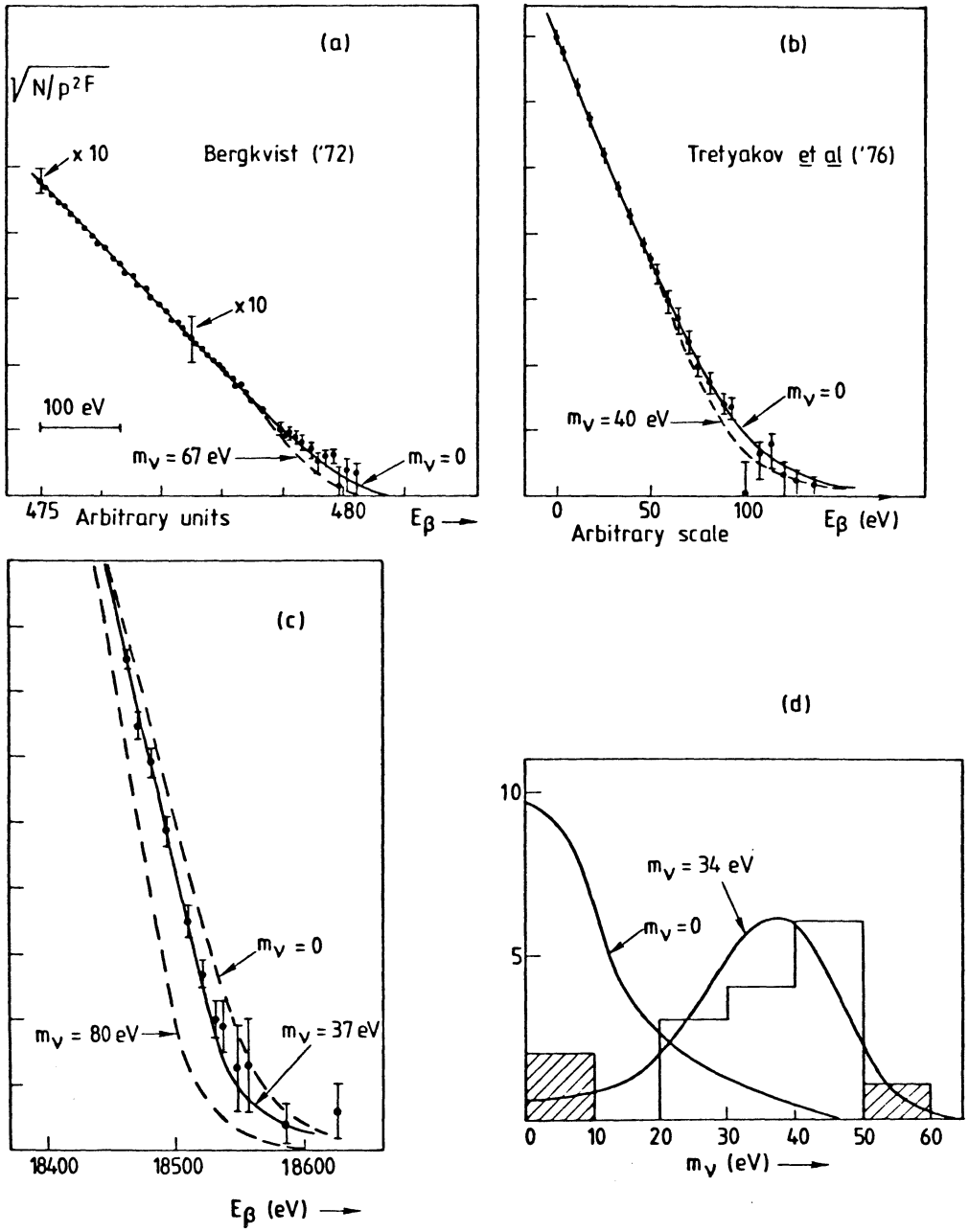

Fig.60 Kurie plots from recent observations of the tritium β-spectrum.

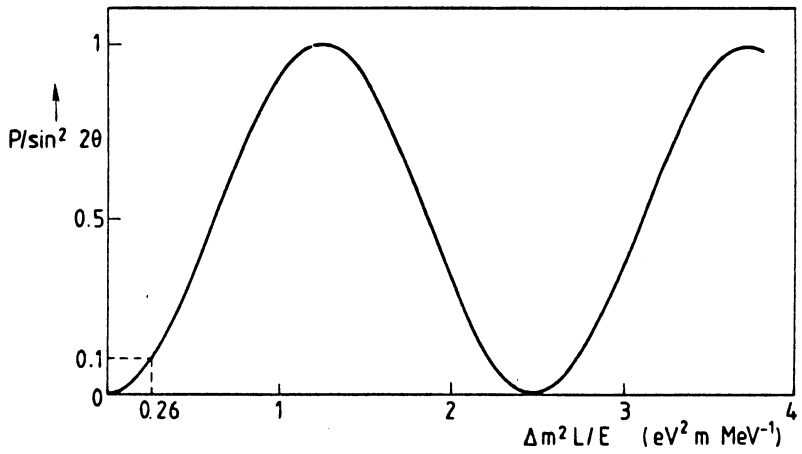

Fig.61 Oscillation amplitude as a function of mass difference, observation length and neutrino energy.

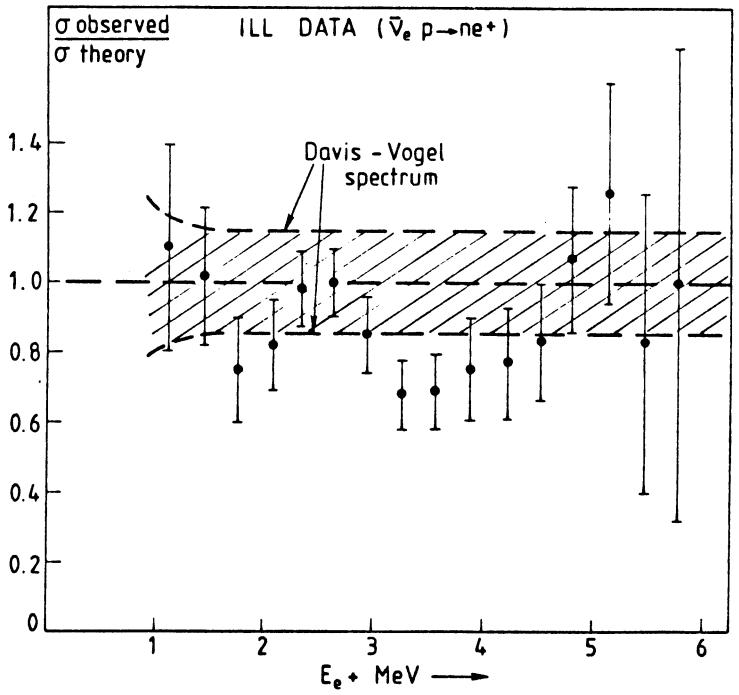

Fig.62 ILL data (Boehm et al 1980) on the ratio of observed to expected rates for $\bar{\nu}_e p \rightarrow ne^+$.

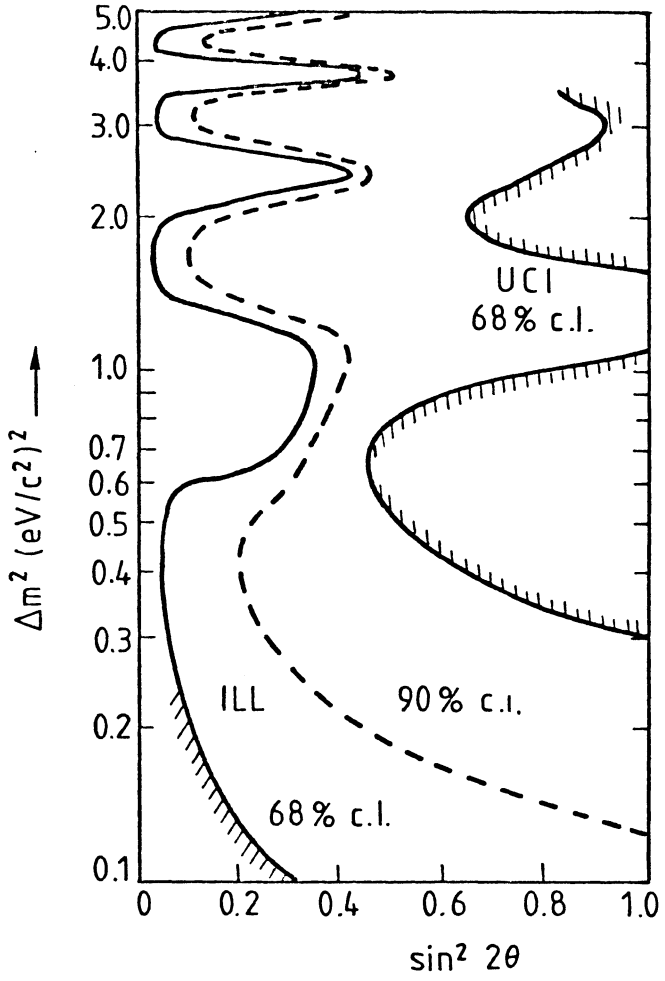

Fig.63 65% and 90% confidence limits from the Savannah River (Reines et al 1980) and Grenoble (Boehm et al 1980) reactor experiments.